STRUCTURAL ASPECTS OF ASC SPECK FORMATION AND ITS POTENTIAL NOVEL FUNCTIONS

by

Ali Can Sahillioğlu

B.S., Molecular Biology and Genetics, Boğaziçi University, 2010

Submitted to the Institute for Graduate Studies in
Science and Engineering in partial fulfillment of
the requirements for the degree of
Master of Science

Graduate Program in Molecular Biology and Genetics
Boğaziçi University

2013

A journey of a thousand miles begins with a single step.

Lao Tzu

ACKNOWLEDGEMENTS

This thesis is the report of my 3 years long hard work, including the outlines of two papers yet to come. At this point I have to pay my respects to a long list of very special people, without them this project would not come to this point.

My greatest acknowledgements are for my thesis supervisor Assoc. Prof. Nesrin Özören for her unconditional support of my ideas and trust in me. The scientific freedom I have tasted in her lab at a very early time point in my career contributed significantly to my scientific thinking skills. I am grateful to Prof. Türkan Haliloğlu and Assoc. Prof. Nesrin Özören for being great mentors and starting an exemplary collaboration between their computational and experimental research groups and giving me the chance to join this project. I also want to thank my colleague Fidan Sümbül as the fellow computational researcher of this collaboration. Fidan Sümbül, M. Sc. and Prof. Türkan Haliloğlu contributed to this project in the prediction of amino acids important for the ASC speck formation and various computational analyses of these residues, which will be discussed in the upcoming paper. Together, we have questioned two basic questions; namely the nature and underlying reasons of the ASC speck formation. We think our pioneering work will be followed by other fellow scientists which will accelerate the pace of scientific discoveries.

Another very special person I want to thank is Assist. Prof. Stefan H. Fuss. I had the opportunity to work in his lab for one year as an undergrad special project student. In his lab, I loved to do research as a result of his mysterious motivation methods. Assist. Prof. Stefan H. Fuss also trained me using the confocal microscope, and his former student İbrahim Taştekin, M. Sc. taught me everything I know about molecular cloning techniques, which I have used excessively in my thesis project.

I also would like to thank to my third jury member Assoc. Prof. Batu Erman for taking time to evaluate my thesis work.

My lab members Serkan Uğurlu, M. D., Elif Eren, M. Sc., Duygu Demiröz, M. Sc., Aybüke Garipcan, M. Sc., Mustafa Yalçınkaya, B. Sc. and former lab member Yetiş Gültekin, M. Sc. were always available when I needed any help. I am grateful for their support.

During this project, we have received reagents from various fellow scientist including, Prof. Masumoto, Prof. Deisseroth, Prof. Nunez, Prof. Soengas, Prof. Gül and Assoc. Prof. Çelik. We are grateful to all of these groups for helping us in this project.

Last but not least, I received tremedous support from my family and my old-time friend Rana N. Özdeşlik for successfully finishing this thesis. These people are the spiritual collaborators of the project.

This project was funded by Tübitak (110T088) and Boğaziçi University (BAP 6524).

ABSTRACT

STRUCTURAL ASPECTS OF ASC SPECK FORMATION AND ITS POTENTIAL NOVEL FUNCTIONS

Inflammasomes are cytoplasmic sensors that detect presence of intracellular pathogens or cellular damage. Activation of NLRP3, NLRC4 and AIM2 inflammasomes is accompanied by formation of a micrometer sized perinuclear structure called the ASC speck which is thought to be the platform for inflammasome activity. We carried out a mutational screen on the EGFP-ASC fusion protein in to determine ASC speck disrupting mutations. The ASC protein has two domains, namely pyrin domain (PYD) and caspase recruitment domain (CARD) which form filament structures when overexpressed in HEK293T cells as seperate domains. A subset of mutations we introduced in the full length ASC protein changed the globular ASC speck structure into filaments, which were similar to the filaments formed by the individual domains of ASC. We repeated a parallel mutational screen on PYD or CARD as seperate domains and found that mutations disrupting the ASC speck in the full length ASC construct also disrupt the filaments in the domain only constructs. The filaments formed by PYD was proposed to be formed by type I interactions. By using the type I binding mode deficient D48A mutant PYD, we showed that D48A-PYD is able to interact with wt PYD filaments, which indicates that PYD has alternative binding modes. Our results suggest that the ASC speck is an organized structure, as single mutations introduced in ASC changes the ultimate structure completely. The second part of the thesis is based on the observation that the ASC speck is able to co-aggregate a wide range of cytosolic proteins on itself. We postulate that antigen co-aggregation of the ASC speck might be important in antigen presentation. The ASC protein has already been implicated in the antigen presentation pathway via inflammasome dependent and independent mechanisms. Co-aggregation of cytosolic proteins on the ASC speck has potential implications in antigen presentation pathway which could be exploited to build better vaccines in the future.

ÖZET

ASC ZERRESİ OLUŞUMUNUN YAPISAL ÖZELLİKLERİ VE POTANSİYEL YENİ İŞLEVLERİ

Enflamazomlar sitoplazmada bulunan patojenleri ve hücresel hasarı tespit eden algılayıcılardır. NLRP3, NLRC4 ve AIM2 enflamazomlarının uyarılması sonucu hücre çekirdeğinin yanında mikrometre boyutlarında ASC zerresi adında, enflamazom aktivitesinin gerçekleştiği platform olduğu düşünülen bir yapı oluşmaktadır. ASC proteini payrin bölgesi (PYD) ve kaspaz bağlanma bölgesi (CARD) isimli iki bölgeden oluşmuştur ve bu bölgeler yüksek miktarda anlatıldığı durumda filament yapıları oluşturmaktadır. EGFP-ASC kaynaşık proteini üzerinde mutasyonlar oluşturarak ASC zerresini bozan mutasyonları taradık. Oluşturduğumuz mutasyonların bir bölümü ASC zerresini, ASC'ı oluşturan bölgelerinin oluşturduğu filament yapılarına benzer yapılara dönüştürdü. Bu mutasyon taramasına paralel olarak, PYD veya CARD ayrışık mutant bölgelerini tek başına anlatarak yaptığımız deneylerde; tam boyutlu ASC proteininde ASC zerrelerini bozan mutasyonların kısaltılmış proteinlerde filament yapısını bozduğunu tespit ettik. PYD'nin oluşturduğu filament yapılarının tip I etkileşmesi sonucu oluştuğu önerilmiştir. Tip I etkileşmesini bozan D48A mutasyonlu PYD kullanarak, yabanıl PYD filamentlerine mutant D48A-PYD'nin bağlanabildiğini gösterdik. Bu sonuç PYD'nin alternatif bağlanma modlarının olduğunu önermektedir. ASC proteininde oluşturduğumuz mutasyonların ASC zerrelerinin yapısını tamamen değiştirmesi, ASC zerre yapısının düzenli bir yapı olduğunu önermektedir. Tezin ikinci kısmı, ASC zerrelerinin sitozolik çeşitli proteinleri ko-agrege edebildiği gözlemine dayanmaktadır. ASC zerrelerinin sitozolik proteinlerini ko-agrege edebilmesinin antijen sunumunda önemli olabileceğini önermekteyiz. ASC proteini halihazırda enflamazoma bağlı ve bağımsız yolaklar ile antijen sunumu ile ilişkilendirilmiştir. ASC zerreleri üzerinde sitoplazmik proteinlerin ko-agregasyonu ve antijen sunumundaki potansiyel ilişkisinden, ileride aşı teknolojisinin geliştirilmesinde yararlanılabilir.

TABLE OF CONTENTS

LIST OF FIGURES

LIST OF TABLES

LIST OF SYMBOLS

a.u.	Arbitrary Unit
bp	Base Pairs
g	Gravity
gr	Gram
kb	Kilobase
kDa	Kilodalton
L	Liter
M	Molar
mA	Milliamper
mg	Milligram
min	Minute
ml	Milliliter
mm	Millimeter
mM	Millimolar
ng	Nanogram
^{o}C	Centigrade Degree
sec	Second
V	Volt
µg	Microgram
µl	Microliter
α	Alpha
β	Beta
γ	Gamma
κ	Kappa

LIST OF ACRONYMS / ABBREVIATIONS

Ab	Antibody
AIM2	Absent in Melanoma 2
Alum	Hydrated Potassium Aluminium Sulfate
APC	Antigen Presenting Cell
APS	Ammonium Persulfate
Ar	Argon
ASC	Apoptosis-Associated Speck-Like Protein Containing a CARD
BF	Bright field
BSA	Bovine Serum Albumin
CARD	Caspase Recruitment Domain
Casp1	Caspase-1
Caspase	Cysteine-Aspartic Proteases
CD	Cluster of Differentiation
CDS	Coding Sequence
cDNA	Complementary DNA
COS-7	CV-1 (simian) in Origin, and Carrying the SV40 7
CpG	C-phosphate-G
C-terminal	Carboxyl-Terminal
CytOVA	Cytoplasmic Ovalbumin
DALIS	Dendritic Cell Aggresome-Like Induced Structures
DAMP	Danger-Associated Molecular-Patterns
DAPI	4',6-diamidino-2-phenylindole
DC	Dendritic Cell
DD	Death Domain
ddH_2O	Double Distilled Water
DED	Death Effector Domain
DISC	Death-Inducing Signaling Complex

DMEM	Dulbecco's Modified Eagle Medium
DMSO	Dimethyl Sulfoxide
DNA	Deoxyribonucleic Acid
dNTP	Four Deoxyribonucleotides
DRiP	Defective Ribosomal Products
dsDNA	Double Stranded DNA
EB	Elution Buffer
ECMV	Encephalomyocarditis Virus
EGFP	Enhanced Green Fluorescent Protein
Em	Emission
ER	Endoplasmic Reticulum
EtBr	Ethidium Bromide
EYFP	Enhanced Yellow Fluorescent Protein
FADD	Fas-Associated Protein with Death Domain
FBS	Fetal Bovine Serum
FRET	Förster Resonance Energy Transfer
g.s.	Gravity Sedimentation
GST	Glutathione S-Transferase
H	Helix
hASC	Human ASC
HBS	HEPES Balanced Salt
HCV	Hepatitis C Virus
HEK	Human Embryonic Kidney
HeNe	Helium–Neon
HEPES	4-(2-hydroxyethyl)-1-piperazineethanesulfonic Acid
HL-60	Human Promyelocytic Leukemia Cells
HRP	Horseradish Peroxidase
IL	Interleukin
IL-1β	Interleukin 1-β
IP	Immunoprecipitation
IPOD	Insoluble Protein Deposit

JUNQ	Juxtanuclear Quality Control
LB	Luria-Bertani Broth
LPS	Lipopolysaccaride
LRR	Leucin Rich Repeat
mCMV	Beta-Herpesvirus Murine Cytomegalovirus
MCS	Multiple Cloning Site
MHC	Major Histocompatibility Complex
MSU	Monosodium Urate
MTOC	Microtubule Organizing Center
MV	Measles Virus
MVA	Modified Vaccinia Virus Ankara
n.s.	Non Spesific
NACHT	NAIP, CIITA, HET-E and TP1
NAIP5	NLR Family, Apoptosis Inhibitory Protein 5
NEAA	Non-esential Amino Acid
neg	Negative
NF-κB	Nuclear Factor Kappa B
NLR	NOD-Like Receptor
NLRC4	NLR family, CARD Domain Containing 4
NLRP3	NLR family, Pyrin Domain Containing 3
NMR	Nuclear Magnetic Resonance
NOD	Nucleotide-Binding Oligomerization Domain
NP	Influenze Nucleoprotein
N-terminal	Amino-Terminal
PAMP	Pathogen-Associated Molecular Pattern
PBS	Phosphate Buffered Saline
PCR	Polymerase Chain Reaction
Pen/Strep	Penicillin/Streptomycin
PFA	Paraform Aldehyde
PLA	Polylactic Acid
PLGA	Poly(lactic-co-glycolic acid)

PMA	Phorbol 12-myristate 13-acetate
proIL-18	Prointerleukin-18
proIL-1β	Prointerleukin-1beta
PYD	Pyrin Domain
RCSB	Research Collaboratory for Structural Bioinformatics
RF	Reverse Flow
RIG-I	Retinoic Acid-Inducible Gene-I
RLR	RIG-I like Receptor
RPM	Rotations per Minute
RT	Room Temperature
SDS	Sodium Dedocyl Sulfate
SDS-PAGE	SDS- Polyacrylamide Gel Electrophoresis
SeV	Sendai Virus
shortASC	Short Isoform of ASC
TAE	Tris-Acetate-EDTA
TBS	Tris Buffered Saline
TBST	Tris Buffered Saline Tween 1,2-diamine
TEMED	N,N,N’,N’-Tetramethylethane-
TLR	Toll-Like Receptor
Tris	Tris(hydroxymethyl)aminomethane
Tween	Polysorbate
UBB	Ubiquitin B
UV	Ultraviolet
v	Volume
VSV	Vesicular Stomatitis Virus
VZV	Varicella-Zoster Virus
w	Weight
WT	Wild-Type

1. INTRODUCTION

1.1. The immune system

The evolutionary history of pathogens goes hand in hand with the development of the immune system. All multicellular organisms, including plants, have a fast responding, simpler form of immunity, called innate immunity [2-6]. This type of immune response depends on antimicrobial peptides and hard-coded pattern recognition receptors [7, 8]. On the other hand, a relatively novel type of immunity, which first evolved in jawless fish, is based on somatic recombination of B- and T-cell receptors, yielding highly specific immune responses against a diverse range of pathogens, called adaptive immunity [9, 10].

1.2. Innate immunity and pattern recognition receptors

Innate immunity is orchestrated by a diverse set of membrane bound and cytoplasmic pattern recognition receptors [11]. Among these, toll-like receptors (TLR) are present on plasma and endosomal membranes. TLRs sense extracellular pathogens and activate the NF-κB pathway. Each TLR has evolved to recognize a particular pathogenic motif such as LPS, flagellin and unmethylated DNA (CpG) recognized by TLR-4,-5 and -9, respectively. Of note, TLR agonists are potent antigen presenting cell (APC) activators and employed in vaccines as proven adjuvant molecules [12]. Others, including RIG-I-like receptors (RLR), NOD-like receptors (NLRs) and the absent in melanoma 2 (AIM2) receptor are cytoplasmic receptors [6, 11].

1.2.1. Inflammasomes

The inflammasomes are cytosolic sensors that detect pathogen associated molecular patterns (PAMPs) and damage associated molecular patterns (DAMPs) [5, 6, 13]. The cellular damage created by pathogens (or other factors) are termed as DAMPs, whereas mo-

lecular patterns on pathogens are called PAMPs. The inflammasome complexes contain receptors (such as NLRP3, NLRC4 and AIM2) that oligomerize upon activation [6].

1.3. Activation mechanisms of inflammasomes

The NLRC4-NAIP5 inflammasome recognizes flagellin [14, 15] and the AIM2 inflammasome recognizes cytosolic dsDNA [16]. NLRC4-NAIP5 and AIM2 have been shown to physically interact with their ligands. On the other hand, the extensively studied NLRP3 inflammasome does not have a specific ligand shown to directly interact with; yet it can be activated by a diverse set of particulate stimulants and membrane permeabilizing agents [5]. It has been postulated that lysosomal damage induced cathepsin B release or potassium ion efflux across the plasma membrane might contribute to downstream signaling events [5].

1.3.1. The NLRP3 inflammasome activation requires a prior priming step

The NLRP3 inflammasome activation takes place in two steps. First, the stimulation of TLR4 by LPS activates NF-κB signalling, which increases cellular levels of NLRP3 as well as immature forms of cytokines proIL-1β and proIL-18. Upregulation of proIL-1β and proIL-18 synthesis is not sufficient for their processing and release, which is accomplished by the second signal. After signal 2, the inflammasome complex is asssembled and cytokines are processed and prepared for secretion [5].

1.3.2. Specific pathogens and their inflammasomes

The inflammasomes can be triggered by a diverse range of bacterial, viral and fungal pathogens. The list of pathogens and their respective inflammasome sensors are summarized in Table 1.1.

Table 1.1. Bacterial, viral and fungal pathogens and their corresponding inflammasomes.

Inflammasome	**Pathogen**	**Type**	**Reference**
NLRC4	*Salmonella*	Bacterial	[17]
	Legionella	Bacterial	
	Pseudomonas	Bacterial	
	Yersinia	Bacterial	
	Shigella	Bacterial	
	A. veronii	Bacterial	
NLRP3	SeV	RNA virus	[18]
	Influenza A	RNA virus	
	ECMV	RNA virus	
	VSV	RNA virus	
	MV	RNA virus	
	HCV	RNA virus	
	Adenovirus	DNA virus	
	MVA	DNA virus	
	Myxoma Virus	DNA virus	
	VZV	DNA virus	
	S. pneumoniae	Bacterial	[17]
	L. monocytogenes	Bacterial	
	S. pyogenes	Bacterial	
	A. hydrophila	Bacterial	
	A. veronii	Bacterial	
	V. vulnificus	Bacterial	
	V. cholerae	Bacterial	
	S. aureus	Bacterial	
	M. marinum	Bacterial	
	M. tuberculosis	Bacterial	
	C. trachomatis	Bacterial	
	C. pneumoniae	Bacterial	
	K. pneumoniae	Bacterial	
	P. gingivalis	Bacterial	
	N. gonorrhoeae	Bacterial	
	C. albicans	Fungal	[19]
AIM2	Vaccinia Virus	DNA virus	[16]
	mCMV	DNA virus	
	F. tularensis	Bacterial	
	LVS	Bacterial	

1.3.3. Sterile inflammation

The NLRP3 inflammasome can be also triggered by stimuli that are not originating from pathogens. These stimuli include extracellular ATP, monosodium urate (MSU) crystals and amyloid-β [20]. Extracelullular ATP is thought to be released from necrotic cells and functions as a ligand for P2X7R, which permeabilizes the plasma membrane for K^+ ions and activates signal 2. MSU crystals and amyloid-β are examples of particulate stimuli that can activate the NLRP3 inflammasome. The NLRP3 inflammasome is also known to be activated by a large range of synthetic particulate stimulants such as alum, silica and asbestos crystals [20].

1.4. Subsequent events following the inflammasome activation

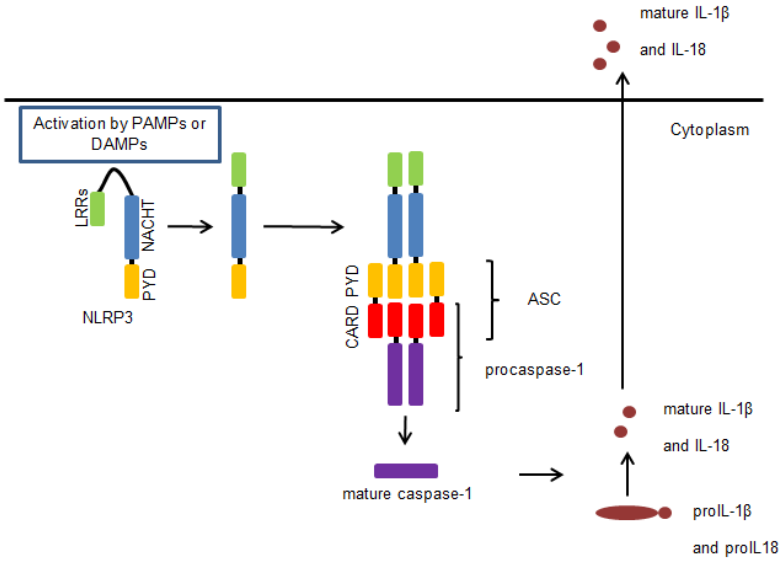

Figure 1.1. Schematic representation of the NLRP3 inflammasome pathway members and their domain compositions.

1.4.1. Assembly of the inflammasome complex

It is generally accepted that monomeric inflammasome components oligomerize upon inflammasome activation. According to the classical model, NLRs change their conformation upon activation in a way that the inhibition of LRR on NACHT domain is abro-

gated (Figure 1.1). The conformational change is followed by oligomerization of NLRs via their NACHT domains [6, 22].

1.4.2. The induced proximity model

The oligomerized inflammasome receptors recruit the ASC protein which interacts with inactive zymogen procaspase-1. Thereby, procaspase-1 proteins that are brought into close proximity cleave each other. The processed mature caspase-1 is capable of hydrolyzing proIL-1β and proIL-18 which are subsequently secreted from the cell. The mechanistic model of caspase self-activation is termed as the induced proximity model [23, 24]. This theory was proposed to explain initiation of inflammatory procaspase-1 as well as apoptotic procaspase-8 and procaspase-9 self-cleavage [25-28]. According to this model; inflammasome complexes, death-inducing signaling complex (DISC) and apoptosome complex are responsible for induced proximity-mediated self-activation of procaspase-1, -8 and -9, respectively [5, 24, 29].

1.4.3. The inflammasome: An oligomeric or a supramolecular activation platform for caspase-1?

The crystal structure of pentameric human DISC, the electron microscope structure of the heptameric human apoptosome, the crystal structure of octameric *Caenorhabditis elegans* apoptosome and the electron microscopy structure of the octameric *Drosophila melanogaster* apoptosome have been revealed [30-33]. However, there is currently no published oligomeric structure of any inflammasome complex. In fact, it has been shown that upon inflammasome activation, inflammasome components form a micrometer-sized supramolecular structure called ASC specks/ASC foci/pyroptosome near the nucleus [34-37]. This structure is implicated in the induced proximity mediated procaspase-1 self-activation [36, 38].

1.4.4. Cytokine processing and secretion

The primary function of the inflammasome complex seems to be the processing of inactive forms of proIL-1β, proIL-18, proIL-33 and their subsequent secretion from the cell (Figure 1.1) [39, 40]. There is evidence that cytokine processing is taking place at the ASC speck [36]. Upon processing of cytokines, IL-1β and IL-18 are released from the cell via an unconventional protein secretion system, which is independent of the ER-Golgi pathway and does not depend on targetting signals [41-47]. The released active IL-1β and IL-18 contribute to progression of local inflammation by promoting fever, edema, lymphocyte activation and leukocyte infiltration at the site of injury or infection.

1.4.5. Pyroptosis

Apart from cytokine processing, inflammasome activation is attributed to another role, which is the caspase-1-dependent pyroptotic cell death [48]. Pyroptotic cell death is observed in macrophages and dendritic cells upon inflammasome stimulation with loss of membrane integrity, similar to necrosis [48, 49]. Pyroptosis was suggested as a mechanism used by macrophages to clear bacterial infection [50, 51]. The ASC protein has been suggested to play a role in the fate of the cell upon stimulation of the NLRC4 inflammasome. According to this model in the absence of ASC, NLRC4 inflammasome activation leads to pyroptotic cell death by direct interaction with procaspase-1, whereas in the presence of ASC, ASC specks favor cytokine processing rather than cell death [34]. However, another report suggested that the ASC speck is responsible for pyroptotic cell death by itself and referred to the ASC speck as “pyroptosome” [36].

1.4.6. Inflammasome inactivation

A recent report has shown that ASC specks are cleared by the autophagy pathway [52]. The clearance of assembled inflammasomes was carried out by their ubiquitination and subsequent recruitment of autophagic adaptor p62. The autophagic removal of the

ASC speck is suggested as a mechanism to limit cytokine processing and pyroptotic cell death [53].

1.4.7. The ASC protein and the inflammasomes

NLRP3 and AIM2 inflammasomes require ASC protein as an adapter in order to interact with procaspase-1. In contrast, NLRC4 can directly interact with procaspase-1 in the absence of ASC. However, NLRC4 activation can also induce ASC speck formation. It has been suggested that ASC-independent NLRC4 activation leads to caspase-1-dependent cell death, called pyroptosis, whereas ASC-dependent NLRC4 activation results in IL-1β secretion [34].

1.5. The structure of the ASC protein

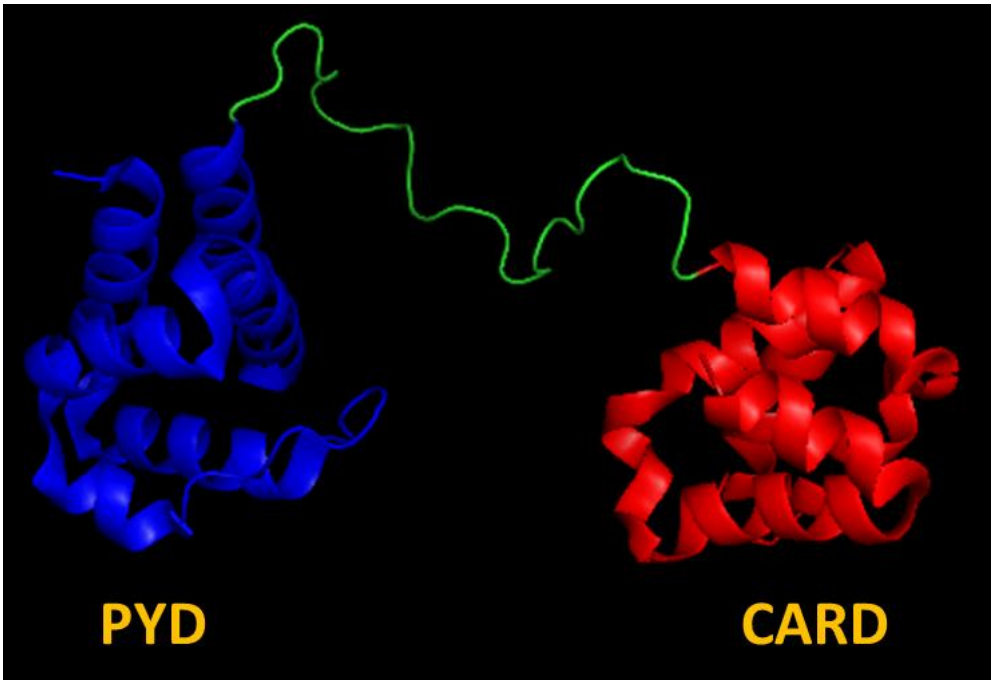

Figure 1.2. The NMR structure of the ASC protein. PYD (blue), CARD (red), linker (green). The structure is created using PYMOL software based on the NMR structure downloaded from RCSB Protein Data Bank with the reference ID: 2KN6 [1].

ASC is a 22kDa, 196 amino acids long protein having an N-terminal pyrin domain (PYD) and a C-terminal caspase recruitment domain (CARD) linked by a 23 amino acids long flexible linker (Figure 1.2) [1, 54]. Both PYD and CARD are members of the death-fold super family. The death-fold superfamily is a conserved folding motif, characterized by a 6-helix bundle structure. Members of the death-fold super family are commonly found in proteins involved in apoptosis and inflammatory pathways. Other members of this folding motif are the death domain (DD) and the death effector domain (DED) [55].

1.5.1. The short isoform of ASC

In humans, the ASC protein has two isoforms. The protein product encoded by the longer transcript is the main isoform and responsible for the compact shape of the ASC speck, whereas the short isoform was reported to form filaments [56]. The shorter isoform encodes in frame PYD and CARD but lacks a 19 amino acids long fragment of the 23 amino acids long linker region between the two domains [56]. The protein product level of the long isoform was reported to be around 10 times higher than that of the short isoform [36, 56]. In reconstitution systems, the short isoform was shown to be able to recruit procaspase-1 for promote IL-1β processing [56]. Interestingly, the compact shape of the ASC speck was reported even in the evolutionarily distant species such as zebrafish [57], which raises the question whether the compact shape of the ASC speck formed by the long isoform has any evolutionarily advantage over the short isoform.

1.5.2. Interaction modes of the death fold super family members

Chronologically, the NMR structure of the PYD of ASC, and then the NMR structure of the full-length ASC protein have been resolved [1, 58]. The NMR structures have revealed two opposing surfaces on the PYD, one surface (H1-H4) having a negative and the other (H2-H3) having a positive electrostatic surface potential. These two surfaces were proposed to be responsible for the filaments formed by PYD, when expressed as a truncated protein [58, 59]. Based on structural studies carried out on other members of the death fold super family, three types of interaction modes have been identified. The interac-

tion mode between H1-H4 and H2-H3 is termed as the type I interaction mode [55]. The type II interaction mode is observed between H4, loop H4-H5 on one surface and the loop H5-H6 on the other surface, and the type III interaction mode is observed between H3 on one surface and the loop H1-H2, loop H3-H4 on the other surface [55]. Yet, it has not been reported whether type II and type III interaction modes are present in PYD or CARD of ASC.

1.5.3. Mutational screens carried out on the ASC protein in the literature

In the first mutational screen paper on the ASC protein, the authors cloned the PYD of ASC, fused it to EGFP and overexpressed it in COS-7 cells. In the wild type PYD-EGFP construct expressing cells, PYD filaments were observed, whereas a subset of the mutations generated on the PYD disrupted the filaments [60]. Later, two studies have been published after this thesis project was initiated. In one of these studies, the authors monitored the effect of mutations they have created on PYD of ASC via co-immunoprecipitation and GST pull-down assays [59]. They have identified which residues are responsible for ASC PYD-ASC PYD, ASC-NLRP3 and ASC-POP1 interactions. They have further claimed that PYD filament structures were formed via type I interaction surfaces on H1-H4 and H2-H3. The last mutational screen paper on ASC was focused on CARD, and identified several mutations that inhibited ASC speck formation and inflammasome activation [61].

1.6. Antigen presentation and adjuvant pathways

Adaptive immunity works in cooperation with innate immunity. $CD4^+$ and $CD8^+$ T-lymphocytes (which are responsible for activation of B-cells and elimination of pathogen-invaded or cancerous cells, respectively) do require activation by innate immune cells, such as dendritic cells and macrophages in a process called antigen presentation [62, 63]. All nucleated cells are capable of presenting degradation products of cytosolic proteins by major histocompatibility class I (MHC-I) molecule to $CD8^+$ T-cells. In addition, specialized antigen presenting cells (APC) can process extracellular antigens, load their degrada-

tion products into major histocompatibility class II (MHC-II) molecules and present to $CD4^+$ T-cells. The antigen presentation ability of cells is greatly enhanced by several innate immunity pathways, which include TLR and NLR pathways, and they are collectively called adjuvant pathways [64].

1.6.1. MHC class I and MHC class II mediated antigen presentation pathways

The MHC class I-mediated antigen presentation pathway surveys cytoplasmic antigens, which can be viral, tumoral or self-antigens [62]. Antigenic proteins are processed in the proteasome and transported to the ER via TAP1/TAP2 proteins, where 8-10 amino acids long short peptides form a complex with MHC-I. Antigen-MHC class I complexes are subsequently transported to the plasma membrane via a secretory pathway for recognition by $CD8^+$ T-cells. Extracellular antigens are engulfed and processed via an endosomal/lysosomal pathway in APCs [65]. This type of antigen presentation depends on MHC class II, which is assembled in the ER. In the late endosome/lysosome, MHC class II is loaded with degradation products of extracellular antigens, which are subsequently transported to the plasma membrane for recognition by $CD4^+$ T-cells [66]. The classical paradigm of MHC class I and class II-dependent presentation of cytoplasmic and extracellular antigens, respectively, is complicated by cross-presentation. Briefly, cross-presentation is the presentation of extracellular antigens via MHC class I and cytoplasmic antigens by MHC class II. There are various pathways proposed for the mechanistic details of cross-presentation, and autophagy has been associated with both types of cross-presentation [67].

1.6.2. Particulate adjuvants

Peptide or protein antigens are loaded to nanometer or micrometer-sized particles in order to facilitate their engulfment by APCs in vaccine development studies. The particles used in the delivery and controlled release of antigens are called particulate adjuvants [68]. Various antigen delivery methods are being actively investigated. Immunostimulant complexes, virus-like particles, gold, silica particles, emulsions, liposomes and polymer-based particles are being used for this purpose. The polymer-based particles can be com-

posed of either biodegradable compounds, such as poly(D,L-lactid) (PLA) and poly(D,L,lactic-co-glycolic acid) (PLGA) or non-biodegradable compounds, such as polystyrene. The other examples of polymer-based antigen delivery methods are layer-by-layer capsules, chitosan particles, micro- and nanogels. By increasing its size, these delivery methods facilitate the engulfment of antigen by APCs [69]. Furthermore, particulate vaccines slow down the enzymatic degradation of the antigens either extracellularly or intracellularly following the engulfment, so that the time period in which antigens stay in the environment increases. All of these factors contribute to enhance the capacity of APCs to present antigens to T cells.

1.6.3. The ASC protein and antigen presentation

The inflammasomes are functional in professional antigen presenting cells such as dendritic cells (DCs) and macrophages as well as in other cell types that are frequently in contact with pathogens, such as keratinocytes and neutrophils [70]. Alum, a widely used adjuvant in human vaccines, has been shown to exert its adjuvant activity via stimulation of NLRP3 inflammasome in an ASC-dependent manner [40, 71]. Furthermore, the ASC protein has also been implicated in antigen presentation via inflammasome-independent mechanisms [72-74].

1.7. The ASC specks and aggresome-like structures: Differences and similarities

The ASC specks were initially discovered in HL-60 human leukemia cells upon induction of cell death by treatment with all-trans retinoic acid [54]. Upon treatment, the ASC specks were observed as micrometer-sized perinuclear protein aggregates. Although these structures were initially linked to the apoptosis pathway due to the conserved CARD that is shared between the ASC protein and the apoptotic protein caspase-9, subsequent evidence showed that ASC specks are mainly involved in IL-1β and IL-18 processing and a specific type of cell death, called pyroptosis, which is dependent on caspase-1.

Formation of the ASC specks upon stimulation of NLRP3, NLRC4 and AIM2 inflammasomes with various pathogenic or sterile challenge conditions were reported before [34-38]. Cellular localization, shape and size of the ASC specks resemble aggresome-like structures. The ASC speck is a perinuclear structure, 1-2 μm in diameter, and composed of mostly inflammasome components [36, 54]. It is reported to co-localize with the microtubule organizing center (MTOC) and surrounded by a vimentin cage [75, 76]. Furthermore, it is associated with proteasomes and inhibited by nocodazole treatment [75, 76]. Recently, it has been reported that inflammasome components in the ASC specks are ubiquitinated and subjected to clearance by autophagy [52]. Once ASC speck formation is started, it takes only minutes for all the cytoplasmic and nuclear ASC protein pool to aggregate into a single ASC speck per cell [36, 76]. The aggresome-like structures are thought to arise from defects or capacity overload in the ubiquitin-proteasome protein degradation pathway [77, 78]. The examples of aggresome-like structures include the aggresome, IPOD, JUNQ and DALIS [77-79].

1.7.1. The aggresomes

The aggresome is a clump of misfolded and ubiquitinated proteins near the nucleus, co-localizing with the MTOC [77]. The aggresome is surrounded by a cage of intermediate filament protein vimentin and it is associated with proteasomes [77, 78]. Aggresome formation can be abrogated by the microtubule inhibitor nocodazole [77]. The process of aggresome formation is a slow process which takes hours [80, 81].

1.7.2. IPOD and JUNQ

Insoluble protein deposit (IPOD) consists of non-ubiquitinated proteins, does not attract proteasomes and localizes at the cell periphery whereas juxtanuclear quality control (JUNQ) is a cytoplasmic structure adjacent to the nucleus, composed of ubiquitinated proteins and associated with proteasomes. It was also shown that proteins residing in the JUNQ are misfolded but soluble which can exchange with the cytoplasmic pool whereas

those proteins at IPODs are mostly aggregated and non-diffusing. Neither IPOD nor JUNQ co-localize with the MTOC [78, 82].

Table 1.2. Comparison of the ASC speck with aggresome-like structures.

	ASC speck	**Aggresome**	**IPOD**	**JUNQ**	**DALIS**
Vimentin cage	+	+	-	-	-
Co-localization with MTOC	+	+	-	-	-
Ubiquitination	+	+	-	+	+
Perinuclear localization	+	+	-	+	-
Time required for formation	Minutes	Hours	Hours	Hours	4 h
Stimulation	Inflam-masome activation	Overexpres-sion, proteasome inhibition	Stress condi-tions	Stress conditions	LPS treatment, enhanced by pro-teasome inhibition
Size/Number per cell	microme-ter sized/one per cell	micrometer sized/usually one per cell	microme-ter sized	microme-ter sized	Dynamic, small DALIS can fuse together to form a bigger one.
Inhibition by microtuble depolymeriza-tion	+	+	+	+	-
Association with proteasome	+	+	-	+	+
References	[36, 52, 75, 76]	[77, 81]	[78, 82]	[78, 82]	[83-86]

1.7.3. DALIS

Dendritic cell aggresome-like induced structures (DALIS) are perinucluear cytoplasmic aggregates of ubiquitinated proteins observed in dendritic cells upon stimulation with LPS [79, 87]. After their initial discovery in DCs, DALIS were observed in several different other cell types including macrophages upon exposure to various stress conditions [83, 85, 88]. DALIS are observed 4 h after and cleared 24-36 h after LPS stimulation. DALIS do not co-localize with MTOC nor are they surrounded by vimentin, unlike aggresomes [79]. DALIS formation requires *de novo* protein synthesis [84]. It has been suggested that transient aggregation of ubiquitinated proteins in DCs might be functional in antigen presentation [79]. This suggestion was supported by the observation of the influenza nucleoprotein (NP) co-localizing at DALIS in influenza virus infected DCs [86].

1.7.4. Similarities and differences of aggresome-like structures with the ASC speck

The comperative analysis of the ASC speck with aggresome-like structures is given in Table 1.2.

2. PURPOSE

The first purpose of this thesis project is to gain insight into the nature of the ASC speck and to determine whether it is an organized structure and if so, obtain as much information as possible about its structural details. To achieve this goal, we carried out two overlapping sets of mutational screens, first on the full length ASC and the second on the isolated domains, pyrin domain (PYD) and caspase recruitment domain (CARD). We have designed experiments to understand how monomeric ASC proteins ultimately form the ASC speck and identify different levels of compaction. Specificity of PYD-PYD and CARD-CARD interactions as well as involvement of alternative interaction modes other than type I for the PYD were investigated.

The second purpose is to understand whether aggresome-like properties of the ASC speck are instrumental biologically. We observed co-aggregation of a set of cytoplasmic proteins on the ASC speck, which might be important in antigen presentation. Shared properties of co-aggregating and non-aggregating proteins (hydrophobicity, ubiquitination) were investigated. We propose three different routes where co-aggregation might be important in antigen presentation. Experimental evidence on the extracellular route involving release of ASC speck upon pyroptosis and subsequent uptake by other cell was obtained.

3. MATERIALS

3.1. Cell Lines

Table 3.1. Cell lines used in this study.

	Catalog number	Main Source	Provider
HEK293(F)T	R700-07	Invitrogen, USA	Kindly provided by Prof. Maria Soengas
THP-1	ATCC TIB-202	ATCC, USA	Kindly provided by Prof. Ahmet Gül

3.2. Chemicals, Plastic and Glassware

Chemicals were purchased from either Sigma-Aldrich (USA), Merck (Germany) or AppliChem (Germany), plasticware from TPP (Switzerland) for cell culture, tips, and tubes from Axygen (USA). All glassware, tips, and tubes were autoclaved at 121^{o}C for 20 minutes for sterilization prior to use.

3.3. Buffers and Solutions

3.3.1. Cell Culture

Table 3.2. Solutions and media used in cell culture.

0.5% Trypsin-EDTA 10X	Gibco Invitrogen, USA
DMSO	AppliChem, Germany

Table 3.2. Solutions and media used in cell culture (cont.).

Dulbecco's Modified Eagle Medium (DMEM)	Gibco Invitrogen, USA
Fetal Bovine Serum (FBS)	Gibco Invitrogen, USA
MEM Non-essential amino acid (NEAA) 100X	Gibco Invitrogen, USA
Penicillin/Streptomycin 100X (5000 u Penicillin + 5000 µg Streptomycin per ml)	Gibco Invitrogen, USA

Table 3.3. Buffers used in cell culture.

Freezing Medium	20% FBS 1X Pen/Strep 100 µM MEM-NEAA 7.5% DMSO
PBS 10X	80 gr NaCl 2 gr KCl 2.4 gr KH_2PO_4 14.4 gr Na_2HPO_4 Add ddH_2O upto 1 lt (pH 7.2)

3.3.2. Cloning and Analytic Digestion

Table 3.4. Enzymes used for cloning.

Restriction Enzymes (NheI, XhoI, EcoRI, HindIII, BglII, NotI)	NEB, USA
T4 DNA Ligase	NEB, USA
High fidelity polymerase (Phusion)	NEB, USA

3.3.3. Agarose Gel Electrophoresis

Table 3.5. Buffers and solutions used for agarose gel electrophoresis.

50X Tris Acetic acid EDTA (TAE)	2 M Tris-acetate 50 mM EDTA pH 8.5
DNA Ladder	DNA Ladder Mix Fermentas, USA
Ethidium Bromide (EtBr)	Merck, USA
Loading Dye	6x Loading Dye Fermentas, USA

Table 3.6. Solutions for liquid and solid bacterial culture.

LB Agar (Solid culture, autoclaved)	1 L LB medium, 15 g Agar
LB Medium (1 L) (Liquid culture, autoclaved)	10 g Tryptone 5 g Yeast Extract, 5 g NaCl
Ampicillin (1000X = 100 mg/ml in 70% EtOH)	AppliChem, Germany
Kanamycin (1000X = 50 mg/ml in ddH20)	Sigma-Aldrich, USA

3.3.4. Transfection of human HEK293T cells via calcium phosphate method.

Table 3.7. Buffers and solutions used in transfection.

2X HBS Buffer	50 mM HEPES pH 7.0 280 mM NaCl, 1.5 mM Na_2HPO_4
Chloroquine	AppliChem, Germany
HEPES	Gibco Invitrogen, USA

3.3.5. Western blotting

Table 3.8. Chemicals for western blotting.

Lumi-Light Western Blotting Substrate	Roche, Switzerland
SDS	AppliChem, Germany
TWEEN	CalbioChem, Canada
Protein Ladders	PageRuler Prestained (SM0671) Fermentas, USA PageRuler Prestained (26616) Thermo, USA

Table 3.9. Recipes for western blotting.

Acrylamide:Bisacrylamide	29.2 gr Acrylamide 0.8 gr bisacryalmide in 100 ml
Ammonium Persulfate	10% APS (w/v)
Blocking Solution	5% BSA in TBS-T
Coomassie Blue Staining Solution	0.1% Coomassie Blue 10% Acetic acid 50% Methanol in ddH_2O
Coomassie Blue Destaining Solution	10% Acetic acid 40% Methanol in ddH_2O
Lysis buffer for sonication	1X PBS including 2mM EDTA+ protease inhibitor cocktail
15% Resolving Gel Stock	50 ml 30% Acrylamide 1 ml 10% SDS 20 ml 1.875M Tris 8.8, 29 ml ddH_2O

Table 3.9. Recipes for western blotting (cont.).

15% Resolving mini gel	4 ml 15% Resolving gel 40 µl 10% APS 4 µl TEMED
Running Buffer	1X Tris-Glycine buffer 0.1% SDS
6X Laemmli Sample Buffer	1.2 gr SDS 0.9 gr DTT 6 mg BPB 4.7 ml Glycerol 1.2 ml Tris 0.5M (pH 6.8) 2.1 ml ddH_2O
4% Stacking Gel Stock	3.3 ml 30% Acrylamide 250 µl 10% SDS 6.3 ml 0.5 M Tris (pH 6.8) 15 ml ddH_2O
4% Stacking gel	1 ml 4% Stacking gel 10 µl 10% APS 1 µl TEMED
10X TBS	90 gr NaCl 121.14 gr Tris base
TBS-TWEEN	1X TBS 0.1% TWEEN 20
10X Tris-Glycine Buffer	15 gr Tris-Base 72 gr Glycine in 0.5 L ddH_2O

3.4. Kits

Table 3.10. Kits used in this study.

High Pure PCR Purification Kit	Roche, Switzerland
High Pure Plasmid Isolation Kit	Roche, Switzerland
Genopure Plasmid Midi & Maxi Kits	Roche, Switzerland

3.5. Equipment

Table 3.11. Equipments used in this study.

Agarose Gel Electrophoresis	Thermo Scientific, USA
Agarose Imaging	Gel Doc XR System, Bio Rad, USA
Autoclaves	MAC 601, Eyela, Japan
	ASB260T, Astell, UK
Centrifuges	Allegra X22-R, Beckman, USA
	Himac CT4200C, Hitachi Koki, Japan
	J2-MC Centrifuge, Beckman, USA
	J2-21 Centrifuge, Beckman, USA
Freezers	2021D, Arçelik, Turkey
	4250T, Arçelik, Turkey
Incubator	Hepa ClassII Forma Series, Thermo, USA
Heat Block	VWR, USA
Laminar Flow Cabinets	Class II A, Tezsan, Turkey
	Class II B, Tezsan, Turkey
Magnetic Stirrer	Yellowline MSH Basic, USA
Microscopes	Zeiss, Axio Observer, Germany
	Z1 Inverted Mic., USA
	Leica, TCSSP5II, Germany
	Nikon, Eclipse TS100, Japan
Microwave oven	Arçelik, Turkey
pH meter	H221, Hanna Instr., USA
Pipettes	Gilson, USA
Plate reader	VersaMax, Molecular Devices, USA
Sonicator	Sonoplus, Bandelin, Germany
Spectrofluorometer	Cary Eclipse, Agilent Technologies, USA
Pipettors	Greiner-bio one, UK
	RatioLab acupetta, Germany
Power Supplies	EC135-90, Thermo Electron Corp
	Power Pac Universal, BIO-RAD, USA
Western blot visualization	Stella, Raytest, Germany
Scales	Precisa XT4200C, Germany

Table 3.11. Equipments used in this study (cont).

SDS-PAGE Electrophoresis System	Mini-PROTEAN 4Cell, BIO-RAD, USA
SDS-PAGE Transfer System	Mini Trans-Blot® Electrophoretic Transfer Cell BIO-RAD, USA
Shakers	Polymax 1010 , USA
	Polymax 1040 , USA
	Heildophl, Germany
Spectrophotometer	Nanodrop ND-100 , Thermo, USA
Vortex	Fisons Whirli Mixer, UK
	GmcLab, Gilson, USA
Water Bath	GFL, Germany
	Memmert, Germany
Water filter	UTES, Turkey

3.6. Fine Chemicals

3.6.1. Antibodies

Table 3.12. Antibodies used in this study.

anti-FLAG	2368S, CST, USA
anti-ASC (monoclonal)	Kindly provided by Prof. Masumoto, Japan
anti-ASC (polyclonal)	AKIL, Turkey
anti-Caspase-1	sc-515, Santa Cruz
anti-EGFP	Vatoz, Turkey
anti-mCherry	Kindly provided by Assoc. Prof. Çelik, Turkey
anti-Rabbit IgG, HRP	7074S, CST, USA
anti-Mouse IgG, HRP	7076S, CST, USA

3.6.2. Plasmids

Table 3.13. Plasmids cloned for this project.

pEGFP-C3-hASC WT	pEGFP-PYD WT
pEGFP-C3-shortASC	pEGFP-PYD E13A
pEGFP-C3-hASC E13A	pEGFP-PYD E19A
pEGFP-C3-hASC E19A	pEGFP-PYD K21A
pEGFP-C3-hASC K21A	pEGFP-PYD L25A
pEGFP-C3-hASC L25A	pEGFP-PYD K26A
pEGFP-C3-hASC L25M	pEGFP-PYD R41A
pEGFP-C3-hASC K26A	pEGFP-PYD D48A
pEGFP-C3-hASC R41A	pEGFP-PYD D51A
pEGFP-C3-hASC D48A	pEGFP-PYD E62A
pEGFP-C3-hASC D51A	pEGFP-PYD E67A
pEGFP-C3-hASC E62A	pEGFP-PYD L68A
pEGFP-C3-hASC G65A	pEGFP-PYD L73A
pEGFP-C3-hASC E67A	pEGFP-peptide_1
pEGFP-C3-hASC L68A	pEGFP-peptide_2
pEGFP-C3-hASC L73A	pEGFP-peptide_3
pEGFP-C3-hASC R74A	pEGFP-peptide_1_19aa
pEGFP-C3-hASC H90A	pEGFP-peptide_1_12aa
pEGFP-C3-hASC G101A	pEGFP-peptide_1_8aa
pEGFP-C3-hASC P103A	pEGFP-hydrophobic_1
pEGFP-C3-hASC H113A	pEGFP-hydrophobic_2
pEGFP-C3-hASC M159A	pEGFP-hydrophilic_1
pEGFP-C3-hASC R160A	pEGFP-hydrophilic_2
pEGFP-C3-hASC C173A	pmCherry
pEGFP-C3-hASC L181A	pmCherry-C3.1
pEGFP-C3-hASC R182A	pmCherry-C3-hASC
pEGFP-C3-hASC K26A-R160	pmCherry-C3-shortASC
pEGFP-C3-hASC L68A-R160	pmCherry-C3-CARD
pLenti-Ef1a-EGFP-hASC	pmCherry-C3-UBB
pFliC-C3-hASC	pEYFP-C1-CytOVA
pEGFP alone	pmCherry alone

Table 3.14. Other plasmids used in the project.

pEGFP-C3	Clontech, USA
pEYFP-N1	Clontech, USA
pcDNA3-hASC	Nunez Lab, University of Michigan, USA
pcDNA3-procaspase-1	Nunez Lab, University of Michigan, USA
pcDNA3-NLRP3-FLAG	Nunez Lab, University of Michigan, USA
pCGN-HA-Ubiquitin	Nunez Lab, University of Michigan, USA
pCMVdeltaR8.74	Deisseroth Lab, Stanford University, USA
pMD2.G	Deisseroth Lab, Stanford University, USA
pLenti-EF1a-hChR2(H134R)-EYFP-WPRE	Deisseroth Lab, Stanford University, USA
pCI-neo-sOVA	Addgene, USA

3.6.3. Primers

Table 3.15. Oligonucleotides used for oligo-annealing procedure.

Peptide_1_19aa_BglII_F	gatcttgtcgcccttattccctttttgcggcattttgccttcctgtttttg
Peptide_1_19aa_EcoRI_R	aattcaaaaaacaggaaggcaaaatgccgcaaaaaagggaataagggcgacaa
Peptide_1_12aa_BglII_F	gatcttgcggcattttgccttcctgtttttg
Peptide_1_12aa_EcoRI_R	aattcaaaaaacaggaaggcaaaatgccgcaa
Peptide_1_8_BglII_F	gatcttcttcctgtttttg
Peptide_1_8_EcoRI_R	aattcaaaaaacaggaagaa
Hydrophobic_1_BglII_F	gatcttatcgtgctgctggtgttcttcctgttcgtgctgttcatcatcatctg
Hydrophobic_1_EcoRI_R	aattcagatgatgatgaacagcacgaacaggaagaacaccagcagcacgataa
Hydrophobic_2_BglII_F	gatcttctgtttatcctgttcgtgattgtgattgtgttcatcttcctgctgtg
Hydrophobic_2_EcoRI_R	aattcacagcaggaagatgaacacaatcacaatcacgaacaggataaacagaa
Hydrophilic_1_BglII_F	gatcttaagaacaacgagagaaaggacaaggacgacgagaacagagagaggtg
Hydrophilic_1_EcoRI_R	aattcacctctctctgttctcgtcgtccttgtcctttctctcgttgttcttaa
Hydrophilic_2_BglII_F	gatcttagagacaacaacagaaaggacaaggaggaggaggaggacaacaggtg
Hydrophilic_2_EcoRI_R	aattcacctgttgtcctcctcctccttgtcctttctgttgttgtctctaa

Table 3.16. Primers used in the study.

Primer Name	Sequence
ASC_E13A_F	gatgcgctggccaacctgaccgccgaggagctc
ASC_E13A_R	ggtcaggttggccagcgcatccaggatggcgtc
ASC_E19_F	accgccgaggccctcaagaagttcaagctgaagc
ASC_E19_R	cttcttgagggcctcggcggtcaggttctcc
ASC_K21A_F	gaggagctcgccaagttcaagctgaagctgctgtc
ASC_K21A_R	gcttgaacttggcgagctcctcggcggtcagg
ASC_L25A_F	gaagttcaaggccaagctgctgtcggtgccgctg
ASC_L25A_R	cagcagcttggccttgaacttcttgagctcctc
ASC_L25M_F	gaagttcaagatgaagctgctgtcggtgccgctg
ASC_L25M_R	cagcagcttcatcttgaacttcttgagctcctc
ASC_K26A_F	aagctggccctgctgtcggtgccgctgcgcgag
ASC_K26A_R	ccgacagcagggccagcttgaacttcttgagc
ASC_R41A_F	cgcatcccggccggcgcgctgctgtccatgg
ASC_R41A_R	agcgcgccggccgggatgcgcccgtagcc
ASC_D48A_F	ctgtccatggccgccttggacctcaccgacaag
ASC_D48A_R	gtccaaggcggccatggacagcagcgcgcc
ASC_D51A_F	gacgccttggccctcaccgacaagctggtcagc
ASC_D51A_R	tcggtgagggccaaggcgtccatggacagcag
ASC_E62A_F	gcttctacctggccacctacggcgccgagctcac
ASC_E62A_R	gccgtaggtggccaggtagaagctgaccagcttg
ASC_G65A_F	gagacctacgccgccgagctcaccgctaac
ASC_G65A_R	agctcggcggcgtaggtctccaggtagaag
ASC_E67A_F	ctacggcgccgccctcaccgctaacgtgctgcg
ASC_E67A_R	gcggtgagggcggcgccgtaggtctccagg
ASC_L68A_F	cgccgaggccaccgctaacgtgctgcgc
ASC_L68A_R	gttagcggtggcctcggcgccgtaggtctc
ASC_L73A_F	gctaacgtggctcgcgacatgggcctgcag
ASC_L73A_R	tgtcgcgagccacgttagcggtgagctc
ASC_R74A_F	cgtgctggctgacatgggcctgcaggag
ASC_R74A_R	gcccatgtcagccagcacgttagcggtgagc
ASC_H90A_F	gccacggcccagggctctggagcc
ASC_H90A_R	gagccctgggccgtggccgcctgcagctg
ASC_G101A_F	gggatcgccgcccctcctcagtcggcagcc
ASC_G101A_R	gaggaggggcggcgatcccagctggcgcggctcc
ASC_P103A_F	caggccgcccctcagtcggcagccaagcc
ASC_P103A_R	cgactgaggggcggcctggatcccagctggc
ASC_H113A_F	gcctggcctttatagaccagcaccgggct

Table 3.16. Primers used in the study (cont.).

ASC_H113A_R	gctggtctataaaggccaggcctggcttggctgc
ASC_M159A_F	caagcaaggcccggaagctcttcagtttcacacc
ASC_M159A_R	aagagcttccgggccttgcttgggttggtgggct
ASC_R160A_F	aagcaagatggccaagctcttcagtttcacaccagc
ASC_R160A_R	ctgaagagcttggccatcttgcttgggttggtgg
ASC_C173A_F	aactggaccgccaaggacttgctcctccagg
ASC_C173A_R	aagtccttggcggtccagttccaggctg
ASC_L181A_F	tccaggccgccagggagtcccagtcctacc
ASC_L181A_R	ggactccctggcggcctggaggagcaagt
ASC_R182A_F	aggccctagccgagtcccagtcctacctggtg
ASC_R182A_R	ctgggactcggctagggcctggaggagcaagt
BglII_Ova_R	ataagatctgagtaaggggaaacacatctgccaaag
CARD_Hind_F	tccaagcttggcctgcactttatagaccag
CMV-F	cgcaaatgggcggtaggcgtg
EcoRI_EGFP_stop_R	tgaattcacttgtacagctcgtccatgc
EcoRI_NotI_Ubb_R	atagaattcgcggccgcttaaccacctctcagacgcagg
Ef1a_F	atggagtttccccacactgag
EGFP-CF	agcacccagtccgccctgagc
FliC_BglII_R	tatagatctgaacgcagtaaagagaggacgttttg
FliC_NheI_F	atgctagcaccatggcacaagtcattaatacaaac
HindIII_Ubb_F	ttaaagcttatgcagattttcgtgaaaacccttac
NheI_Kozak_CytOVA_F	atagctagcaccatgagcaccaggacacagataaataag
NheI_mCherry_F	gctagcaccatggtgtctaagggcgaaga
Peptide_1_BglII_F	ataagatcttatgagtattcaacatttccgtgtc
Peptide_1_EcoRI_R	tgaattcaaaaaacaggaaggcaaaatgcc
Peptide_2_BglII_F	tctagatcttgctcacccagaaacgctggtg
Peptide_2_EcoRI_R	tgaattcagtaacccactcgtgcacccaac
Peptide_3_BglII_F	ataagatcttatcgaactggatctcaacagcg
Peptide_3_EcoRI_R	tgaattcacattggaaaacgttcttcgg
PYD_EcoRI_R	tgaattcctggtgcgtggccgcctg
shortASC_F	accagggcctgcactttatagaccag
shortASC_R	ctataaagtgcaggccctggtgcgtggccg
SV40-pArev	cctctacaaatgtggtatgg
WPRE_R	agaataccagtcaatctttcac
XhoI_mCherry_R	ctcgagtttcttgtacagctcgtccat

4. METHODS

4.1. Molecular Cloning

4.1.1. Plasmid DNA isolation

Plasmid DNA isolation was conducted according to manufacturer's instructions (Table 3.15). 8 ml of bacterial liquid culture for mini-scale, 200 ml liquid culture for midi-scale and 500 ml liquid culture for maxi-scale DNA isolation were used. In mini-scale DNA isolation, DNA was eluted from the mini-spin column using 50 ul EB. For midi and maxi-scale DNA isolations, DNA was resuspended in 1 ml ddH_20.

4.1.2. High-fidelity PCR reaction

DNA fragments to be cloned into plasmid vectors were amplified using the proof reading polymerase (Phusion® High-Fidelity DNA Polymerase, NEB, USA). PCR reactions were carried out according to manufacturer's instructions. The protocol is summarized in Table 4.1.

Table 4.1. PCR protocol using the Phusion polymerase.

Step #no	Description	Temperature (°C)	Duration
1	Initial denaturation	98	30 s
2	Denaturation	98	5 s
3	Annealing	Primer specific T_m	30 s
4	Elongation	72	20 s per 1 kb
5	Return to step 2 (32x)		
6	Final elongation	72	5 min

4.1.3. Restriction enzyme digestion of plasmids and PCR products

Plasmid DNA or purified PCR products were digested with suitable restriction enzymes for molecular cloning purposes. Restriction enzymes from NEB (USA) were preferred and digestion reactions were carried out according to manufacturer's instructions using the appropriate digestion buffers and temperatures, specific for each restriction enzyme.

4.1.4. Agarose gel electrophoresis

DNA fragments were run on agarose gels for diagnostic purposes and agarose gel extraction procedure. For routine applications, 1% agarose gel was employed. In order to differentiate large DNA fragments between 5-10 kb, low percent agarose gels (0.7%); for small DNA fragments (50-200 bp), high percent agarose gels (2%) were used. 400 ml of 1% agarose gel stock solution was prepared from 4 g agarose resuspended in 400 ml of 1X TAE buffer. The stock solution was boiled in a microwave until the agarose was completely dissolved. For one mini-agarose gel, around 50 ml of stock solution was mixed with 3 µl of EtBr under fume hood. The rest of the stock solution was kept in 65 °C oven until later use. DNA samples were run in 1X TAE buffer containing gel electrophoresis tanks. Orange G was used in all experiments as the loading dye.

4.1.5. PCR purification and agarose gel extraction

PCR products and restriction enzyme digested DNA fragments were purified with spin columns using the PCR purification kit according to manufacturer's instructions (High Pure PCR Purification Kit, Roche, Switzerland), when the PCR products or the digested DNA fragments were composed of one type of DNA fragment. Primer dimers or other small DNA fragments smaller than 100 bp do not efficiently bind to spin columns, so that DNA fragment of interest can be purified from small DNA fragments using PCR purification method. In other cases, where there are several DNA fragments larger than 100 bp, the

DNA sample was run on agarose gel and the DNA fragment of interest was cut using a razor under UV light. The DNA was extracted using the agarose gel extraction protocol according to manufacturer's instructions (High Pure PCR Purification Kit, Roche, Switzerland).

4.1.6. Oligo-annealing

In order to clone short DNA fragments (less than 100bp) into plasmid vectors, 2 complementary oligonucleotides were designed so that upon annealing of oligonucleotides to each other, the desired sticky restriction enzyme cutting sites were formed, without the need of actually cutting the DNA fragment. To anneal oligonucleotides, 1 µl of each oligonucleotide (100 pmole/µl) was mixed with 1 µl of 10X ligation buffer and 7 µl of ddH_20. The annealing reaction was incubated at 95 °C for 5 minutes and gradually cooled to room temperature in 1 hour using a PCR machine.

4.1.7. Ligation of DNA fragments

Restriction enzyme digested plasmid vectors and inserts were ligated using T4 polymerase (NEB, USA). In all ligation reactions, vector and insert concentrations were adjusted in a way that 1:5 (vector : insert) ratio was established. In each ligation reaction 10-30 ng of vector and corresponding amount of insert DNA were added, without exceeding the threshold of 100 ng (vector+insert) per 10 µl ligation reaction.

For example, in order to ligate 4000 bp vector and 1000bp insert, 20 ng of vector and (20 X 5) / 4 = 25ng of insert were added to ligation reaction. 1 µl of 10X ligation buffer and 0.5 µl T4 ligase were added and reaction was added up to 10 µl using ddH_20. The ligation reaction was incubated at 4 °C overnight. It is important to aliquot 10X ligation buffer for single use only since repeated freeze-thawing destroys ATP which decreases ligation efficiency.

4.1.8. Transformation of plasmids into competent bacteria strains

The ligated DNA fragments or plasmids were transformed into competent bacterial strains. For molecular cloning and re-transformation purposes, Top10 strain of *E. Coli* was used. Top10 strain does produce enzymes that methylate plasmid DNA. In order to obtain dam or dcm methylation free plasmid DNA, the plasmids were transformed into SCS110 strain when necessary.

Half of the ligation reactions or 1-2 ng of plasmid to be re-transformed were added on top of the Top10 strain competent cell aliquots. Efficiency of re-transformation into SCS110 competent cells is very low and it requires around 5-10 µg of plasmid DNA for re-transformation. Competent cells + DNA were incubated on ice for 20 minutes and then incubated at 42 °C for 45 s in water bath (heat shock). 100 µl of antibiotic-free LB was added on competent cells and incubated at 37 °C at rocking agitation (recovery). Finally, cells were plated on pre-warmed LB-agar plates including suitable antibiotics and incubated at 37 °C for 16 h.

4.1.9. Colony PCR

16 h after ligation products were transformed into competent cells, colony PCR procedure were executed to screen for positive colonies. Briefly, 20 µl of ddH_20 was aliquoted into 8-strip PCR tubes. One backup plate with suitable antibiotics was marked with grids and numbered. With sterile micropipette tips, colonies were sampled, then touched to backup plate and then into PCR tubes. Bacterial samples in ddH_20 were incubated at 95 °C for 15 minutes (lysis). Then, PCR mixtures were added on top (Table 4.2) and the PCR reaction was executed (Table 4.3). Primer pairs used in colony PCR reaction were chosen in a way that the size of the resulting band can be differentiated from negative colonies (empty vector plasmid containing). Ideally, one of the primers anneals to the vector and the second primer anneals to the insert so that only the recombinant, newly synthesized constuct is able to give the correct band.

Table 4.2. PCR mixture for the colony PCR reaction.

Reagent	Initial concentration	Volume (µl)
Buffer	10X	3
$MgCl_2$	50mM	1.05
dNTP	10mM	0.6
Forward primer	10 pmole/µl	1.5
Reverse primer	10 pmole/µl	1.5
Template		+
Taq		1
ddH_20		20 + 1.35
Total		30

Table 4.3. PCR protocol for the colony PCR reaction.

Step #no	Description	Temperature (°C)	Duration
1	Initial denaturation	95	30 s
2	Denaturation	95	5 s
3	Annealing	Primer specific Tm	30 s
4	Elongation	72	60 s per 1 kb
5	Return to step 2 (32x)		
6	Final elongation	72	5 min

4.1.10. Analytic digestion (Diagnostic digestion)

Positive colonies identified with the colony PCR procedure were screened via analytical digestion reactions. Briefly, positive colonies were picked with a sterile tip from the backup plate and put into LB with the suitable antibiotics (liquid bacterial culture). Bacteria were grown at 37 °C for 16 h with rocking agitation. Mini-scale DNA isolation was executed as in Section 4.1.1. Subsequently, isolated plasmid DNA was digested as in 4.1.3 using a restriction enzyme pair that gives rise to a pattern that can be distinguished from negative colonies (empty vector plasmid containing).

4.1.11. Sequencing of plasmid constructs

Each construct used in this study was checked using Sanger sequencing. Sequencing service was purchased from Macrogen Inc, Korea.

4.2. Cloning strategies

4.2.1. pEGFP-C3-hASC plasmid

In order to create a plasmid encoding a fusion protein of EGFP and ASC, cDNA of ASC was obtained by digesting pcDNA3-ASC plasmid with HindIII and EcoRI restriction enzymes. The empty vector pEGFP-C3 which encodes cDNA of EGFP and a C-terminal multiple cloning site, was digested with the same restriction enzyme pair. Vector and insert fragments were purified as in Section 4.1.5 and ligated as in Section 4.1.7. Colonies were screened via colony PCR using the GFP_F and SV40_pA_R primer pair as in Section 4.1.9. Positive colonies were further analyzed using diagnostic digestion using the BamHI enzyme as in Section 4.1.10. Colonies were further checked using Sanger sequencing using CMV_F and SV40_pA_R primers.

4.2.2. Site-directed mutations on pEGFP-C3-ASC construct

The desired mutations were introduced in pEGFP-C3-ASC plasmid using a PCR based site-directed mutation approach. Briefly, mutations were introduced on complementary primer pairs, annotated as ASC_mutation_F and ASC_mutation_R in Figure 4.1. In the first step of PCR, EGFP_F and ASC_mutation_R primer pair were used to amplifiy the left fragment of ASC and thereby introducing the mutation at the 3’ end. Simultaneously, in another tube ASC_mutation_F and SV40_pA_R were used to amplify the right framgent of ASC, introducing a mutation at the 5’ end. The left and right fragments were purified from the gel, mixed in an equal molar ratio and used as a template in the second step. 3’ and 5’ ends of the left and right fragments do share around 20-25 base pairs of identical

sequences, respectively. For this reason, when EGFP_F and SV40_pA_R primers were added into the PCR reaction, the left and right fragments annealed from their 3' and 5' ends respectively, and an overlapping DNA fragment encoding the mutated ASC cDNA was synthesized. The PCR product was purified using spin columns, then digested using HindIII and EcoRI enzmyes, and the desired fragment was extracted from the gel. The insert encoding cDNA of mutant ASC was ligated into pEGFP-C3 vector as in Section 4.2.1

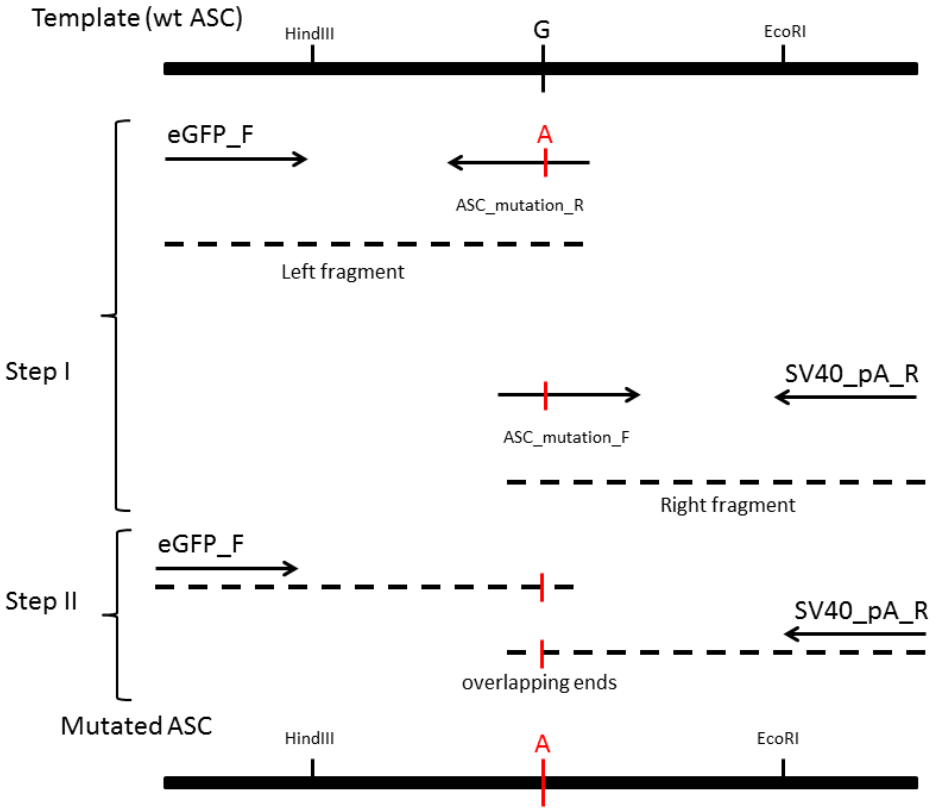

Figure 4.1. Site-directed mutagenesis strategy to clone EGFP-ASC mutants.

Primers used for site-directed mutagenesis of ASC were listed in Table 3.14. Double mutation carrying pEGFP-ASC constructs (K26A-R160A and L68A-R160A) were cloned sequentially, using pEGFP-ASC R160A as a template in the mutagenesis procedure. All constructs were checked by Sanger sequencing in order to verify the presence of desired site-directed mutations and absence of unexpected mutatations.

4.2.3. pEGFP-PYD plasmid

A fusion protein of only the PYD of ASC (amino acids between 1-90) and EGFP at its N-terminal was cloned. For this cloning, PYD encoding DNA was amplified via PCR using the EGFP-CF and PYD_EcoRI_R primer pair and pEGFP-C3-hASC as a template. The resulting band was cloned into the pEGFP-C3 vector between HindIII and EcoRI sites as described in Section 4.1.

4.2.4. pEGFP-PYD mutant constructs

In total, 12 EGFP-PYD mutant encoding plasmids (E13A, E19A, K21A, L25A, K26A, R41A, D48A, D51A, E62A, E67A, L68A, L73A) were cloned as described in Section 4.2.3 using pEGFP-C3-hASC mutant plasmids as templates.

4.2.5. pEGFP-C3-shortASC

The short isoform of ASC (shortASC) encoding DNA fragment was obtained using overlap PCR as in Section 4.2.2. Briefly, an overlapping primer pair (shortASC_F and shortASC_R) pointing at inverse directions as described in Figure 4.1 was designed so that at the end of the two step overlap PCR procedure, the resulting DNA fragment encoded cDNA of short isoform of the ASC.

4.2.6. pmCherry-C3.1

For mCherry labeled fusion proteins, firstly an empty vector with mCherry followed by a multiple cloning site was cloned. This empty vector is referred as pmCherry-C3.1. pmCherry-C3.1 vector was cloned via PCR amplification of mCherry encoding DNA with the NheI_mCherry_F and XhoI_mCherry _R primer pair using pcDNA3 IFP 1.4 plasmid as a template. The resulting band was digested with NheI and XhoI enzymes

and swapped with the EGFP coding sequence (CDS) in the pEGFP-C3 plasmid. The resulting plasmid, pmCherry-C3.1 has the same MCS as the pEGFP-C3 plasmid except for the BglII cutting site.

4.2.7. pmCherry-C3-hASC

A fusion protein of mCherry and ASC encoding plasmid was cloned by digesting hASC encoding fragment from the pcDNA3-hASC plasmid using HindIII and EcoRI restriction enzymes and cloning into the MCS of pmCherry-C3.1 as described in Section 4.1.

4.2.8. pmCherry-C3-shortASC

A fusion protein of mCherry and short isoform of ASC encoding plasmid was cloned by digesting out shortASC encoding fragment from the pEGFP-C3-shortASC plasmid using HindIII and EcoRI restriction enzymes and cloning into the MCS of pmCherry-C3.1 as described in Section 4.1.

4.2.9. pmCherry-C3-CARD

A fusion protein of mCherry and CARD of ASC (amino acids between 111-195) encoding plasmid was cloned. For this purpose, CARD was amplified via PCR using the CARD_Hind_F and SV40-pArev primer pair and pEGFP-C3-hASC as a template. The resulting band was digested using HindIII and EcoRI enzymes and cloned to pmCherry-C3.1 vector as described in Section 4.1.

4.2.10. pmCherry-UBB

A fusion protein of mCherry and 1X UBB (human ubiquitin B) encoding plasmid was cloned. For this purpose, 1X UBB was amplified with PCR using HindIII_Ubb_F and

EcoRI_NotI_Ubb_R primer pair and pCGN-HA-Ubiquitin plasmid as a template. The resulting band was digested using HindIII and EcoRI enzymes and cloned into pmCherry-C3.1 plasmid as in Section 4.1.

4.2.11. pEYFP-N1-CytOVA

A fusion protein of cytoplasmic ovalbumin (CytOVA) and EYFP protein was cloned. For this cloning, the secretion signal sequence (first 48 amino acids) of ovalbumin was deleted during the PCR reaction. The CytOVA was amplified via PCR using the NheI_Kozak_CytOVA_F and BglII_Ova_R primer pair and pCI-neo-sOVA plasmid as a template.

4.2.12. pFliC-C3-hASC

A fusion protein of flagellin and ASC protein was created. For this purpose, flagellin encoding gene (FliC) was amplified from the genomic DNA of *S. typhimurium* using the FliC _NheI_F and FliC _BglII_R primer pair. The resulting band was digested using NheI and BglII enzymes and cloned into pEGFP-C3-hASC vector to replace EGFP as described in Section 4.1. *S. typhimurium* was purchased from Refik Saydam Culture Collection (Ankara, Turkey).

4.2.13. pEGFP-peptide_1, pEGFP-peptide_2, pEGFP-peptide_3

26 amino acids long short peptides from the ampicillin resistance gene peptide_1, peptide_2 and peptide_3 were cloned to the C-terminus of EGFP. For these clonings; the BglII_peptide_1_F and EcoRI_peptide_1_R, BglII_peptide_2_F and EcoRI_peptide_2_R, and BglII_peptide_3_F and EcoRI_peptide_3_R primer pairs were used to amplify peptide_1, peptide_2 and peptide_3, respectively. Resulting bands were digested using BglII and EcoRI and cloned into pEGFP-C3 vector as described in Section 4.1.

4.2.14. pEGFP-peptide_1_19aa, pEGFP-peptide_1_12aa, pEGFP-peptide_1_8aa, pEGFP-hydrophobic_1, pEGFP-hydrophobic_2, pEGFP-hydrophilic_1, pEGFP-hydrophilic_2, pEGFP-C3_19aa

EGFP protein CDS was fused with a series of short peptide CDS; peptide_1_19aa, peptide_1_12aa, peptide_1_8aa, hydrophobic_1, hydrophobic_2, hydrophilic_1 and hydrophilic_2. For these clonings, oligonucleotides listed in Table 3.13 were subjected to oligo-annealing procedure as described in Section 4.1.6. The resulting oligos were cloned into pEGFP-C3 vector as described in Section 4.1. A shorter version of C3 peptide was cloned by BglII and EcoRI digestion of pEGFP-C3 and re-ligation on itself.

4.2.15. pLenti-Ef1a-EGFP-hASC plasmid

The lentiviral construct encoding the EGFP-ASC fusion protein was cloned into pLenti-Ef1a backbone. For this purpose, a modified version of the pLenti-Ef1a vector with a MCS with ClaI, NheI, HindIII, XbaI, EcoRI, NotI, EcoRV, NdeI cutting sites was cloned via oligo annealing as described in Section 4.1.6. The plasmid backbone was originally derived from the pLenti-EF1a-hChR2(H134R)-EYFP-WPRE plasmid. EGFP-ASC encoding DNA was digested out from pEGFP-C3-hASC plasmid using NheI-NotI enzymes and cloned into pLenti-Ef1a vector as described in Section 4.1. Positive colonies were screened via colony PCR using the Ef1a_F and WPRE_R primers.

4.2.16. pEGFP alone and pmCherry alone plasmids

pEGFP alone plasmids has the same vector backbone as pEGFP-C3 but lacks the short peptide encoded by the MCS. The plasmid was cloned by amplifying CDS of EGFP with CMV-F and EcoRI_EGFP_stop_R primer pair and pEGFP-C3 as a template. The PCR product was digested with NheI and EcoRI enzymes and cloned to pEGFP-C3 backbone between same restriction enzyme cutting sites. Similarly, pmCherry alone plasmid was obtained by amplifying CDS of mCherry from the pmCherry-C3 plasmid using CMV-

F and EcoRI_EGFP_stop_R primer pair. The PCR product was digested similarly with NheI and EcoRI enzymes and cloned to pEGFP-C3 backbone between same restriction enzyme cutting sites as in Section 4.1.

4.2.17. pETM20-mCherry plasmid

CDS of mCherry was cloned into pETM-20 vector for bacterial expression. Briefly, CDS of mCherry was obtained from the pmCherry plasmid by NcoI and BamHI (partial digestion) restriction enzyme digestion. The obtained DNA fragment was cloned into the pETM-20 vector having a modified MCS.

4.3. Western blotting analysis

4.3.1. Preperation of samples

Cell culture samples were collected in lysis buffer (Table 3.9) using a scraper. Typically, 200 µl of lysis buffer was added on a well of 6-well plate (10^6 cells) and cells were collected. Subsequently, samples were sonicated via executing the sonication program for 3 times (5 seconds, 3 cycles, 50% power) on ice in 15 ml falcon tubes. Subsequently, tubes were briefly spinned down at low speed to collect droplets on the walls. Samples were transferred into 1.5 ml tubes and 40 µl 6X Laemli buffer (Table 3.9) was added. Samples were denaturated at 95 °C for 5 minutes, and stored at -20 °C until later use.

4.3.2. Preperation of SDS-PAGE gels

For routine use, 0.75mm 15-well SDS-PAGE gels were casted. Briefly, liquid 15% gel solution (4 ml per gel) was mixed with 40 µl 10% APS and 4 µl TEMED (resolving gel). The gel solution was mixed thoroughly and put between casting glasses. The gel was immediately covered with n-butanol to ensure a flat surface. Once the resolving gel was

polymerized (around 30 minutes), n-butanol was drained off. Stacking gel mixture was prepared. 1 ml per gel 4% gel solution was mixed with 10 ul 10% APS and 1 µl TEMED. The mixture was added on top of the resolving gel and the comb was inserted. After polymerization was completed, the gel was wrapped with tissue paper and wetted with ddH_20, put in a plastic bag and kept at 4 °C until later use, for no longer than 1 week.

4.3.3. Protein Gel Electrophoresis

SDS-PAGE gels were run in vertical electrophoresis tanks in 1X TGS buffer. Prior to electrophoresis, samples were briefly incubated at 95 °C for 2 minutes and vortexed. 10 µl of sample were loaded to each well in 0.75mm 15-well SDS-PAGE gels. Empty wells were loaded with blank sample (PBS mixed with 6X laemli) to avoid “smile effect”. Samples were run at 80 V until they enter resolving gel, then the voltage was increased to 130 V. The gel electrophoresis was stopped as the dye front reached the end of gel.

4.3.4. Wet transfer

Proteins in the SDS-PAGE gels were transferred onto nitrocellulose membranes using the wet transfer method. Briefly, a sandwich of fiber pad, 2 filter papers, SDS-PAGE gel, nitrocellulose membrane, 2 filter papers and a fiber pad was prepared in a tank filled with transfer buffer. Bubbles between sandwich layers were removed with a falcon tube used as a roller. The gel-membrane sandwich was inserted into the transfer apparatus with the correct orientation (the proteins run towards positive pole). Transfer was executed in the 4 °C room. Ice blocks at -80 ° were inserted into the transfer apparatus for cooling. The transfer was completed at 100 V for 1 h.

4.3.5. Membrane blocking

The nitrocellulose membrane was taken into a plastic tank for subsequent incubations with the protein side facing upwards. The membrane was washed for 5 minutes with

TBS-T and blocked with 5% BSA for 1 h at RT. After blocking, the membrane was washed for 5 minutes with TBS-T.

4.3.6. Antibody incubations

The membranes were incubated with the primary antibody solutions at 4 °C overnight. Sodium azide was added into the primary antibody solution to inhibit microbial growth. When the incubation was finished, the primary antibody was stored at 4 °C for repeated usage. The membrane was washed 3 times after primary antibody incubation with TBS-T, then incubated with a secondary antibody solution at RT for 1 hour. Sodium azide was not included into secondary antibody solution, as it inhibits HRP on the secondary antibody. The secondary antibody was chosen according to the animal in which primary antibody was raised (either mouse or rabbit in our study). After secordary antibody incubation, the membrane was washed 3 times with TBS-T.

4.3.7. Visualization of the membrane

Color reagents were mixed with one-to-one ratio and added on the membrane which was placed on a glass slab (Lumi-Light Western Blotting Substrate, Roche, Switzerland). The surface of membrane was covered with transparent film and bubbles were removed. Membrane was imaged using a digital visualization device (Stella, Raytest, Germany).

4.4. Confocal analysis

4.4.1. Seeding cells on coverslips

The confocal microscope used in this study is an upright microscope. Therefore, cells need to be plated onto coverslips and inverted by putting onto a glass slide. For this

purpose, glass coverslips were put on 6-well plates and treated under UV for at least 1 h. HEK293T or THP-1 cells were plated on coverglass containing wells afterwards.

4.4.2. PFA fixation, DAPI and lysotracker-red stainings

Cells were fixed in 4% PFA solution at room temperature for 5 minutes. PFA was then removed and cells were kept in PBS and stored in dark at 4 °C until analysis. 1 mg/ml (200X) DAPI stock solution was aliquoted and stored in -20 °C. The stock solution was diluted in PBS to 1X concentration. 1X DAPI solution was added dropwise on fixed cells attached to the coverslips. Cells were incubated at RT for at least 5 minutes. Subsequently, the wells were washed once with PBS. Cells were stained with 50nM lysotracker red containing medium for 30 minutes at cell culture conditions and washed once with PBS.

4.4.3. Visualization by the confocal microscope

Fluorochromes were excited using appropriate wavelengths and emitted photons were scanned using the ranges given in Table 4.4. Image acquisition was carried out using LAS AF software. Images were acquired using 20X (immersion in PBS) or 63X (immersion in glycerol) lenses.

Table 4.4. Excitation and emission wavelengths used in confocal microscopy analysis.

Fluorochrome	Laser	Excitation (nm)	Emission range (nm)
DAPI	Diode, 50 mW	405	410-450
EGFP	Ar, 65 mW	488	490-535
EYFP	Ar, 65 mW	514	520-560
mCherry	HeNe, 1 mW	543	570-680
Lysotracker red	HeNe, 1 mW	543	585-630

4.4.4. Time-lapse imaging

PMA differentiated THP-1 macrophage cells were observed by time-lapse confocal microscopy. Cells were imaged using in house produced growth chambers that keep cells viable for at least half an hour. Briefly, 60mm cell culture plates were filled with agarose and a rectangular piece of gel was carved. The whole plate was equilibriated at 37 °C and the space was filled with warm cell culture media. Cells plated on the glass coverslips were inversely placed on the growth chamber by removing the air bubbles between the glass slide and the chamber.

4.5. Cell culture

4.5.1. Maintainance of THP-1 cells

THP-1 is an established monocytic cell line derived from a leukemia patient [89]. The cell line displays macrophage-like characteristics upon differentiation with PMA [90]. Undifferentiated THP-1 cells were cultured in suspension with RPMI supplemented with supplemented with 1x MEM Non-Essential Aminoacids, 2mM L-Glutamine, 100 U/ml penicilin, 100 µg/ml streptomycin and 10% FBS. THP-1 cells were not allowed to exceed the maximum confluency of 10^6 per 1 ml. Freezing of THP-1 cells was carried out in 50% FBS and 5% DMSO containing full RPMI medium. Aliquotes of THP-1 cells were stored at -150 °C indefinetely in the freezing media using cryotubes. Frozen vials were thawed using a water bath at 37 °C. Freezing media were changed with full RPMI medium suppel-emented with 20% FBS. Cultures were maintained in 20% FBS containing RPMI until cells acquired their normal morphology.

4.5.2. PMA differentiation and MSU treatment of THP-1 cells

$5x10^6$ THP-1 cells were differentiated in 60 mm plates in 0.5 µM PMA containing RPMI for 3 h. Subsequently, cells were collected by scraping. Cells were incubated for

24 h in PMA-free RPMI. PMA differentiated THP-1 cells were treated with 150 μg/ml MSU crystals for 4 h. MSU crystals are water insoluble, so that stock solutions must be thoroughly mixed before pipetting.

4.5.3. Maintainance of HEK293T cells

HEK293(F)T cells (Invitrogen, USA) are widely used for protein overexpression and lentiviral packaging purposes. These cells were derived from HEK293F cells which stably express the SV40 large T antigen from the pCMVSPORT6TAg.neo plasmid. HEK293T cells were cultured with high glucose DMEM supplemented with supplemented with 1x MEM Non-Essential Aminoacids, 2mM L-Glutamine, 100 U/ml penicilin, 100 μg/ml streptomycin and 10% FBS.

4.5.4. Calcium Phosphate Transfection

HEK293T cells were efficiently transfected via the calcium phosphate transfection method. This procedure produces insoluble precipitates of plasmid DNA and calcium phosphate, which are subsequently engulfed by HEK293T cells [91]. Briefly, plasmid DNA to be transfected were mixed with ddH_20, 2M $CaCl_2$ and 2X HBS solution in the given order, with the amounts indicated at Table 4.5. Incubation time after $CaCl_2$ and 2XHBS addition does change size of the calcium-phospate-DNA co-precipitates which affects transfection efficiency. The incubation time is determined empirically as 5 minutes after addition of $CaCl_2$ and 2XHBS. Vortexing the transfection mixture should be avoided as it decreases transfection efficiency.

4.5.5. Lentiviral Transduction

Lentiviral transduction procedure was used to infect THP-1 monocytes which could not be easily transfected by transient transfection protocols such as calcium phosphate transfection. Also, stable HEK293T cells expressing EGFP-ASC or mCherry-ASC fusion

proteins were prepared using the same procedure. The advantage of lentiviral transduction is its ability to infect a broad range of cell types and stable integration of the gene of interest into the genome of transduced cell.

Table 4.5. Preperation of transfection reagents for calcium phosphate transfection method.

	DNA	**ddH_20 (add up to)**	**2M $CaCl_2$**	**2XHBS**
6-well plate	0.5-1 µg	219 µl	30.5 µl	250 µl
100 mm dish	4 µg	439 µl	61 µl	500 µl
150 mm dish	12 µg	1317 µl	183 µl	1500 µl

Three plasmids, two of the plasmids encoding genes for lentiviral packaging (pCMVdeltaR8.74 and pMD2.G) and one encoding the desired construct of interest in pLenti-Ef1a vector backbone were co-transfected into HEK293T cells for producing lentiviral particles by calcium phosphate transfection method as in Section 4.4.5. Briefly, $5x10^6$ cells were plated on 100mm dishes the evening before transfection. In the morning, cell culture media was carefully changed and 25 µl of 10mM chloroquine was added. Tranfection mixture was prepared using 4 µg of each three plasmids as in Section 4.4.5 and added dropwise on cells. Cells were incubated for 8 h, and the culture media was carefully refreshed. 2 days after transfection, cell culture media, which now contains lentiviral particles, was taken into a 10 ml syringe. 10 µl of 4mg/ml stock solution of polybrene was added into the tip of the syringe, sucked carefully into the syringe and a 0.45 µm syringe filter was inserted at the tip of the syringe. The syringe was mixed gently, and the lentiviral particles were added dropwise onto the cells. Cell culture media was changed 24 h after transduction.

4.6. In vitro FRET experiment

$15x10^6$ cells per 150mm plate were transfected with 12 µg of pmCherry-PYD wt and either pEGFP alone, pEGFP-PYD wt, pEGFP-PYD R41A and pEGFP-PYD D48A plasmids as in Section 4.5.5. Cells were collected by scraping in 3 ml PBS + PIC + 2mM

EDTA 24 h later and sonicated 3 times (5 seconds, 3 cycles, 50% power) on ice. Lysates were added inside a quartz cuvette and analyzed using a spectrofluorometer (Cary Eclipse, Agilent Technologies, USA). Samples were excited sequentially at 488 nm and 587 nm and fluorescence emission spectrum of each sample was measured for 2 times. The experiment was done in duplicate.

4.7. Purification of ASC specks from HEK293T cells

4.7.1. Crude extraction

Transfection of ASC encoding plasmids was carried out via calcium phosphate method as in Section 4.5.5. Cells were collected 24 h after transfection by scraping in 3 ml PBS for each 150mm dish. Cells were combined in 50 ml falcon tube and sonication program was run for 5 times, 5 seconds 3x10%, 50% power program in ice. The lysate was centrifuged at 200 g at RT for 5 minutes in Beckmann falcon centrifuge. Due to micrometer size of the ASC specks, they were found in the low speed centrifugation pellet. Soluble proteins remained in the supernatant which was discarded.

4.7.2. High purity isolation of ASC specks

Typical results of ASC speck purification procedure were shown in Appendix B (Figure B.1 and Figure B.2) .Transfection of ASC encoding plasmids was carried out via calcium phosphate method as in Section 4.5.5. Cells were collected 24 h after transfection by scraping in 3 ml PBS for each 150mm dish. Lysates of 3x150mm dishes were combined in a 50 ml falcon tube. Sonication program was run for 5 times, 5 seconds 3x10%, 50% power program in ice. The lysate was centrifuged at 2400 g for 5 minutes at RT in Beckmann falcon centrifuge. The pellet was resuspended by vigorous vortexing. After complete resuspension, lysates were left to sediment for 5 minutes. The first gravity sedimenting filamentous pellet was observed to be rich in nucleic acids and granular proteins but deficient in ASC protein (See Appendix B, Figure B.3). Taking advantage of this observation, this

cycle was repeated until sufficient purity was achieved. Upon gravity sedimentation, the supernatant was transferred into a new falcon tube. The supernatant was centrifuged at 200 g for 5 minutes at RT in Beckmann falcon centrifuge. The supernatant was discarded and pellet was resuspended in 10 ml PBS. The pellet was resuspended by vigorous vortexing. The lysate was left for gravitiy sedimentation for 5 minutes and the suparnatant was carefully saved. The supernatant was centrifuged for 60 minutes at 200 g at RT. The pellet was resuspended on 30 ml PBS. After sequential gravity sedimentation, granular particles smaller than ASC specks were removed by first passing the sample through a 5 μm syringe filter and then re-applying PBS in the opposite direction (reverse flow, see Appendix B, Figure B.4). By this method, not only ASC specks greater than 5 μm but smaller specks were recovered as well, possibly due to uneven size distribution of the filter. 30 ml sample was passed from the syringe filter in 6 cycles and at the end of each cycle reverse flow was applied. Sequential passing of the sample is necessary not to clog the filter. Finally, the sample was centrigufed at 2400 g for 60 minutes. The pellet was resuspended in 0.5 ml PBS. The typical yield of this method is around 100-200 μg of ASC specks per $5x10^7$ HEK293T cells. It is important not to centrifuge ASC specks at high speed (ex. 20 000 g) as high speed centrifugation pellets could not be resuspended.

4.8. Intradermal injection of mCherry-ASC specks

50 μg of mCherry-ASC specks and its fluorescence equivalent purified mCherry protein were injected intradermally, side-by-side to the back of 4 Balb/c mice. mCherry-ASC specks were purified as in Section 4.6.2 and mCherry protein was purified from *E. Coli* as in Section 4.7.1. Mice were anesthetized during procedure with 100mg/kg ketamine and 10mg/kg xylasine mixture injected intraperitoneally.

4.8.1. Expression and purification of mCherry from *E.Coli*

pETM-20 mCherry plasmid was transformed into Rosetta2 pLysS strain of *E. Coli* as in Section 4.1.8. Transformed bacteria were plated on ampicillin and chloroamphenicol containing LB-agar plates. A single colony was picked and cultured in ampicillin and chlo-

roamphenicol containing 5 ml LB starter culture. Next day, 0.5 ml of the starter culture was added on 100 ml ampicillin and chloroamphenicol terrific broth. The culture was shaked for 4 h and 50 min at 37 °C until the OD reached 0.85. At this time point, 40 µl of 1 M IPTG (0.4 mM final concentration) was added on 100 ml culture and shaked overnight at 25 °C (cold IPTG induction). The next day, culture was splitted into 2x50 ml falcon tubes. The pellet was resuspended in 1 ml equilibriation buffer (PBS + 10mM imidazole) and sonicated thoroughly (run 15 times, 5 seconds each, 3 cycles, 50% power on ice). The Ni-NTA spin column was equilibriated with equilibriation buffer (700g, 2 min). The sonicated lysate was centrifuged for 15 min at 13000 rpm at 4 °C. The lysate was then applied to the column in 500 µl aliquotes (30 min each, RT on shaker). The spin column was centrifuged for 5 min at 270 g. The column was washed for 3 times with wash buffer (PBS + 25mM imidazole) and centrifuged for 2 min at 700 g. The column was eluted for 3 times with elution buffer (PBS + 250 mM imidazole). The sample was dialyzed against PBS at 4 °C overnight. The purity of the sample was monitored by SDS-PAGE and Coomassie staining and the concentration was measured by Bradford assay.

4.8.2. Calculation of the relative fluorescence

mCherry protein extracted from *E. Coli* and mCherry-ASC specks extracted from HEK293T cells had different purities (See Appendix B, Figure B.5). In order to normalize these two samples according to their fluorescence intensities, serial dilutions of samples were imaged under UV light (Gel Doc, Bio-Rad, USA). Triplicates of 5 µl serial dilutions of samples were dropped on a UV transparent tray. The image was quantified using ImageJ and a standard curve was plotted, which permitted the calculation of relative fluorescence intensities of both samples (See Appendix B, Figure B.5).

5. RESULTS

5.1. THP-1 EGFP-ASC Stable Cell Line Does Form ASC Specks upon Stimulation with MSU Crystals

In the absence of inflammasome stimulation, ASC protein displays a diffused expression throughout the cell. We have created a stable THP-1 cell line which expresses EGFP-ASC fusion protein. Upon PMA differentiation followed by treatment with MSU crystals, the ASC proteins in the cytosol and the nucleus change their cellular localization and form a micrometer sized structure next to the nucleus inside the cytosol, called the ASC speck (Figure 5.1).

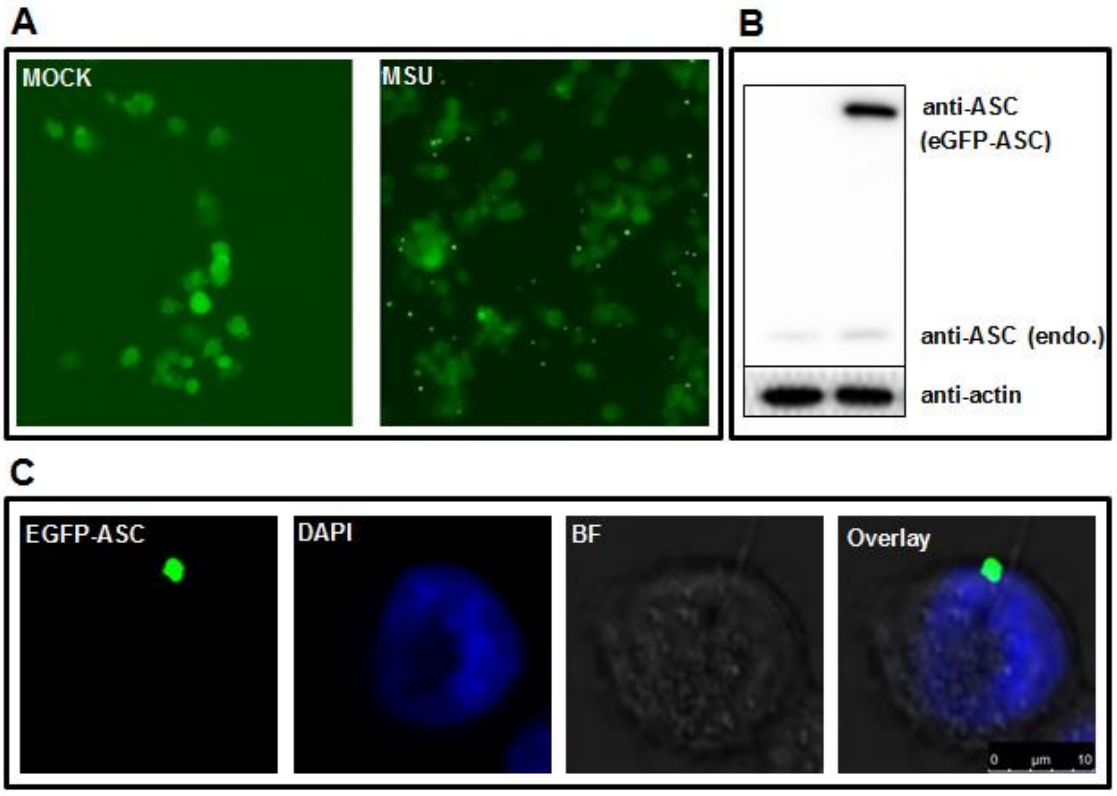

Figure 5.1. PMA differentiated THP-1 EGFP-ASC stable cells. (A) PMA differentiated THP-1 EGFP-ASC cells were treated with either mock or 150 ug/ml MSU for 4 h. (B) Western blot analysis of THP-1 EGFP-ASC stable cells. Lane 1: wt THP-1. Lane 2: EGFP-ASC stable THP-1. (C) Confocal micrograph of a THP-1 EGFP-ASC stable cell stimulated with MSU crystals. DAPI: Nucleus. BF: Bright field.

5.2. Mutational Screen on the EGFP-ASC construct

Upon establishing the participation of our EGFP-ASC fusion protein into the ASC speck following inflammasome stimulation, we performed a mutational screen by expressing mutant EGFP-ASC constructs in HEK293T cells. The EGFP-ASC fusion protein does form spontaneous ASC specks when expressed in HEK293T cells at 72.7 ± 2.37 % frequency.

The spontaneous ASC speck formation upon overexpression of ASC was reported before [54, 76, 92]. The probable reason of spontaneous ASC speck formation in HEK293T cells is the excess of critical ASC concentration by overexpression so that the ASC speck does form without the need for activation by inflammasome receptors (such as NLRP3, NLRC4 and AIM2). The ASC speck formation was described as a "low probability event" before the start of speck nucleation, but later turns into a "high probability event" once the ASC speck starts to grow, and therefore only one ASC speck per cell is observed in an all-or-none fashion [76]. In our study, overexpression of the EGFP-ASC construct is probably resposible for increasing the likelihood of this "low probability event". The cellular localization of ASC specks formed in THP-1 and HEK293T cells (perinuclear) as well as the shape of the ASC speck (compact, globular) were observed to be similar (Figure 5.2, 5.3).

To understand which amino acids in the pyrin domain (PYD) and caspase recruitment domain (CARD) of ASC are important for ASC speck formation, we generated a series of mutations. Overall, 23 amino acid residues were mutated into alanine. Cells were transfected with EGFP-ASC mutant encoding plasmids, observed under the confocal microscope and scored on the basis of the ASC speck formation. In total, 12 single amino acid mutations on ASC protein were found to have no effect on ASC speck formation, whereas 11 single amino acid mutations disrupted the ASC speck formation (E13A, E19A, K21A, K26A, R41A, D48A, D51A, L68A, L73A, M159A and R160A, Figure 5.2, 5.3, Table 5.1). In these cells, filament structures were observed, which were similar to the

structures observed upon expression of single PYD or CARD alone or expression of the short isoform of the ASC (See Section 5.4).

Interestingly, the L25A mutation showed a different phenotype displaying a shape in between ASC specks and filaments formed by other ASC mutants. The structure formed by the L25A mutation, referred in this thesis as Medusa's head, is a perinuclear structure, similar to the size of the ASC speck but has characteristic radial filament extension pointing outwards from its center (Figure 5.3). Although ASC protein is conserved between human and mouse with 71.8% protein sequence identitiy, mouse ASC protein has a methionine at this posititon. Since such kind of a structure has not been reported in previous studies using mouse cells, we hypothesized that a methionine residue at position 25 might substitute for a leucine residue present in the human ASC protein. Indeed, when EGFP-ASC L25M mutant is expressed in HEK293T cells, a globular speck structure phenotype has been recovered (Figure 5.3). Phenotypes of the mutations were summarized in Table 5.1.

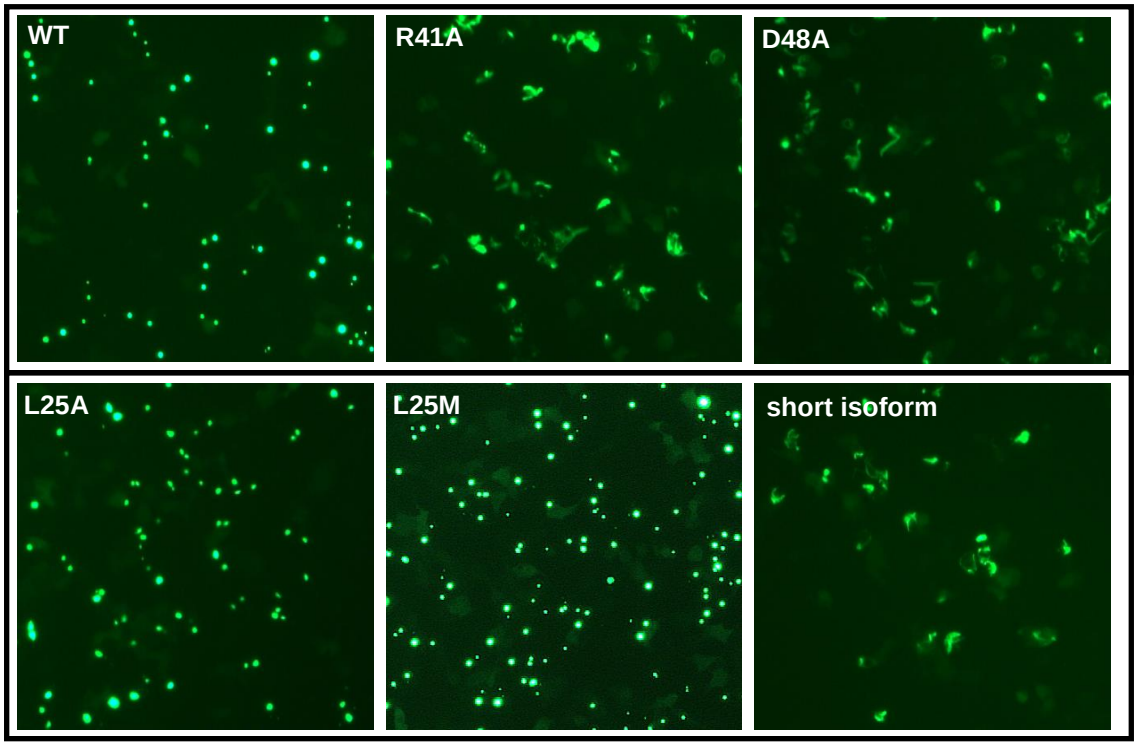

Figure 5.2. General view of HEK293T cells transfected with either EGFP-ASC wt, R41A, D48A, L25A, L25M or short isform encoding plasmids.

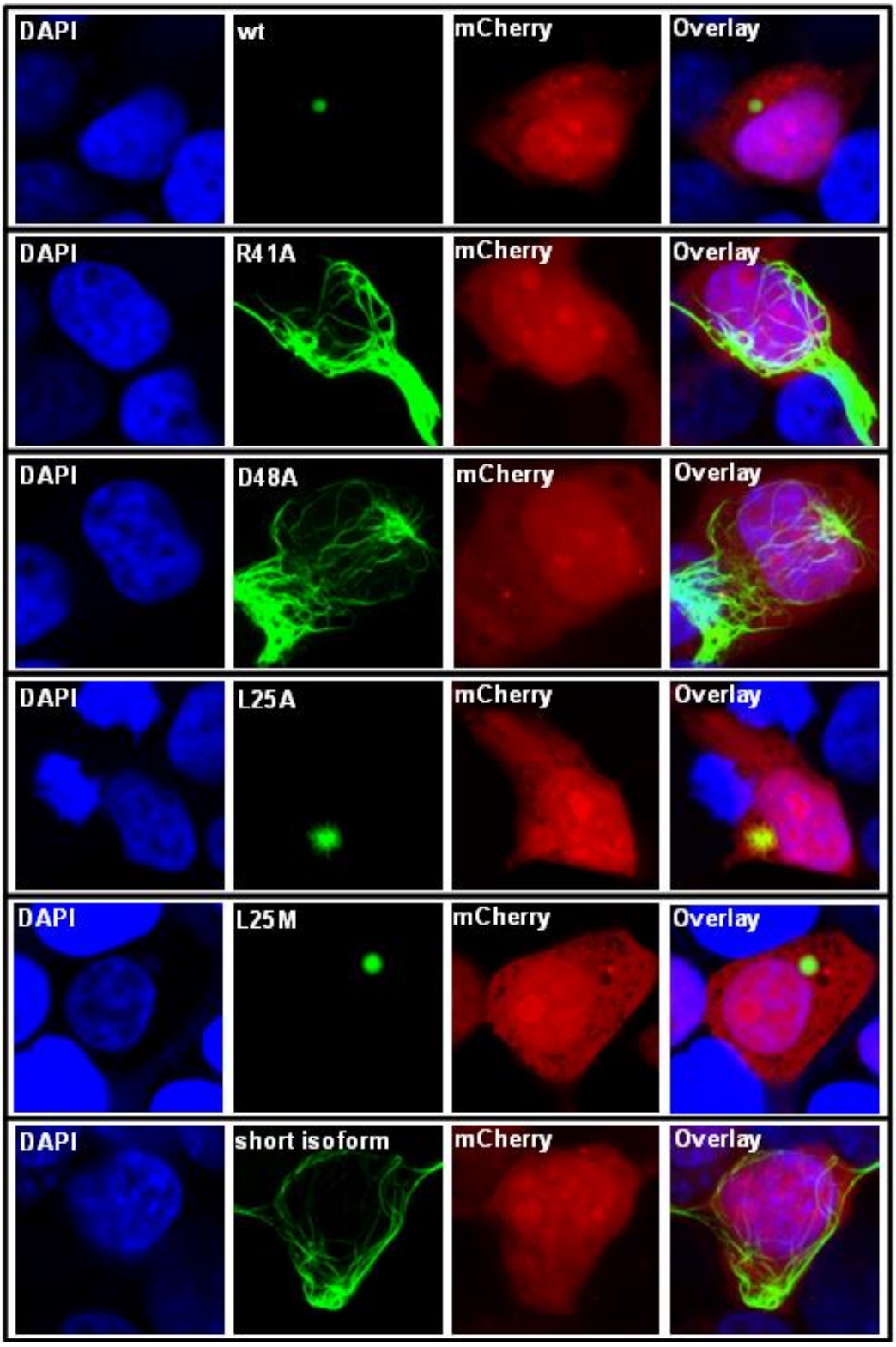

Figure 5.3. R41A and D48A mutations disrupt the ASC speck whereas L25A mutant displays a novel phenotype. Confocal micrographs of HEK293T cells transfected with either EGFP-ASC wt, R41A, D48A, L25A, L25M or short isoform encoding plasmids. DAPI: Nucleus. mCherry alone: Cytosol + Nucleus.

Table 5.1. Phenotypes of the mutations on the EGFP-ASC construct.

ASC variant	Phenotype	Location
wt	speck	-
E13A	filament	PYD
E19A	filament	PYD
K21A	filament	PYD
L25A	Medusa's head	PYD
L25M	speck	PYD
K26A	filament	PYD
R41A	filament	PYD
D48A	filament	PYD
D51A	filament	PYD
E62A	speck	PYD
G65A	speck	PYD
E67A	speck	PYD
L68A	filament	PYD
L73A	filament	PYD
R74A	speck	PYD
H90A	speck	PYD
G101A	speck	linker
P103A	speck	linker
H113A	speck	CARD
M159A	filament	CARD
R160A	filament	CARD
C173A	speck	CARD
L181A	speck	CARD
R182A	speck	CARD
K26A-R160	soluble	PYD + CARD
L68A-R160	soluble	PYD + CARD
short isoform	filament	No linker

5.2.1. Western Blot Analysis of EGFP-ASC Mutants

We have analyzed EGFP-ASC expressing cells by Western blotting to check whether mutations introduced in the construct alter the size of the protein product (Figure 5.4). Since truncated domains of the ASC protein, namely PYD and CARD do form fila-

ment structures instead of ASC specks, we wanted to rule out the possibility of protein shortening. We did not find any evidence of protein truncation due to mutations introduced into the constructs. All proteins synthesized by the constructs except for the short isoform of ASC have the same size.

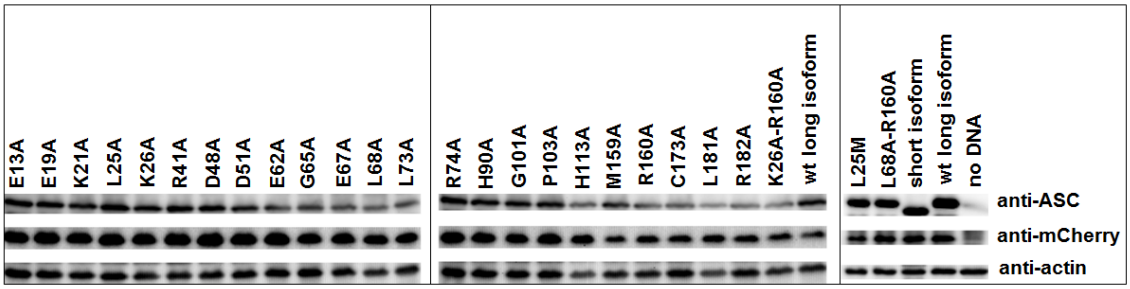

Figure 5.4. Western blot analysis of EGFP-ASC mutants. Plasmids encoding the indicated constructs were co-transfected with mCherry (transfection contol).

5.2.2. Double mutations on the ASC protein completely inhibit the ASC speck and filament formation

Since we observed that single mutations on PYD or CARD of full-length ASC protein resulted in filament formation instead of ASC speck formation, we hyphothesized that the remaining intact domain should be responsible for filament formation. To prove this idea, two combinations of double ASC mutants were cloned (K26A-R160A and L68A-R160A). We observed that double mutant EGFP-ASC constructs failed to form the ASC speck or filament (Figure 5.5).

5.3. PYD and CARD isolated domains form mutually exclusive filaments

We created fusion proteins of PYD and CARD of ASC with EGFP and mCherry fluorescent proteins, respectively. When HEK293T cells were co-transfected with these constructs, we observed mutually exclusive filaments of PYD and CARD, which shows that PYD-PYD and CARD-CARD interactions are highly specific (Figure 5.6). Further-

more, we realized that L68A and R160A mutations destroyed filaments of PYD and CARD truncated proteins, respectively (Figure 5.6).

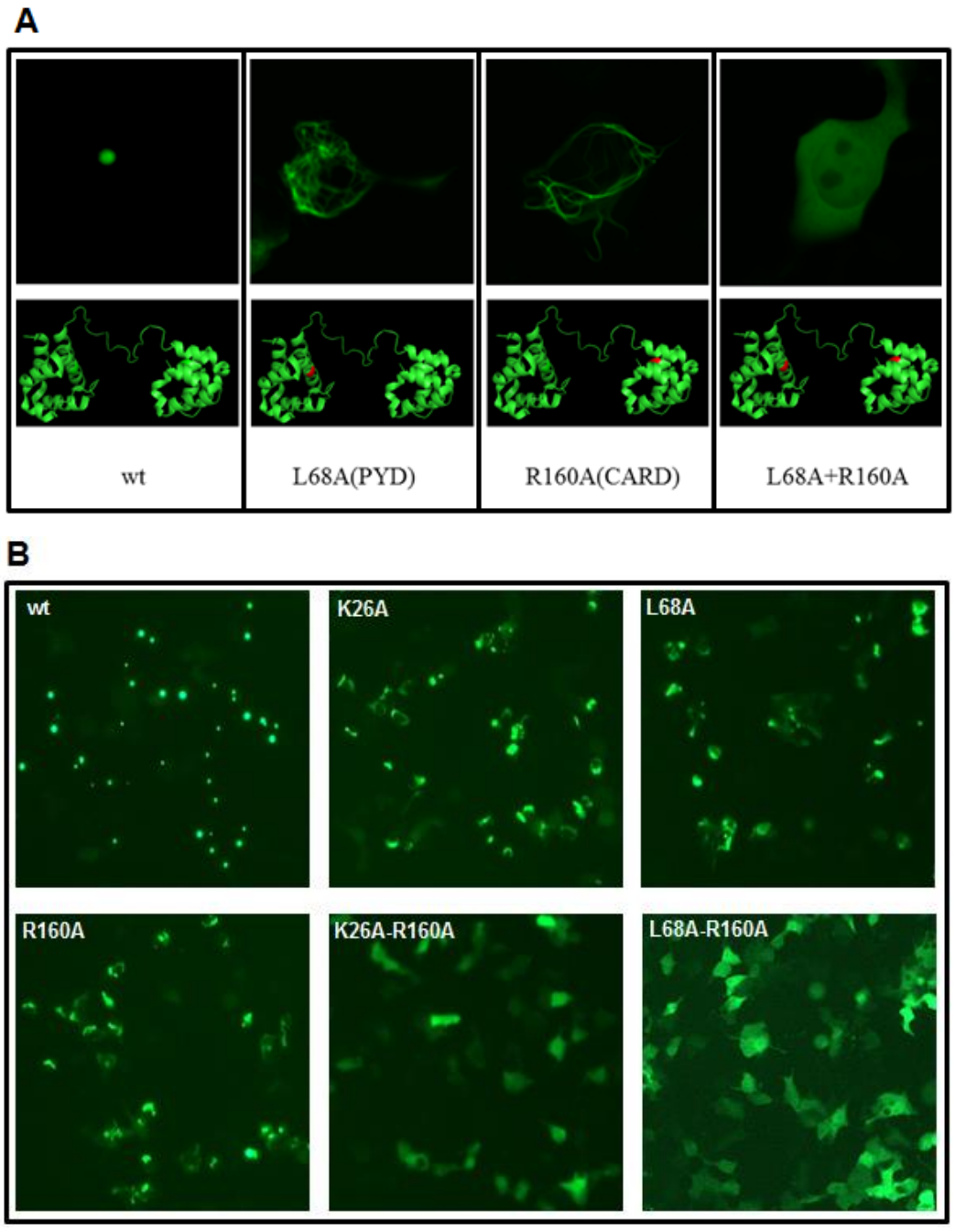

Figure 5.5. Double mutations on PYD and CARD disrupt speck and filament formation. (A) Confocal micrographs of wt, L68A, R160A and L68A-R160A mutant EGFP-ASC expressing HEK293T cells (upper lane) and locations of the mutation on the NMR model (lower lane). (B) General view of HEK293T cells transfected with wt, K26A, L68A, R160A, K26A-R160 and L68A-R160A EGFP-ASC encoding plasmids.

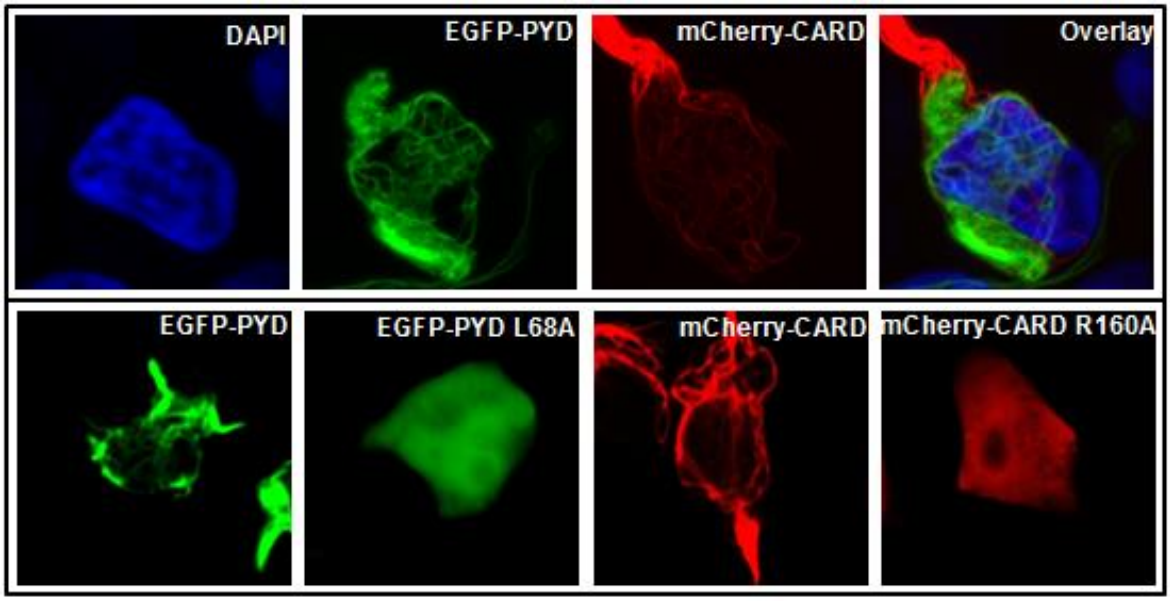

Figure 5.6. PYD and CARD form mutually exclusive filaments which can be inhibited by single mutations. (A) EGFP-PYD and mCherry-CARD filaments do not co-localize in HEK293T cells co-transfected both plasmids. EGFP-PYD (B) and mCherry-CARD (D) filaments are inhibited by L68A (C) and R160A (E) mutations. DAPI: Nucleus.

5.4. The same set of mutations that destroy ASC specks formed by full-length ASC protein also inhibits filaments of PYD- or CARD-only truncated protein

Based on the results in Section 5.5, we decided to run a parallel experiment on EGFP-PYD truncated protein using an overlapping set of mutations. All ASC speck disrupting mutations and two non-disrupting mutations were re-created on the EGFP-PYD construct. It was observed that every mutation tested that has disrupted the ASC speck on full-length ASC protein, also inhibited EGFP-PYD filaments and vice versa. The degree of inhibition was gradual, ranging from complete inhibition to reducing the frequency of filament formation by half (Figure 5.7, 5.8). The unique mutation L25A, which formed Medusa's head phenotype in full-length ASC protein, does not have an effect on EGFP-PYD filament formation, indicating that the effect of the mutation is not related to the disruption of the PYD-PYD interaction (Figure 5.7).

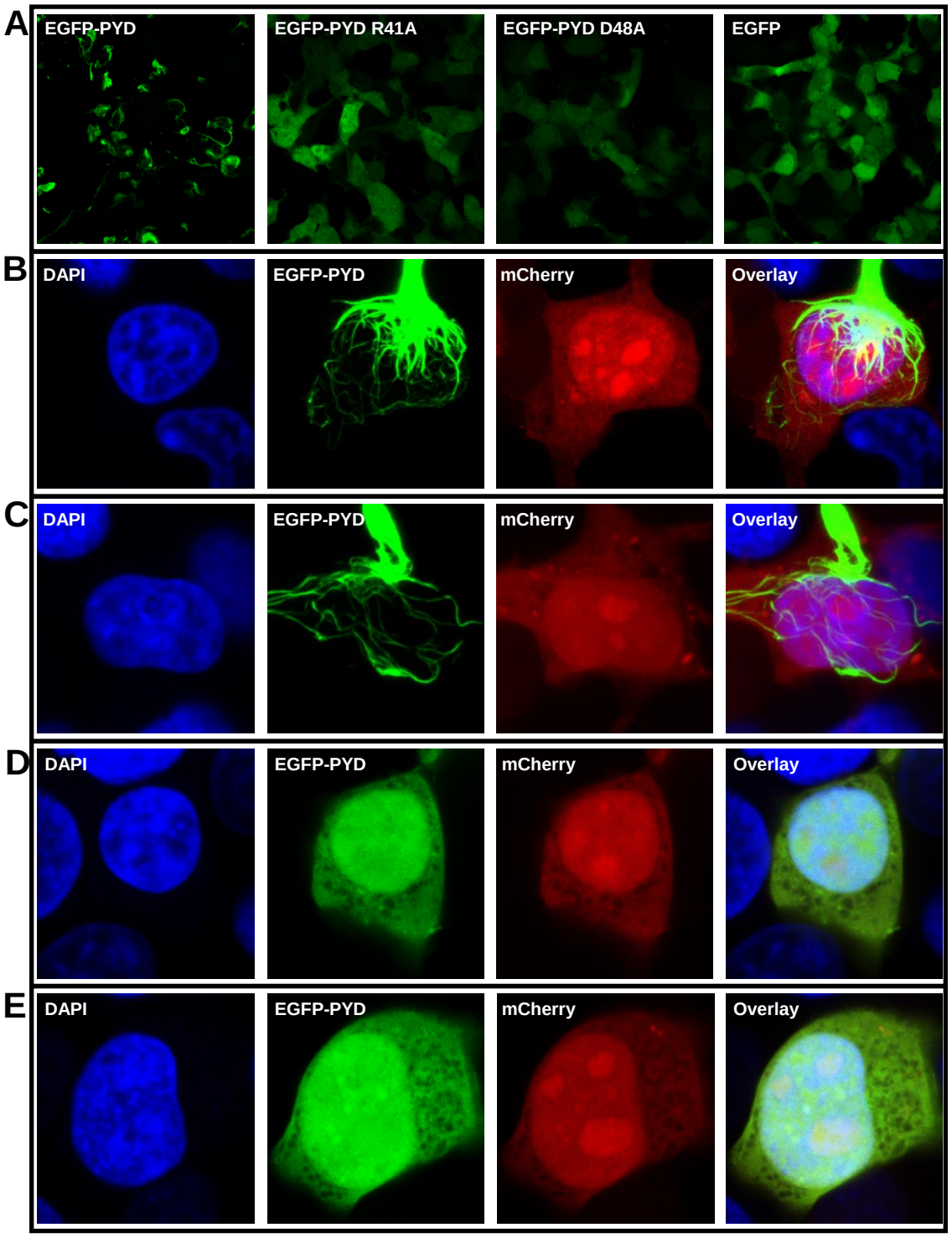

Figure 5.7. Representative mutations on EGFP-PYD construct. (A) General view of HEK293T cells transfected with EGFP PYD wt, R41A, D48A or EGFP only. Confocal micrographs of HEK293T cells expressing EGFP-PYD wt (B), L25A (C), R41A (D), D48A (E). DAPI: Nucleus. mCherry alone: Cytosol + Nucleus.

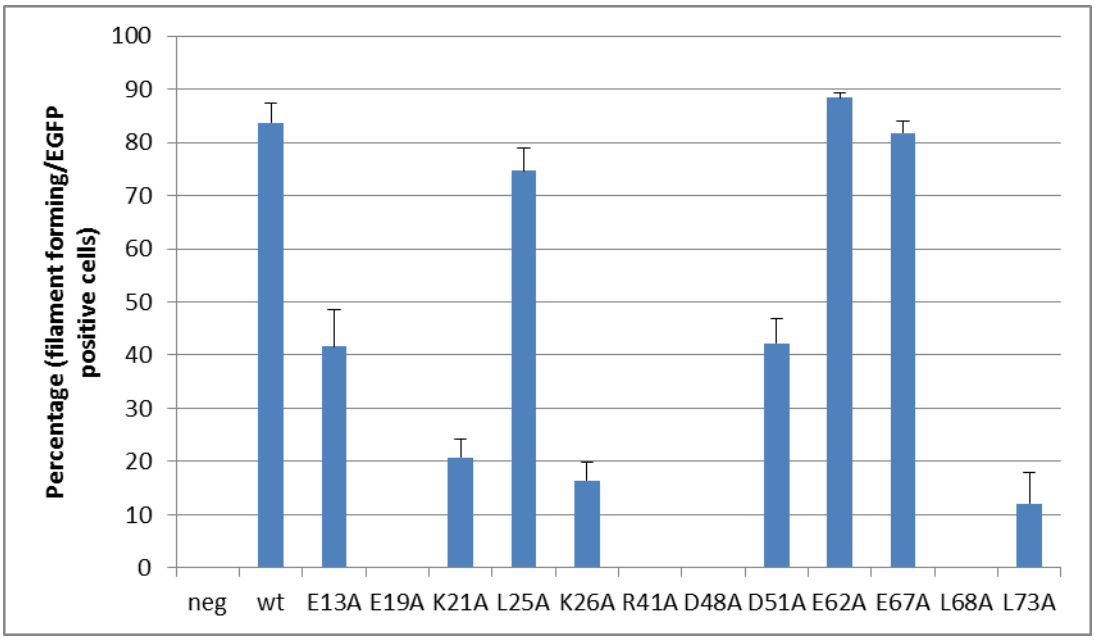

Figure 5.8. Mutations that disrupt ASC speck formation also inhibit PYD filament formation on EGFP-PYD construct.

5.4.1. Western blot analysis of EGFP-PYD mutant constructs

To confirm proper expression of mutant EGFP-PYD constructs, we analyzed transfected cells with western blot. We did not observe any changes in the size of the protein products as a result of the mutations (Figure 5.9).

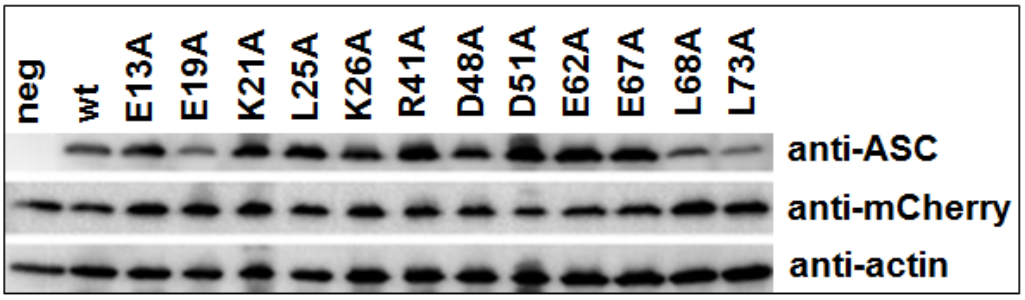

Figure 5.9. Western blot analysis of mutations created on EGFP-PYD construct. HEK293T cells transfected with either EGFP (neg) or indicated EGFP-PYD constructs were analyzed by western blotting. mCherry encoding plasmid was co-transfected as transfection control.

5.5. PYD of ASC uses alternative interaction modes.

R41A and D48A residues are present at the putative type I interaction surfaces of the PYD [59]. Upon observation of the complete loss of filament formation by R41A and D48A single mutations on EGFP-PYD construct, we designed an experiment to test whether type I interaction is the only interaction mode possible between PYDs of ASC protein. In this experimental setup, wt PYD labeled with a red fluorescent marker was co-expressed with type I interaction mode mutant PYD labeled with a green fluorescent marker. In such an experimental setup, there are three potential experimental outcomes (Figure 5.10). In scenario number one, the mutant PYD is able to interact with wt PYD filaments using its intact surface but not the mutated surface. In such a case, we would expect to observe competition of mutant PYD with wt PYD and inhibition of filament formation. In case of number two, we would not observe inhibition of filament formation but co-localization of mutant PYD on wt PYD filaments. Such an interaction can only be possible if mutant PYD is able to interact with alternative binding surfaces such as type II or type III interaction modes. In the third scenario, we would observe wt filament formation but no co-localization of mutant PYD on filaments. This scenario would imply that the mutation introduced in PYD did excert its effect not only on the surface it resides but on the other interaction surface(s) of PYD.

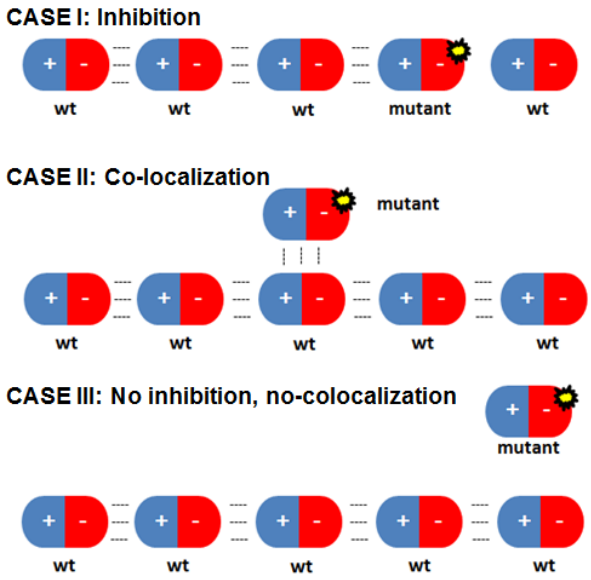

Figure 5.10. Schematic representation of potential experimental outcomes.

5.5.1. Co-localization of mutant PYD with wt PYD filaments.

To monitor the interaction of mutant PYD with wt PYD filaments or potential inhibition of wt PYD filaments, we analyzed co-transfected cells with confocal microscopy. We observed the full co-localization EGFP-PYD D48A with mCherry-PYD wt filaments. Thus, it is clear that disruption of the type I interaction surface was not suffient to inhibit interaction of D48A mutant PYD with wt PYD filaments, suggesting the presence of alternative binding modes. We did not observe complete co-localization for EGFP-PYD R41A, although there was a weak co-localization at spots where mCherry-PYD wt filaments were dense (Figure 5.11).

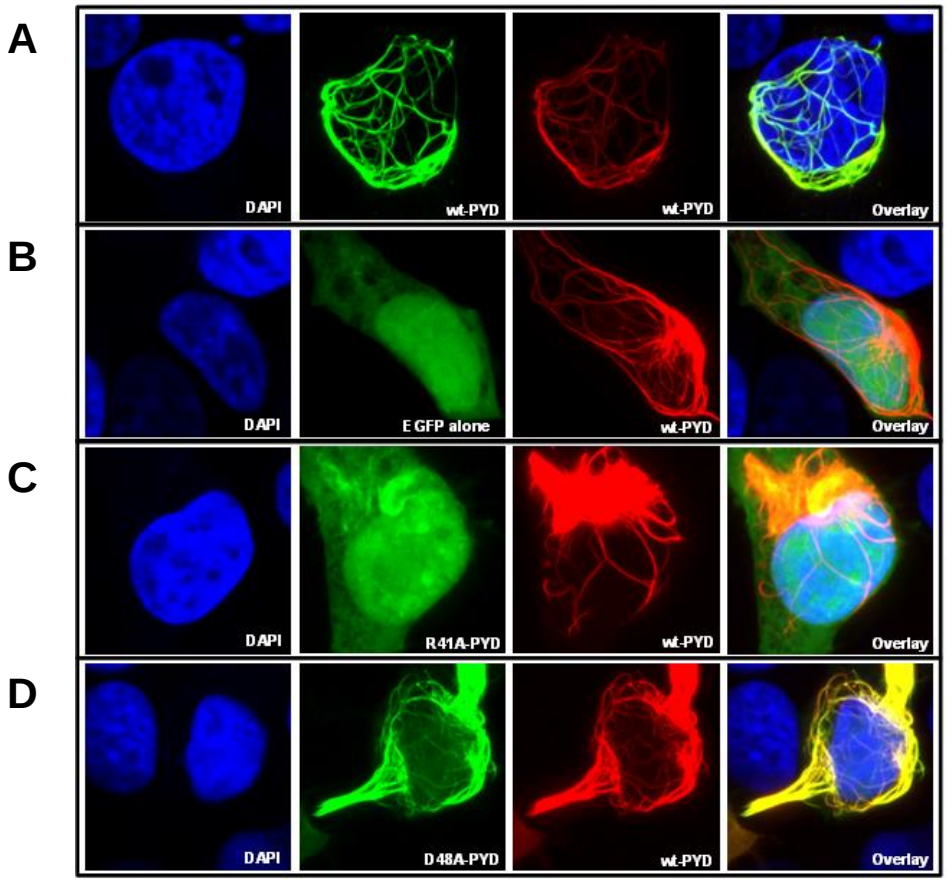

Figure 5.11. Co-localization of type I interaction surface mutant EGFP-PYD with mCherry-PYD wt filaments. (A) Positive control. EGFP-PYD wt fully co-localizes with mCherry-PYD wt filaments (B) Negative control. EGFP alone does not co-localize with mCherry wt filaments. (C) EGFP-PYD R41A was observed to partially co-localize with mCherry-PYD wt filaments where filaments are dense. (D) EGFP-PYD D48A was observed to fully co-localize with mCherry-PYD wt filaments. DAPI: Nucleus.

5.5.2. In vitro FRET experiment to analyze mutant PYD binding to wt PYD filaments.

To quantitate the degree of co-localization, lysates of HEK293T cells co-transfected with mutant and wt PYD encoding plasmids were analyzed using a spectrofluorometer to run an intermolecular FRET experiment (Figure 5.12). Briefly, this experiment measures the relative proximity of fluorescent markers, as the FRET efficiency is inversely correlated with the distance between probes.

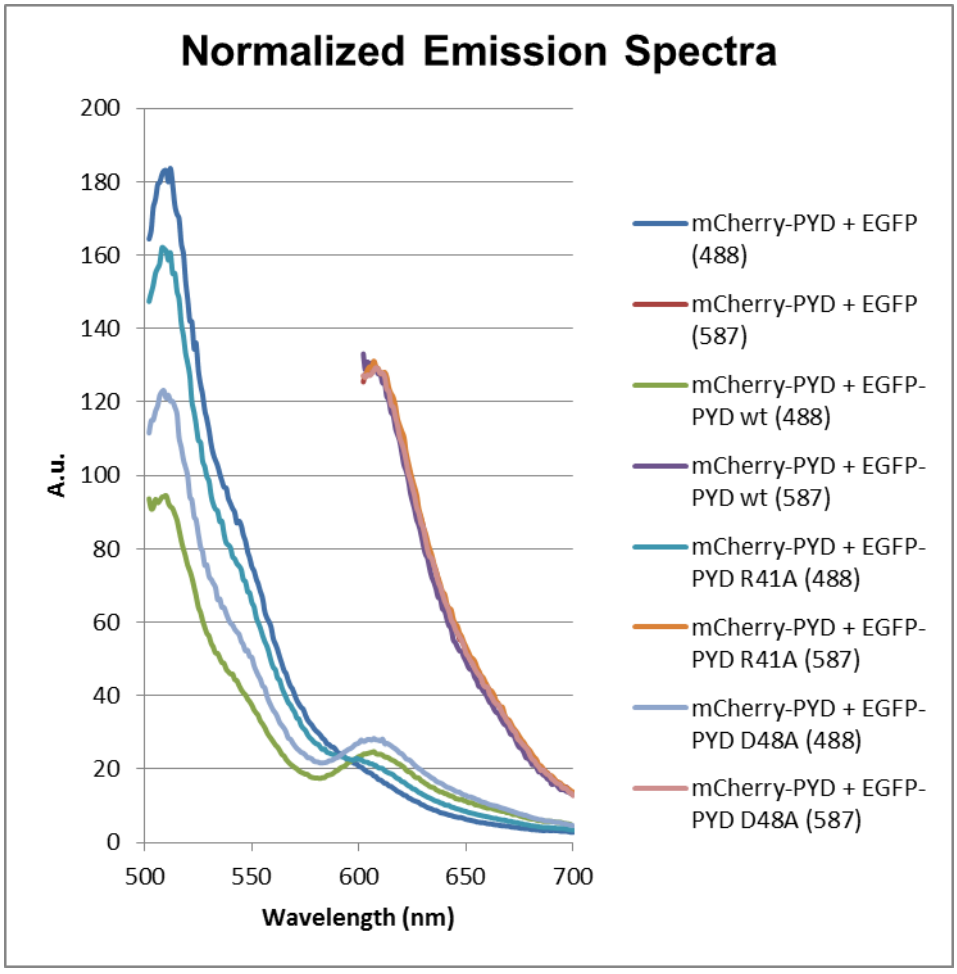

Figure 5.12. Normalized emission spectra of mCherry-PYD and either EGFP, EGFP-PYD wt, R41A or D48A expressing HEK293T cell lysates upon excitation with 488nm (EGFP) or 587nm (mCherry). The experiment measures intermolecular FRET between EGFP, EGFP-PYD wt, R41A or D48A and mCherry-PYD wt. Emission peaks were normalized to emission maximum of mCherry at 610nm.

We compared the FRET efficiencies of EGFP-PYD R41A and D48A constructs with the positive (EGFP-PYD wt) and negative (EGFP) controls, by taking the ratio of FRET acceptor vs donor emission peaks (Em 610/Em 509). While both R41A and D48A constructs' relative FRET efficiencies were significantly higher than the negative control, relative FRET efficiency of D48A has been found to be closer to the positive control, in accordance with the full co-localization of D48A PYD on wt PYD filaments (Figure 5.13). The ability of type I interaction surface mutant PYD D48A to co-localize with wt PYD filaments suggests that the PYD of ASC is able to use alternative interaction modes other than type I. Aliquotes of cell lysates were analyzed by Western blotting (Figure 5.14).

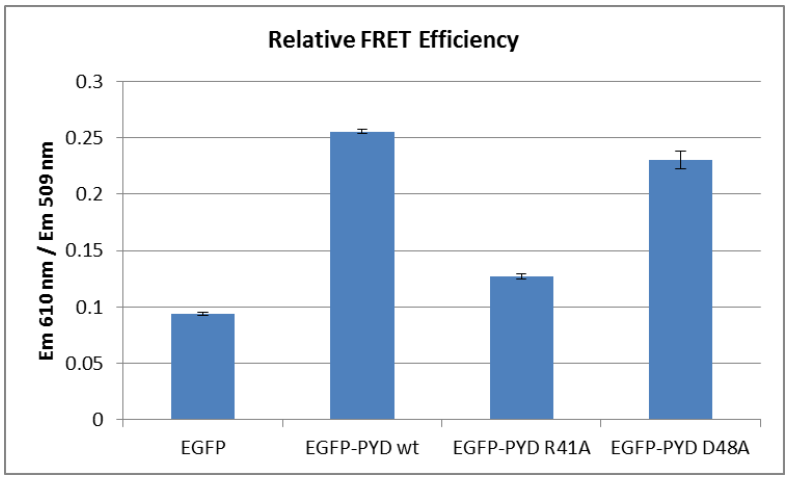

Figure 5.13. Relative FRET efficiencies of mutant EGFP-PYD constructs with mCherry-PYD wt filaments.

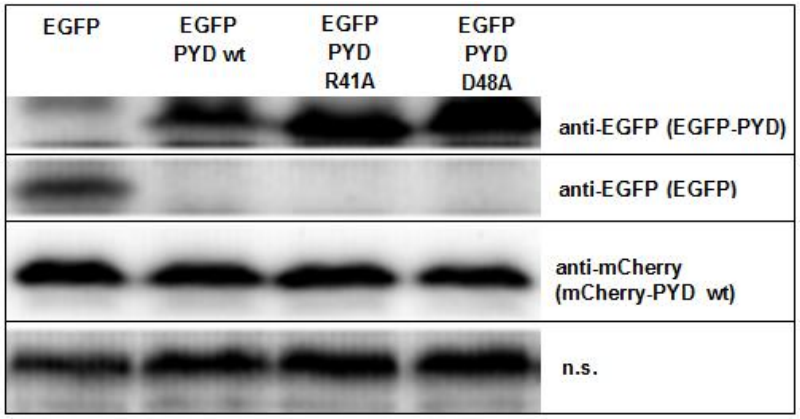

Figure 5.14. Western blot analysis of cell lysates used in the FRET experiment. n.s.: non-specific (loading control)

5.6. Co-aggregation of cytosolic proteins on the ASC speck

Accidentally, we observed that the ASC speck is capable of accumulating cytosolic proteins on its surface. The initial observation was done by co-transfecting HEK293T cells with plasmids encoding mCherry-ASC and EGFP-C3. EGFP-C3 is a fusion protein encoded by the commercial plasmid pEGFP-C3 (Clontech, USA). C3 refers to the 26 amino acid long peptide encoded by the multiple cloning site at the C-terminus of EGFP. We observed the accumulation of EGFP-C3 on the mCherry-ASC speck in co-transfected cells, but EGFP alone failed to localize with mCherry-ASC specks (Figure 5.15).

We found this unexpected co-localization of cytosolic proteins on the ASC speck very interesting, as aggregation of cytosolic proteins in APCs were previously shown to be important for antigen presentation. Given the importance of the ASC protein in the antigen presentation via inflammasome-dependent and -independent mechanisms, such an aggresome-like property of the ASC specks might be the answer to the long-standing question: what is the ASC speck good for?

Later, we cloned a series of EGFP-peptide fusion constructs and performed the same experiment we had done for EGFP-C3 (Figure 5.15). Three fusion constructs, in which 26 amino acid long peptides chosen from the ampicillin resistance gene were cloned at the C-terminus of EGFP. When the same experiment was repeated with these constructs, one out of three constructs accumulated on the mCherry-ASC speck (EGFP-peptide_1). Next, we looked into the charge/hydrophobicity properties of peptides that were accumulated on the ASC specks (Figure 5.16). While peptide_1 shows an obvious hydrophobic amino acids distribution, for C3 this was less apparent. We cloned 2 randomly generated hydrophobic and 2 hydrophilic peptides at the C-terminus of the EGFP, and observed that EGFP-hydrophobic peptides localized with the ASC speck but not EGFP-hydrophilic peptides. We also generated shorter versions of C3 and peptide_1, as C3_19aa failed but peptide_1_19aa succeeded to accumulate on mCherry-ASC specks. Finally, we repeated the same experiment using the model antigen ovalbumin. We have deleted the N-terminal 48 amino acid long secretion signal of the ovalbumin and fused EYFP to its C-terminal. This

construct, referred here as CytOVA-EYFP, accumulated on the mCherry-ASC speck but EYFP alone failed to localize on the mCherry-ASC speck.

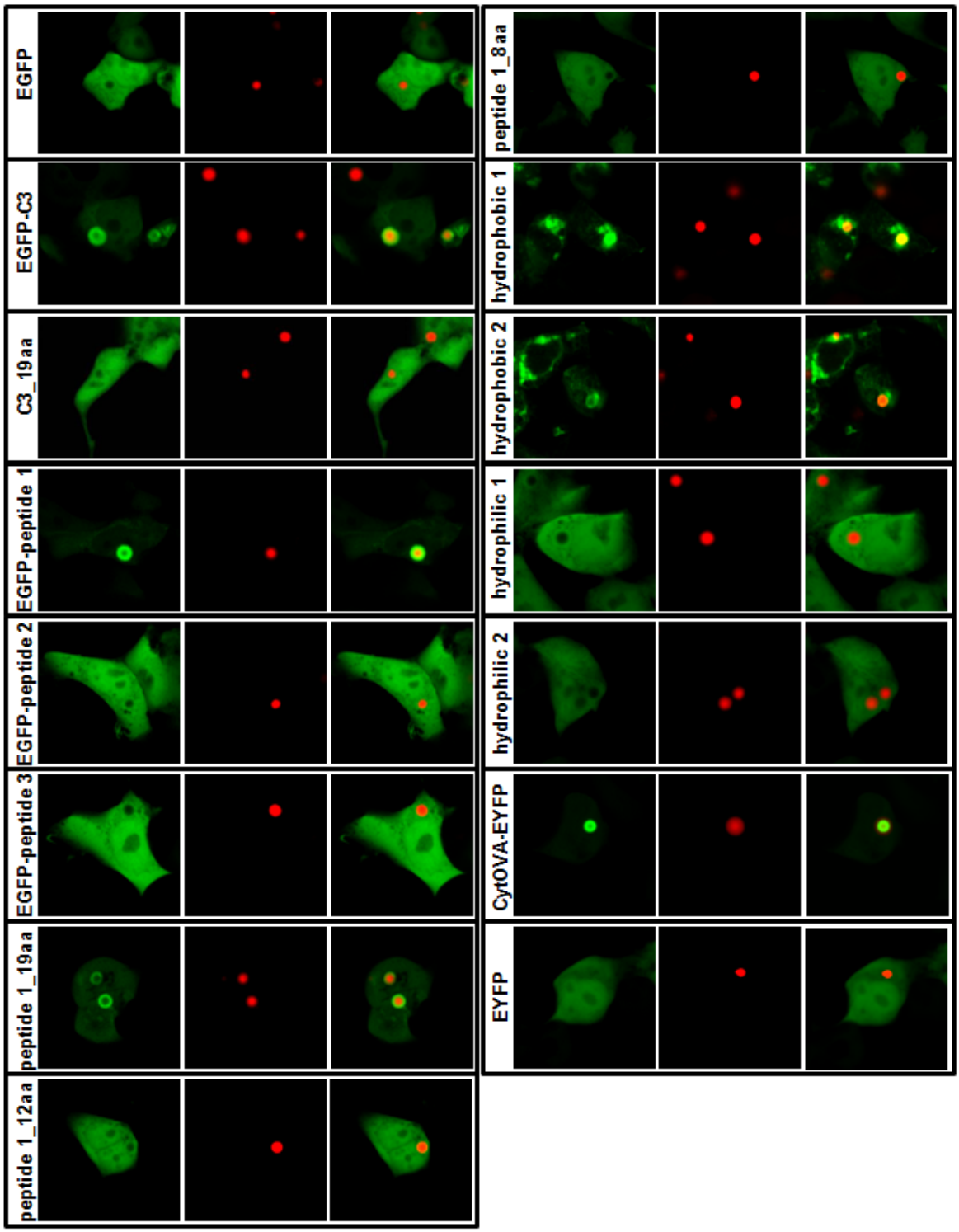

Figure 5.15. The co-aggregation panel of fluorescently labelled constructs on the mCherry-ASC speck.

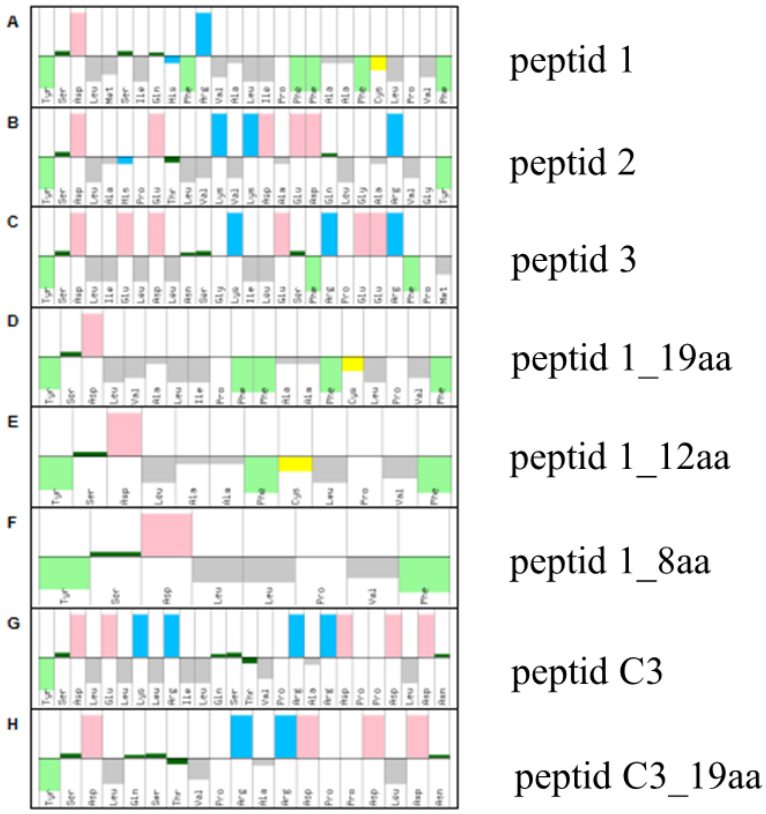

Figure 5.16. Hydrophobicity plots of peptides fused to EGFP at C-terminal.

5.6.1. The accumulation of cytosolic proteins on the ASC specks is not due to interactions between fluorescent reporters

To rule out the possibility that the accumulation of cytosolic proteins on ASC specks might be due to interactions between fluorescent reporters, we co-transfected HEK293T cells with or without non-labelled inflammasome components together with CytOVA-EYFP. We observed that when CytOVA-EYFP construct was transfected alone, it displayed a diffused distribution throughout the cell. However, when all inflammasome components were co-transfected along with the CytOVA-EYFP, speck-like aggregates of CytOVA-EYFP were observed nearly in every cell (Figure 5.17). Samples were also analyzed by Western blotting (Figure 5.18).

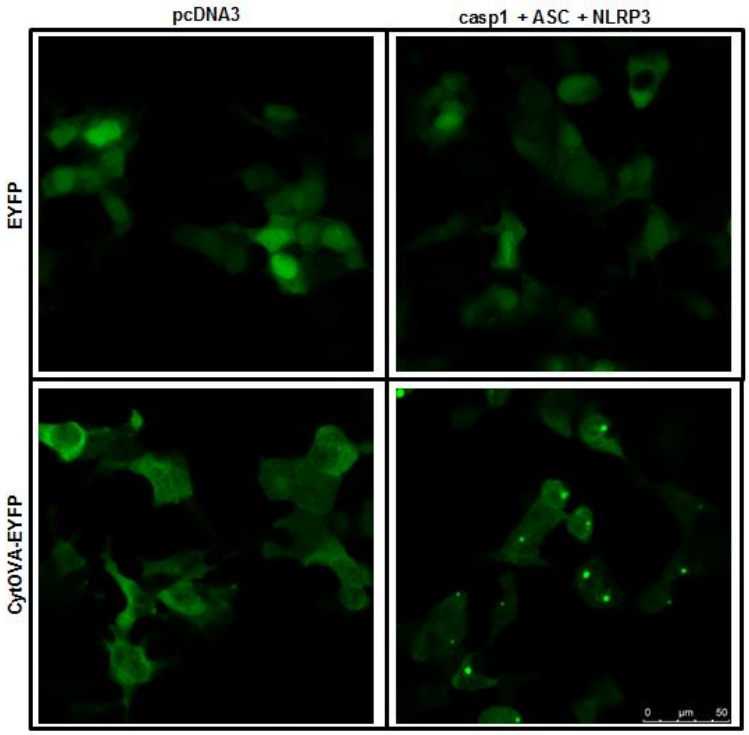

Figure 5.17. Tagging control. CytOVA-EYFP construct was transfected either alone or together with non-labelled inflammasome components procaspase-1, ASC and NLRP3.

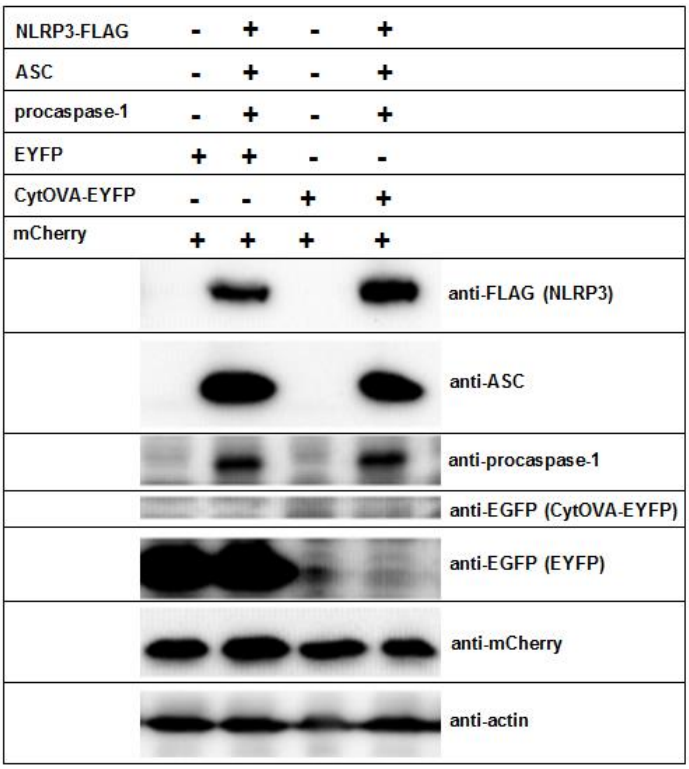

Figure 5.18. Western blot analysis of the transfection set in “tagging control” experiment

5.6.2. The accumulation of cytosolic proteins on the ASC speck is not due to co-existence in a membrane enclosed organelle

The co-localization of the ASC speck and cytosolic proteins might be due to their co-existence at the same membrane enclosed organelle at the same time, such as the autophagosome. To test this possibility, we extracted mCherry-ASC specks with EGFP-C3 accumulated on its surface by extensive sonication and enrichment by low speed centrifugation. We observed that EGFP-C3 remained on the mCherry-ASC specks even after ASC specks were extracted from HEK293T cells. Moreover, co-localization was preserved even after prolonged incubation of extracted specks at 37 °C for 4 weeks in PBS, which indicates that cytosolic protein-ASC speck co-aggregates are remarkably stable (Figure 5.19).

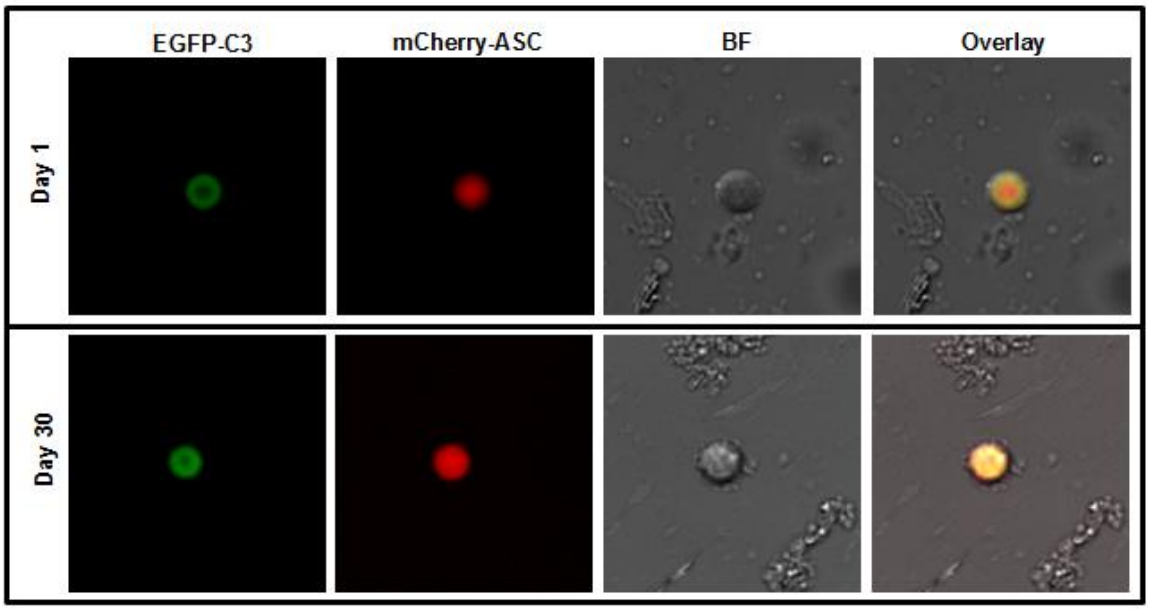

Figure 5.19. ASC speck co-aggregates are remarkably stable. EGFP-C3 proteins remained on the ASC speck after the purification step, which includes rigorous sonication. ASC speck co-aggregates also survived prolonged incubation at 37 °C in PBS solution for 30 days. The brightness of images is not proportional with actual signal intensity. BF: Bright field.

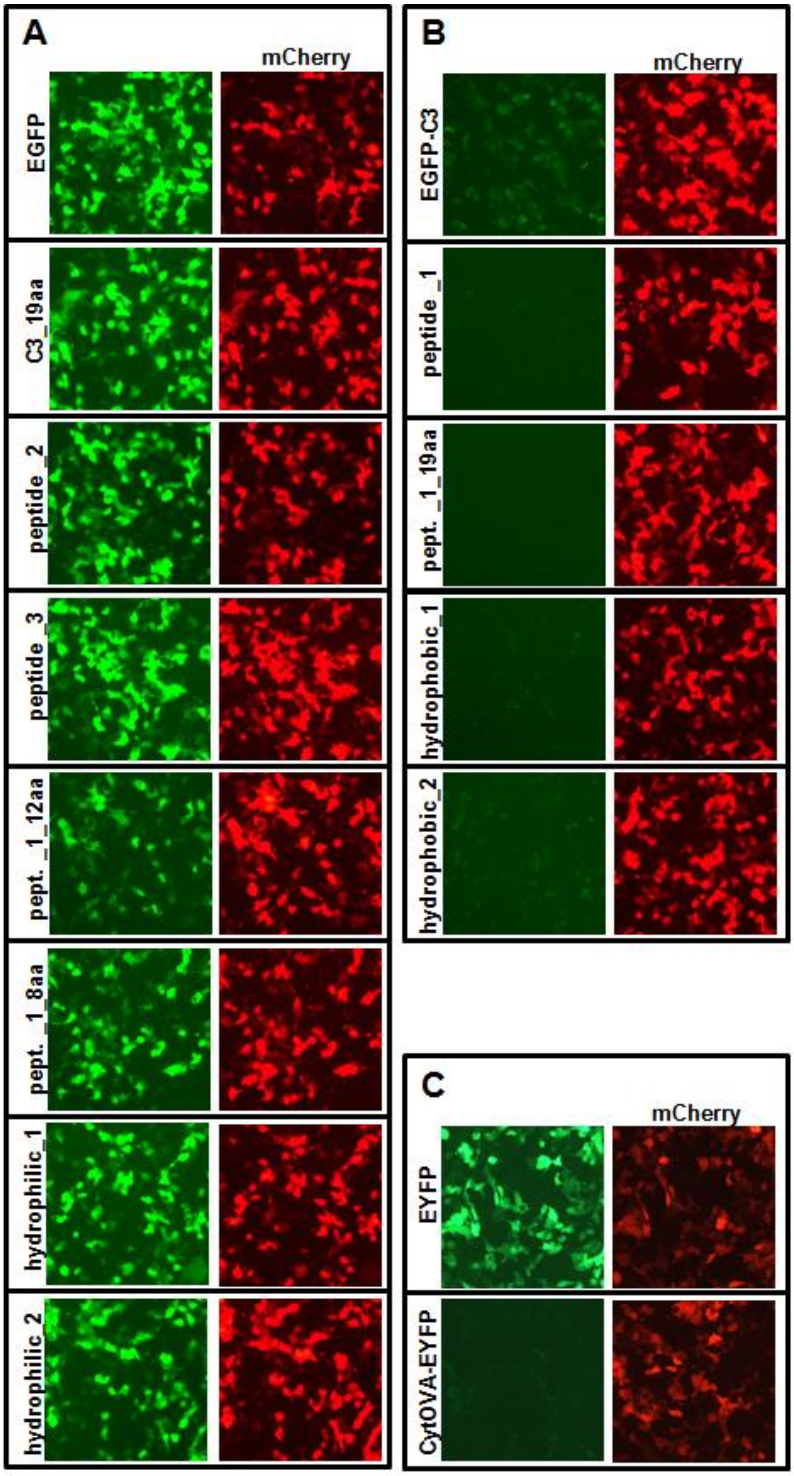

Figure 5.20. Relative fluorescence intensity of constructs accumulating or not accumulating on the ASC speck. (A) EGFP-peptide constructs that do not accumulate on the ASC speck. (B) EGFP-peptide constructs that accumulate on the ASC speck. Exposure times between images in (A) and (B) are equal. (C) Relative fluorescence of EYFP and CytOVA-EYFP constructs. Exposure times between images in (C) are equal. Each construct was co-transfected with mCherry as a control.

5.7. Proteins that accumulated on the ASC speck are expressed poorly.

Apart from the hyrophobicity of EGFP-peptide fusion constructs, another common property of all ASC speck accumulating fusion proteins is their relatively low expression level. We have first noticed this in the relative brightness of transfected cells and later confirmed our observation by Western blotting (Figure 5.20, 5.21). We hypothesized that constructs that accumulated on the ASC speck might be misfolded and/or ubiquitinated proteins with a short lifespan in the cell. It was already shown that the ASC speck itself is ubiquitinated and shares a wide range of common properties with aggresomes and other aggresome-like structures as discussed in detail in Section 1.7.

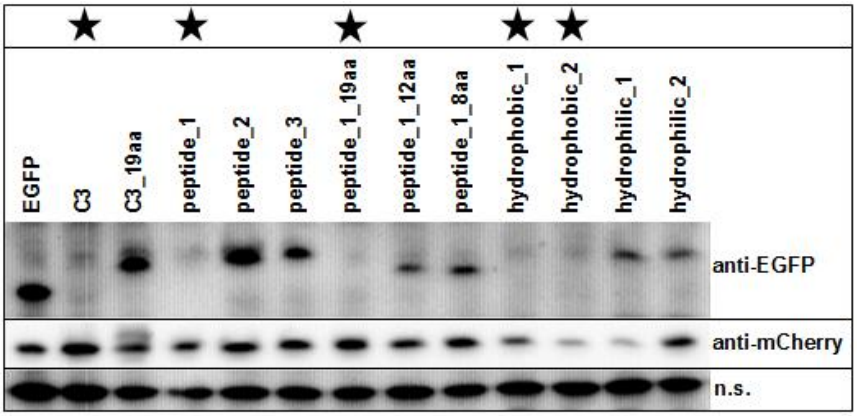

Figure 5.21. Western blot analysis of EGFP-peptide constructs. Constructs that accumulate on the ASC speck are marked with stars, and are characterized with poor expression levels. mCherry was used as transfection control. n.s.: non-specific (loading control).

5.7.1. The ASC specks are ubiquitinated

We confirmed the ubiqutination of ASC specks using HEK293T cells stably expressing EGFP-ASC fusion protein. These cells express low levels of EGFP-ASC protein showing a diffused distribution throughout the cell. When EGFP-ASC stable HEK293T cells were transfected with NLRP3 encoding plasmid, 50% of cells display perinuclear ASC specks, whereas NLRP3 plasmid untransfected cells display less than 1% spontaneous ASC speck formation. We have shown that mCherry-UBB construct displayed near

complete co-localization with ASC specks in mCherry-UBB (+), ASC speck forming stable cells, whereas mCherry reporter alone failed to co-localize with the ASC speck (Figure 5.22). Samples were further analyzed by Western blotting (Figure 5.23). Western blot analysis revealed a strong smear after mCherry-UBB, which is thought to be due to ubiquitin conjugation. Also, co-transfection of NLRP3-FLAG with mCherry-UBB caused a higher molecular weight smear, which is thought to represent NLRP3-mCherry-UBB conjugates. Co-transfection of ASC with mCherry-UBB did not affect its molecular weight.

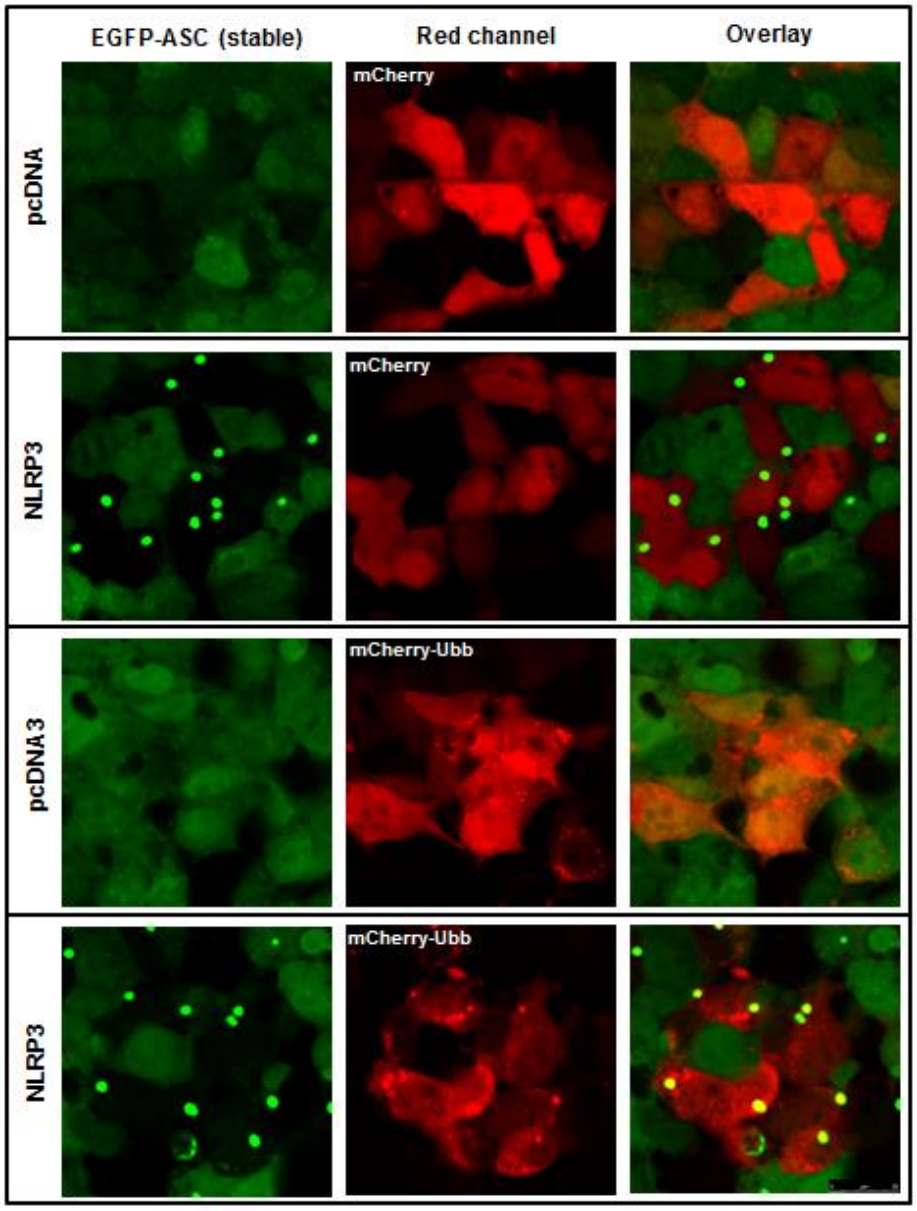

Figure 5.22. The ASC speck is ubiquitinated. The ASC specks formed in EGFP-ASC stable HEK293T cells upon NLRP3 overexpression co-localize with mCherry-UBB but not with mCherry alone.

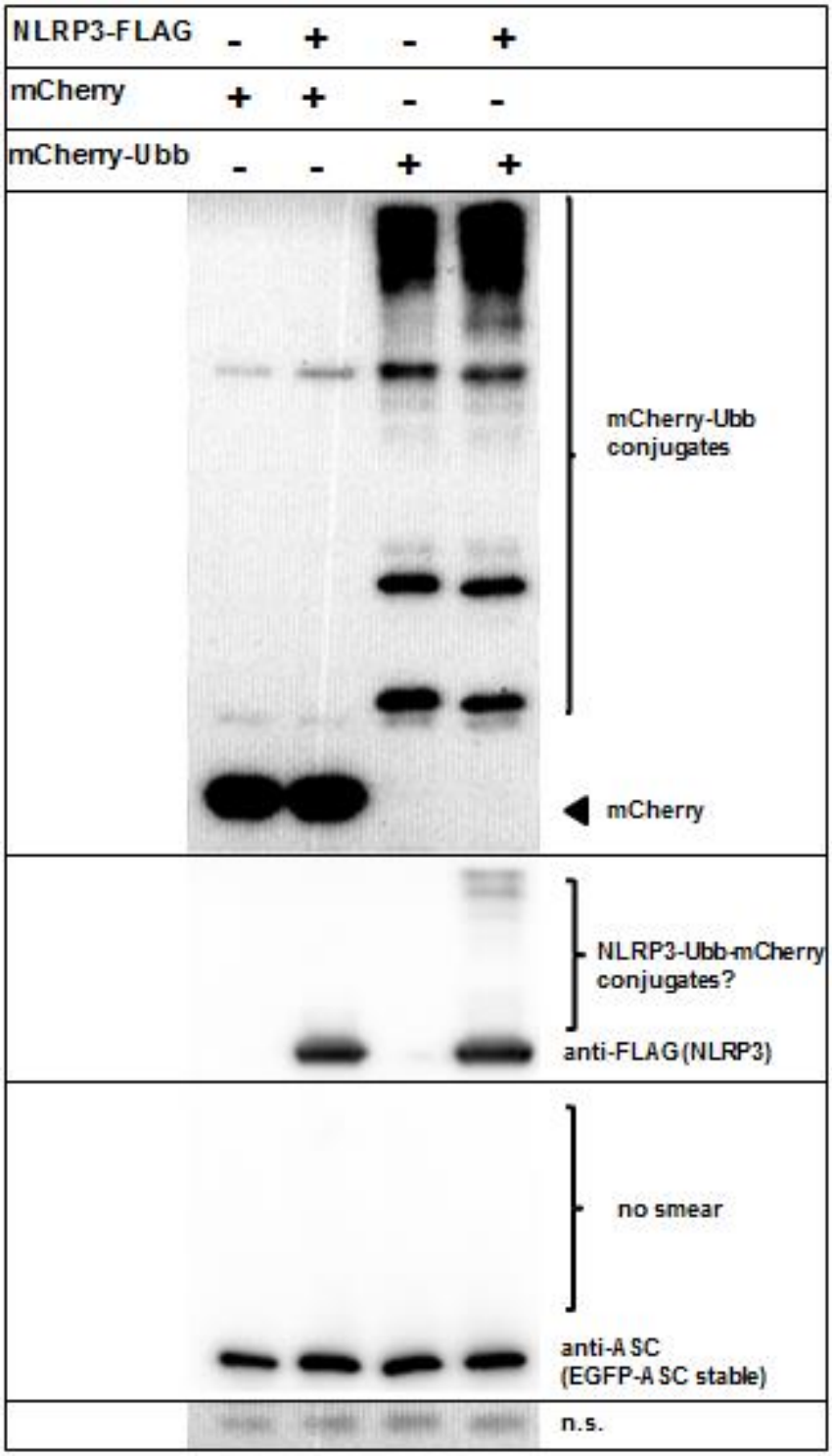

Figure 5.23. Western blot analysis of the samples in the Figure 5.22. Strong smears after mCherry-UBB and NLRP3-FLAG bands were detected. No smear was detected after ASC.

5.7.2. CytOVA-EYFP construct co-localizes with NLRP3 induced ASC specks formed in mCherry-ASC stable HEK293T cells

We ran a similar experiment using NLRP3-induced ASC speck formation in mCherry-ASC stable HEK293T cells using the CytOVA-EYFP construct. Similar to Section 5.11, mCherry-ASC stable HEK293T cells produce perinuclear ASC specks when transfected with NLRP3 encoding plasmid (Figure 5.24, 5.25). These ASC specks co-localized with CytOVA-EYFP construct at 4.63 ± 0.83 % frequency, which increased to 31.3 ± 4.4 % upon MG132 treatment (Figure 5.26). The cellular levels of CytOVA-EYFP construct upon MG132 treatment was also increased as shown by Western blot and increased brightness in fluorescence microscopy (Figure 5.26, 5.27). MG132 treatment has no detectable effect on ASC speck formation frequency (mock: 363.8 ±32.3 versus MG132: 379.5 ± 27.8 per visual field) or protein levels of mCherry-ASC and NLRP-FLAG in our experimental system (Figure 5.27). As a control, we showed that EYFP alone did not co-localize with the ASC speck in the presence or absence of MG132 treatment (Figure 5.24, 5.25). Our results suggest that co-aggregation of cytosolic proteins on the ASC speck is enhanced by relative abundance of the co-aggregating protein and proteasomal inhibition.

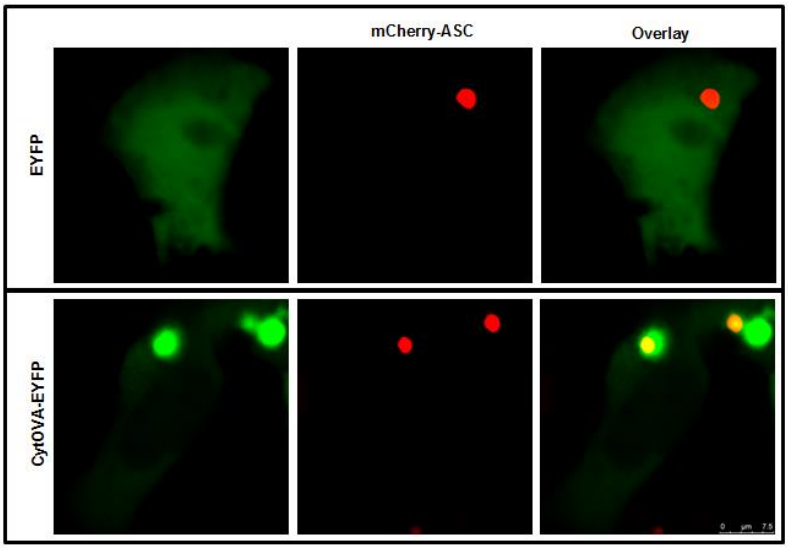

Figure 5.24. CytOVA-EYFP construct co-localizes with the ASC speck in mCherry-ASC stable cells. Speck formation was induced in mCherry-ASC stable cells by NLRP3 overexpression. CytOVA-EYFP but not EYFP alone was observed to co-localize with the ASC speck.

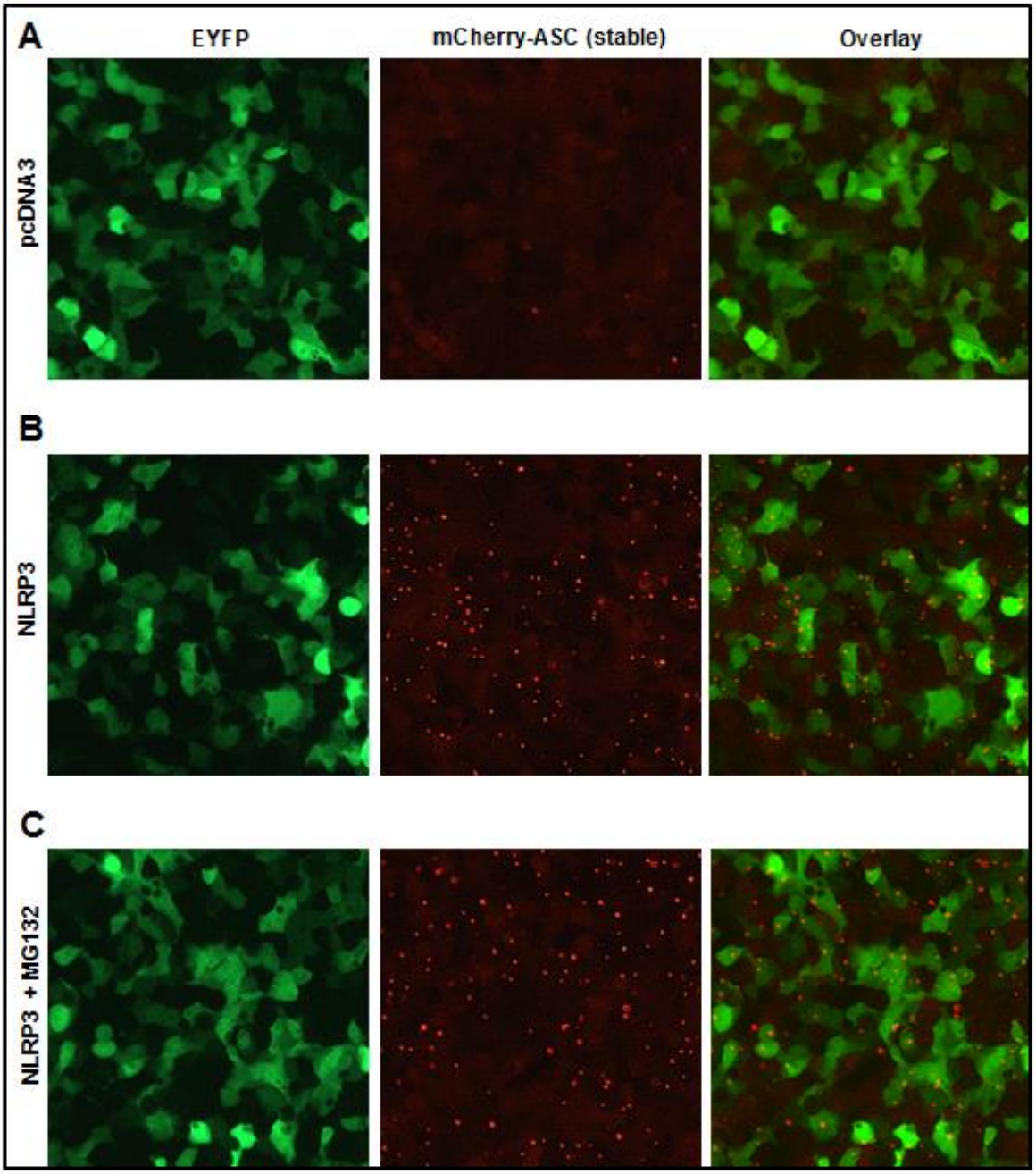

Figure 5.25. NLRP3 overexpression induced ASC speck formation in mCherry-ASC stable HEK293T cells. General view of mCherry-ASC stable HEK293T cells transfected with either empty plasmid pcDNA3 (A), NLRP3 encoding plasmid (B) or NLRP3 encoding plasmid + 10 μM MG132 treatment for 6 h, 24 h after transfection (C). Exposure times between images are equal. EYFP alone did not co-localize with the ASC speck in the presence or absence of MG132.

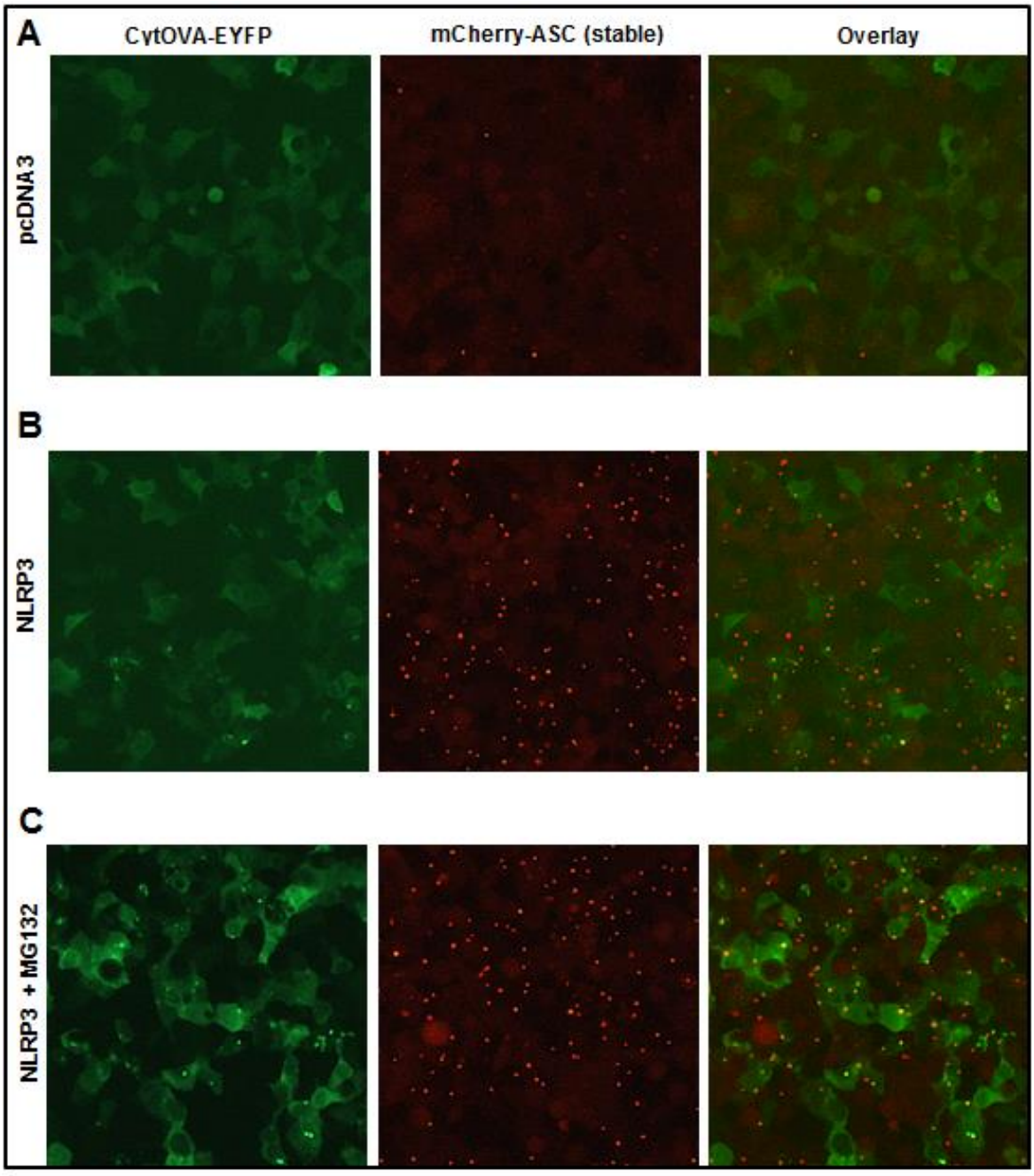

Figure 5.26. Co-localization frequency of CytOVA-EYFP construct increases with MG132 treatment in mCherry-ASC stable cells. General view of mCherry-ASC stable HEK293T cells transfected with either empty plasmid pcDNA3 (A), NLRP3 encoding plasmid (B) or NLRP3 encoding plasmid + 10 μM MG132 treatment for 6 h, 24 h after transfection (C). Exposure times between images in this figure are equal. Exposure times of EYFP channel in this figure are 5X higher compared to Figure 5.25. An obvious signal increase of CytOVA-EYFP construct upon MG132 treatment was observed.

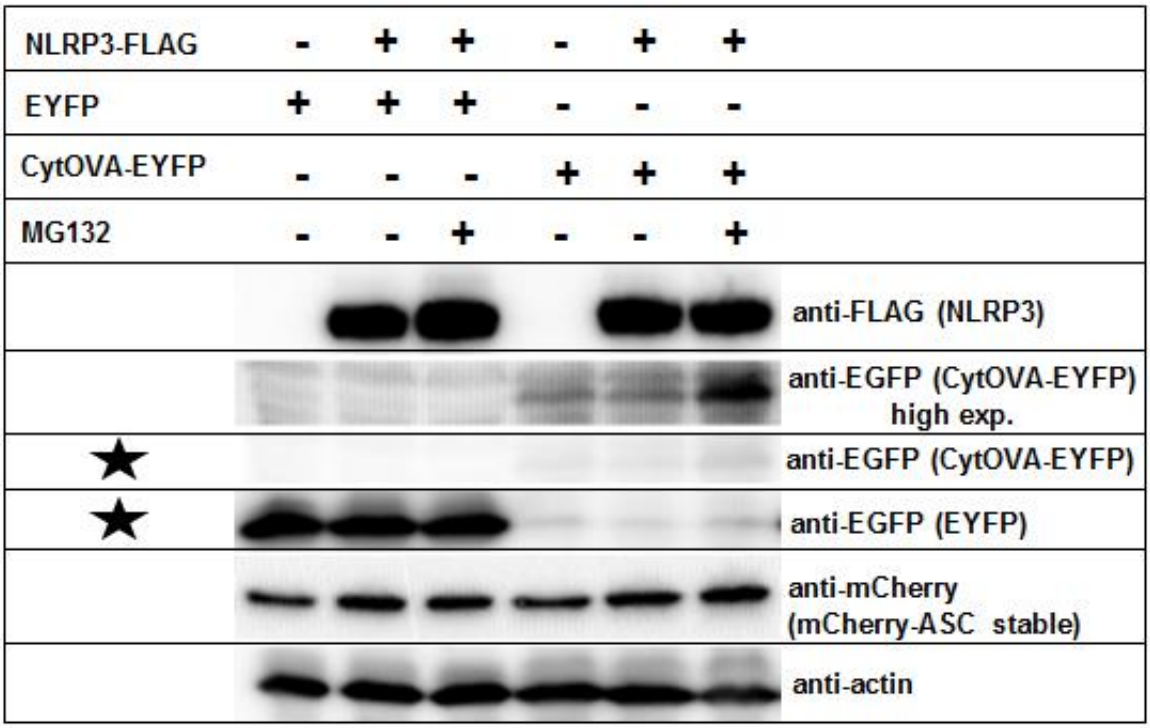

Figure 5.27. Western blot analysis of the samples in Figure 5.25 and Figure 5.26. Exposure times of the rows with the stars are equal. Notice high intensity difference of CytOVA-EYFP and EYFP bands.

5.8. ASC specks are observed extracellularly when PMA differentiated EGFP-ASC stable THP-1 cells are treated with MSU cystals

What happens after inflammasome activation is an ongoing debate. While a series of reports show that pyroptotic cell death is following inflammasome activation, it is evident that not every immune cell undergoes cell death upon inflammasome activation. In parallel with the pyroptosis model, when PMA differenctiated THP-1 EGFP-ASC stable cells were treated with MSU crystals for prolonged incubation (24 h), we observed free EGFP-ASC specks in the extracellular space (Figure 5.28).

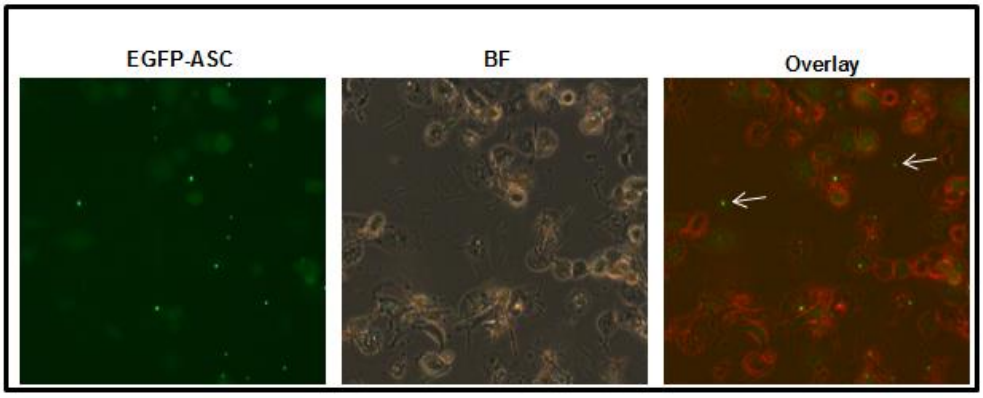

Figure 5.28. Extracellular ASC specks were observed upon treatment of PMA differentiated THP-1 EGFP-ASC stable cells with MSU crystals. Extracellular EGFP-ASC specks were detected 24 h after MSU treatment in cell culture. BF was converted into the red channel for the overlay image. BF: Bright field.

5.8.1. PMA differentiated THP-1 cells are able to engulf extracellular ASC specks

Upon observation of free ASC specks originating from MSU treated THP-1 cells and co-aggregation of cytosolic proteins on the ASC speck, we tested whether other THP-1 cells are able to engulf extracellular ASC specks. Indeed, mCherry-ASC specks purified from HEK293T cells were engulfed by EGFP-ASC stable THP-1 macrophages. We observed that engulfed mCherry-ASC specks and cytosolic EGFP-ASC pool did not co-localize (Figure 5.29).

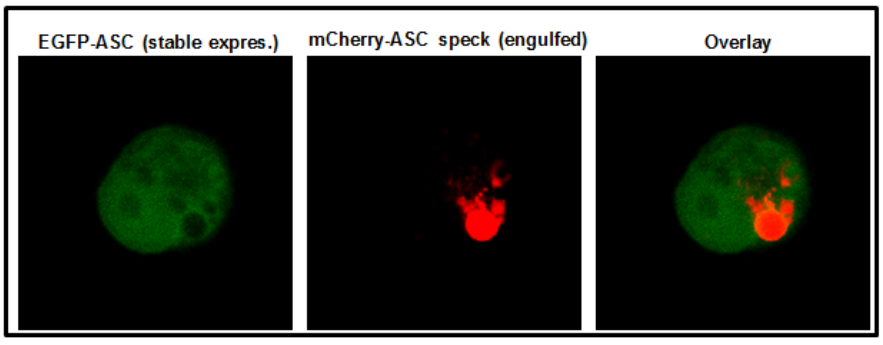

Figure 5.29. THP-1 cells are able to engulf purified ASC specks. THP-1 EGFP-ASC stable cells were incubated with purified mCherry-ASC specks for 3 h. Note the largely intact spherical mCherry-ASC speck and vesicles leaving the phagosome. The cellular pool of EGFP-ASC and engulfed mCherry-ASC specks were localized exclusively.

5.8.2. Engulfed ASC specks are present in an acidic organelle

By lysotracker red staining, we have shown that engulfed ASC specks are present in an acidic organelle. Given the size of the engulfed ASC speck, this organelle is likely to be the phagolysosome (Figure 5.30).

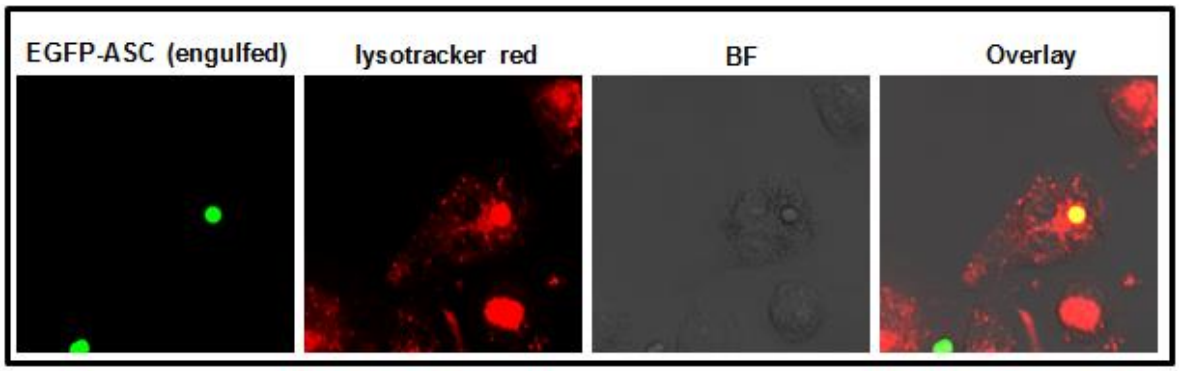

Figure 5.30. Engulfed ASC specks are present in an acidic organelle. PMA differentiatied THP-1 cells were incubated with purified EGFP-ASC specks and stained for acidic organelles using lysotracker red.

5.8.3. Time-lapse imaging of engulfed ASC specks in THP-1 cells reveal globular and tubular vesicles pinching-off from the phagosome

The next question is the fate of the engulfed ASC specks inside the macrophage cells. We investigated mCherry-ASC specks engulfed by EGFP-ASC stable THP-1 cells using time-lapse confocal microscopy. We observed that the bulk of the engulfed ASC speck remained intact during the observation period, and globular and tubular vesicles containing mCherry reporter coming from the engulfed ASC speck to be pinching-off from the phagosome (Figure 5.31). Our results suggest that engulfed ASC specks enter into endosomal trafficking pathway so that its cargo is likely to be presented to the plasma membrane by MHC molecules.

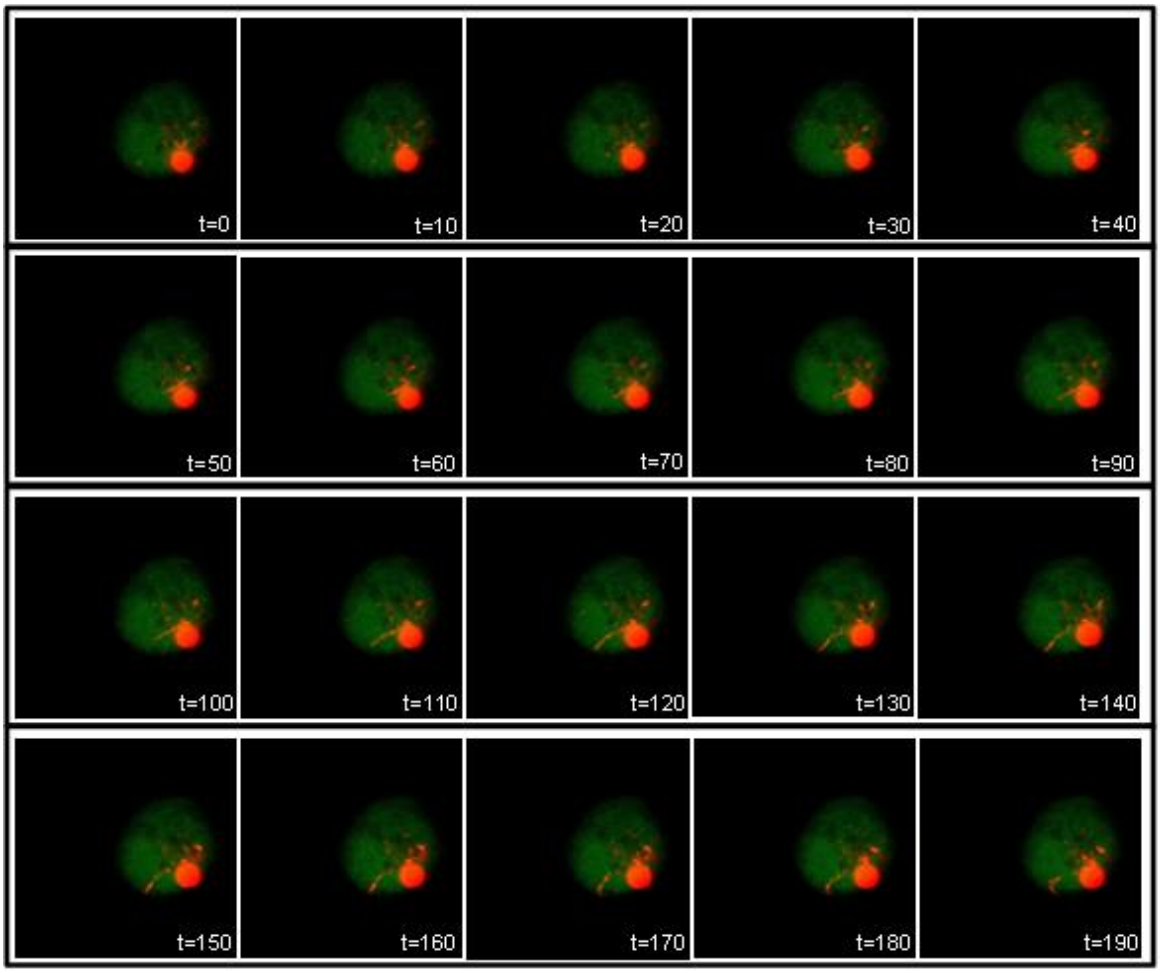

Figure 5.31. Time-lapse imaging of engulfed mCherry-ASC specks in THP-1 EGFP-ASC stable cells. PMA differentiated THP-1 EGFP-stable cells were incubated with purified mCherry-ASC specks for 3 hours. Cells were subsequently imaged by confocal microscopy using an in-house produced growth chamber for 30 minutes. A 90 second long section of the time-lapse movie is shown. Notice tubular vesicles pinching off from the phagosome.

5.8.4. Time-lapse imaging of the ASC speck engulfed by the THP-1 cell reveal controlled release of mCherry reporter

When the same experiment in Section 5.8.3 was repeated without usage of growth chambers that maintain cell culture conditions during time lapse imaging, we observed that THP-1 cells underwent membrane blebbing. As the cell dies by apoptosis, the membrane surrounding the mCherry-ASC speck loosened and became visible. At this time point, the

space between the intact engulfed ASC speck and the phagosomal membrane became visible, which is filled with mCherry signal with a much lower fluorescence intensity compared to the intact ASC speck (Figure 5.32).

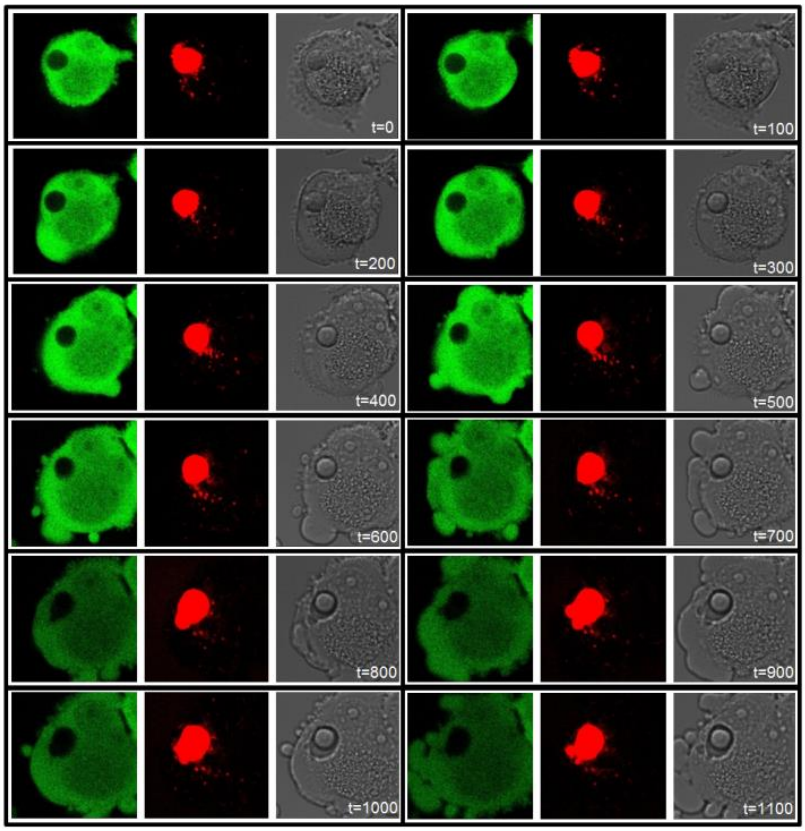

Figure 5.32. Engulfed ASC specks are degraded gradually. PMA differentiated THP-1 EGFP-stable cells were incubated with purified mCherry-ASC specks for 3 hours. Cells were subsequently imaged under a confocal microscope without a growth chamber for 30 minutes. Cells imaged without growth chamber died within this time interval. While cells were undergoing membrane blebbing, the space between the phagosomal membrane and engulfed ASC speck became visible, which was filled with mCherry signal.

5.9. Short isoform of ASC fails to co-localize with EGFP-C3

We have observed that shortASC filaments are incapable of co-aggregating cytosolic proteins unlike the ASC speck formed by the longer isoform (Figure 5.33). Given the knowledge that shortASC can recruit procaspase-1 and contribute to cytokine processing

but it is not the main isoform in humans [56], and that the compact shaped speck structures are observed physiologically unlike shortASC filaments in different organisms, we suggest that the evolutionarily preference of long isoform over short isoform might arise from its ability to accumulate cytosolic proteins, which are probably important in antigen presentation.

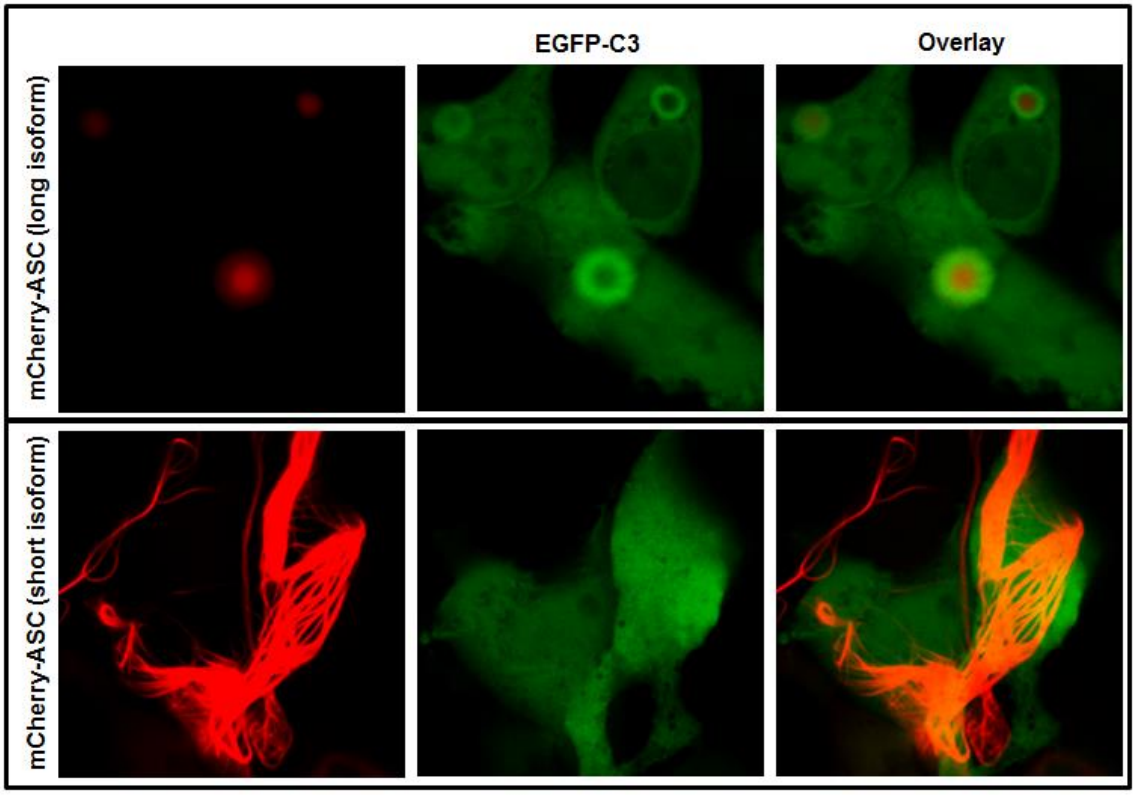

Figure 5.33. Short isoform of ASC fails to co-aggregate EGFP-C3. HEK293T cells were co-transfected with mCherry-labeled long or short ASC isoforms together with EGFP-C3. EGFP-C3 accumulated on ASC specks (upper row). ShortASC filaments did not co-localize with EGFP-C3 yet (lower row).

5.9.1. The abundance of the long isoform determines ultimate shape of the ASC speck

It has been reported that the long isoform is expressed at around 10 times higher levels compared to the short isoform [36, 56]. In HEK293T cells using different color labelled isoforms, we did co-transfection experiments in which either isoforms were trans-

fected 10 times more concentrated compared to the other. We observed that the ultimate shape is determined by the concentration of the more abundant isoform, and co-localization of the 2 isoforms (Figure 5.34). So, the higher amount of the long isoform will favor the ASC speck formation, even in the presence of the short isoform.

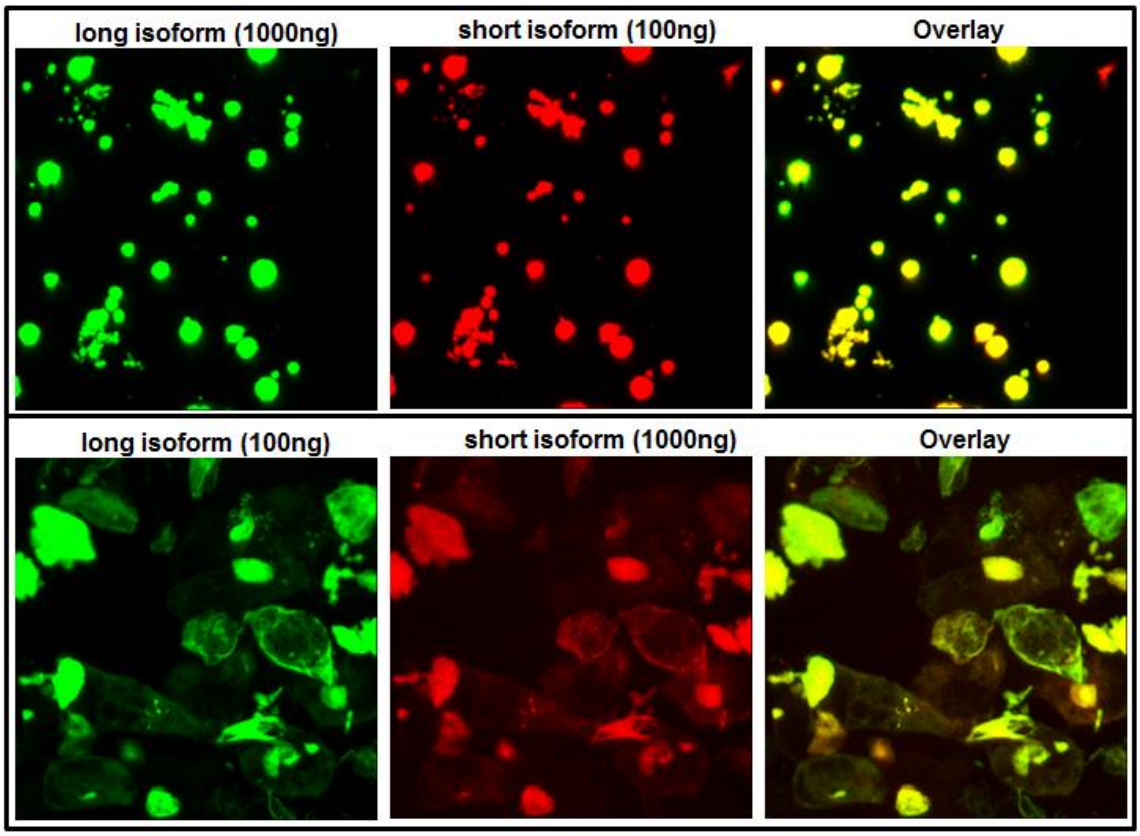

Figure 5.34. Relative abundance of either isoform dictates the overall shape of the ASC speck. HEK293T cells were co-transfected with different color labeled short and long ASC isoforms at indicated concentrations. Notice the compact shape of ASC specks in the upper row and filamentous structures in the lower row.

5.10. ASC specks as particulate antigen delivery vehicles

Targeting APCs with particulate antigen delivery vehicles decorated with adjuvant molecules is an active field of research as discussed in Section 1.6.2. Based on the observation that macrophage cells are able to engulf ASC specks and degrade gradually within the cell, we suggested that ASC specks can be used in antigen delivery applications. For the purpose of using the ASC speck as an antigen delivery vehicle, we filed a national pa-

tent application on 24.04.2012 with the reference number 32178-01 and a corresponding international application (PCT/IB2013/053079).

5.10.1. Intradermal injection of mCherry-ASC specks

One advantage of particulate delivery systems is to prolong antigen stability within a system in order to increase the duration of antigen presentation. We designed an *in vivo* experiment in which we injected mCherry-labeled ASC specks intradermally at the dorsal right and mCherry alone at the dorsal left of the shaved balb/c mice. We observed fluorescence intensity of injected areas using a stereo fluorescent microscope. Injected areas were photographed at days 0, 1, 2, 7 and 15. We noticed that just after injection, ASC specks accumulated in a confined area unlike mCherry alone, which was dispersed in a larger area (Figure 5.35). The mCherry only signal vanished at day 2. On the other hand, the mCherry-ASC signal was detectable at days 2 and 7, but was eliminated at day 15 (Figure 5.36). We concluded that coupling of mCherry to the ASC speck increases its persistence in the system.

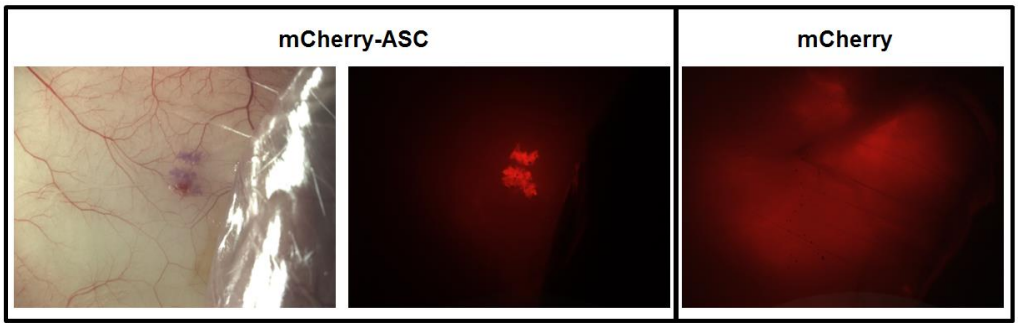

Figure 5.35. Intradermal localization of the injected sample. One mouse was sacrificed and opened-up after being injected with mCherry-ASC specks at dorsal right and with mCherry at dorsal left intradermally.

5.10.2. Flagellin-ASC specks activate NF-κB signaling

Particulate vaccines are often decorated with ligands that activate adjuvant pathways such as TLR ligands [68]. Flagellin is known to activate TLR5 and NF- κB pathway in the downstream signaling events [93]. We cloned flagellin encoding gene (FliC) from *S.*

typhimurium and fused it to ASC. Then, we extracted FliC-ASC specks from HEK293T cells and incubated PMA differentiated THP-1 cells with FliC-ASC specks. FliC-ASC specks were observed to activate NF-κB pathway in THP-1 cells as reported by an increase in phospho I-kappa beta alpha levels over a period of 90 minutes and temporary degradation on I-kappa beta alpha in the first 30-60 minutes followed by an increase to normal levels (Figure 5.37).

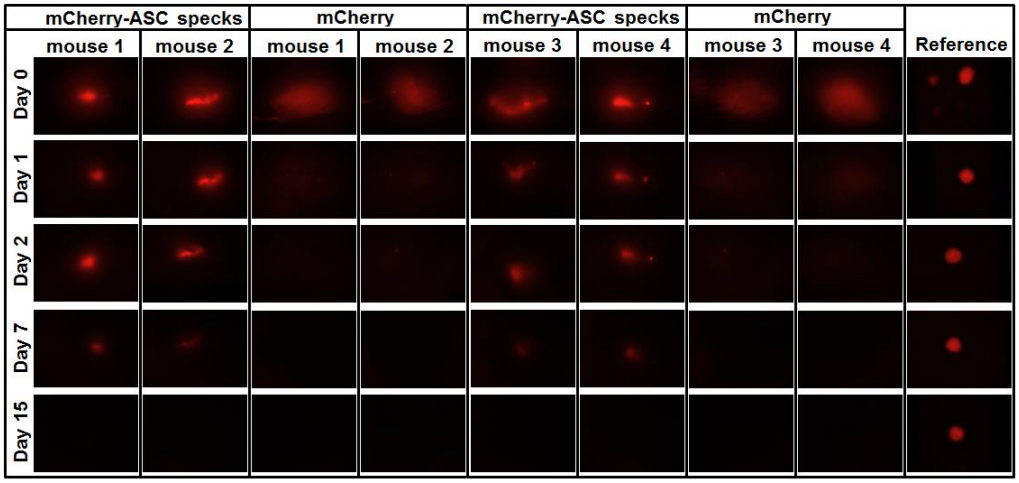

Figure 5.36. Intradermal injection of mCherry-ASC specks. Mice were photographed with a stereo fluorescent microscope at days 0, 1, 2, 7, 15. In order to monitor fluctuations in the fluorescence intensity of the light bulb, a reference of mCherry protein dropped on a filter paper was used.

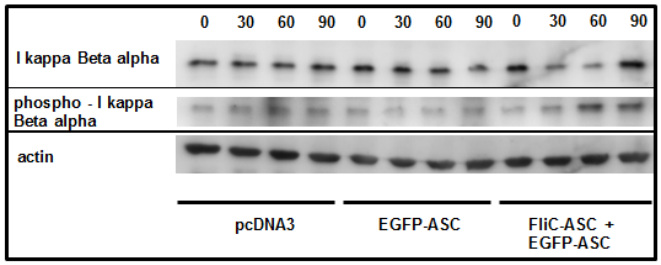

Figure 5.37. Flagellin-ASC specks activate NF-κBsignaling. ASC speck extraction procedure was applied to pcDNA3 (neg. control), EGFP-ASC and FliC-ASC+EGFP-ASC transfected HEK293T cells. PMA differentiated purified specks were incubated with THP-1 cells and cells were analyzed by Western blot, to monitor NF-κB activation. Flagellin-loaded ASC specks were observed to induce I-kappa beta alpha phosphorylation from 0 to 90 minutes and degradation of I-kappa-beta-alpha from 0 to 60 minutes which was recovered 90 minutes after induction.

6. DISCUSSION

The micrometer-sized structure formed by the ASC protein, namely the ASC speck was discovered before the function of ASC as an adaptor protein was assigned in different inflammasome pathways [54]. Later, the ASC speck was proposed to be the activation platform for caspase-1-dependent cytokine processing [36]. The ASC speck is often referred to as an aggregate due to its compact shape and size. Indeed, the ASC speck shares similar properties with aggresome and other aggresome-like structures, as comparatively listed in Table 1.2. One important difference of the ASC speck compared to the aggresome is its rapid formation kinetics, as the redistribution of ASC monomers into a single focus takes only a few minutes compared to the formation of aggresome for hours. The rapid formation of the ASC speck can be explained by highly specific PYD-PYD (pyrin domain) and CARD-CARD (caspase recruitment domain) interactions, which consume the complete pool of ASC monomers in an oligomerization cascade and form a single ASC speck per cell. In an immunological context, the rapid formation kinetics of the ASC speck is meaningful, as response times in other innate immune pathways, such as NF-κB, are measured in minutes to fulfill "the first line of the protection" duty.

Due to similarities between the ASC speck, aggresome and other aggresome-like structures, it remained as an open question whether the ASC speck is formed by non-specific interactions in the traditional way aggregate formation occurs (non-specific hydrophobic interactions) or via PYD- and CARD-dependent specific interactions. The mutational screen we carried out on the full-length ASC protein points out the second option is a more likely scenario. We have shown that mutations inhibiting PYD-PYD and CARD-CARD interactions also disrupt the ASC speck formation (Figure 5.3, 5.7, 5.8, Table 5.1). If it was the case that ASC specks were formed simply by aggregation of non-specific hydrophobic patches of ASC proteins, then the expectation would be that mutations important for PYD-PYD and CARD-CARD interactions should have little or no importance. Our observations point in the opposite direction.

In total, 11 out of 23 mutations we have created on the full length ASC protein disrupted the ASC speck and instead, filament structures were observed. We hypothesized that these filaments formed by mutant full-length ASC proteins could arise due to the remaining intact domain. Indeed, two combinations of PYD-CARD double mutations (K26A-R160A and L68A-R160A) destroyed filaments completely (Figure 5.5). We observed filaments formed by isolated wt PYD and wt CARD as well, which were inhibited in mutated PYD and CARD isolated domain constructs (Figure 5.6).

Presently, there are two published mutational screens focusing on the PYD and one focusing on the CARD of ASC [59-61]. The comparative listing of results in our study and previous work focused on PYD of ASC were summarized in Table 6.1. We observed a discrepancy between our work and a previous PYD filament formation study for mutations E13A, L25A, E62A, E67A and L73A [60]. Regardless, our mutational screen results in PYD isolated domain and full-length ASC, and the results from Co-IP/GST-pull down experiments by another group are in agreement with each other [59].

Table 6.1. Comparison of the results in our study and previous studies focused on PYD of ASC.

PYD mutant	Filament formation our study	Filament formation previous study [60]	Co-IP/GST pull-down previous study [59]
wt	+	+	+
E13A	-	+	-
E19A	-	-	N/A
K21A	-	-	-
L25A	+	-	+
K26A	-	-	-
R41A	-	-	-
D48A	-	-	-
D51A	-	-	-
E62A	+	-	N/A
E67A	+	-	+
E68A	-	-	N/A
L73A	-	+	N/A

The mutational screen focused on the CARD of ASC has only one overlapping mutation with our study, which is arginine residue at point 160 substituted with glutamic acid (charge swapping mutation) [61]. Independent of this study, we have identified M159A and R160A residues as CARD filament and ASC speck-disrupting mutations. We have observed the disruption of the ASC speck in agreement with their work. However, in their sudy it has not been stated that ASC speck-disrupting mutations displayed filament structures, possibly due to low image magnification.

Filaments formed by isolated PYD and CARD were proposed to arise due to specific PYD-PYD and CARD-CARD interactions. Indeed, the mutations that were observed to inhibit filament formation in our study (Figure 5.7, 5.8) were also reported to inhibit PYD-PYD interactions by Co-IP and GST-pull down experiments (and vice versa) by another group [59]. The overlapping results of both studies strongly suggest that filament formation by isolated PYD is due to specific interactions between domains. Another evidence of the filament formation specificity is the loss of co-localization of PYD and CARD filaments in co-transfected cells (Figure 5.6). In a previous study however, PYD and CARD filaments were shown to co-localize in COS-7 cells [94]. This co-localization could be due to a cell specific factor that could interact with both domains. It is generally accepted that PYD and CARD containing proteins associate via homotypic PYD-PYD and CARD-CARD interactions [95, 96]. Our results also suggest that the self association of ASC is due to homotypic interactions between domains rather than heterotypic interactions (Figure 5.6).

PYD and CARD are members of the death-fold super family domains. Other members of this family were shown to be able to establish at least three different interaction modes. Recently, it has been suggested that PYD filaments are formed as a result of type I interaction mode, which employs helices 1-4 on one surface and helices 2-3 on the other. PYD and CARD filaments observed in HEK293T cells extend through the cytosol and branch. The branches in filaments suggest that PYD might employ more than one interaction surface. To further prove this idea, we exploited filament formation deficient PYD constructs mutated on the putative type I interaction surface. We observed the full co-localization of D48A mutant PYD on wt PYD filaments, whereas R41A mutant PYD

showed only partial co-localization (Figure 5.11). We confirmed co-localization of D48A PYD on the wt PYD filaments by an *in vitro* FRET experiment which gave a very close relative FRET efficiency compared to the positive control (Figure 5.12, 5.13). In contrast, relative FRET efficiency of R41A PYD is closer to but still significantly higher than the negative control. Our results suggest that PYD of ASC is able to exploit alternative interaction modes other than type I.

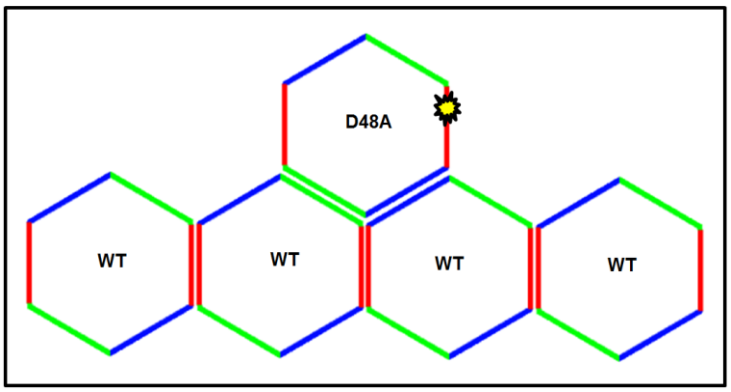

Figure 6.1. The proposed model for alternative interaction modes on the PYD filaments. Red stands for type I whereas green and blue stand for alternative interaction surfaces. D48A mutation was indicated by a star on the type I interaction surface. This model explains: 1) Deficiency of D48A PYD to form filaments, 2) Co-localization of D48A on wt PYD filaments and 3) Absence of interaction in Co-IP and GST pull-down assays.

Note that in a previous study, D48A PYD was reported to be unable to interact with wt PYD according to Co-IP and GST pull-down assays [59]. Both assays monitor interactions between soluble proteins. In our results, we observe filament formation deficiency of D48A PYD by itself, yet it can interact with insoluble wt PYD filaments. The combinatorial results suggest that D48A PYD – wt PYD filament binding interface consists of more than one wt PYDs (Figure 6.1). A similar alignment was shown for FAS/FADD-DISC based on the crystal structure [31, 55].

Our results demonstrate that both domains of the ASC are indispensible for the ASC speck formation. In addition to that, the 23 amino acid long flexible linker between

both domains is also crucial for the ASC speck. The NMR structure of ASC indicates that in solution, ASC is able to adopt a variety of conformations due to the flexibility of the linker [1]. Without the linker, as in the naturally occuring short isoform of the ASC [56], we observe filaments instead of the ASC speck (Figure 5.2, 5.3). One can suggest that the conformational flexibility ensured by the linker avoids sterical hinderance as ASC proteins self-associate. With increased conformational flexibility, PYD and CARD might have more freedom to establish homotypic interactions, which ultimately leads to the highly compact ASC speck.

In one study, the ASC speck imaged under higher magnification was shown to display filamanet extrusions at the periphery of the ASC speck [92]. At least with our imaging setup, we did not observe such obvious filaments at the periphery of the wt ASC speck. However, L25A mutant full length ASC displayed a unique phenotype with short filaments radially pointing outwards from the center of an ASC speck sized structure as we called Medusa's head in this study (Figure 5.3). L25 residue is not conserved between rodents and men, as methionine residue is present at position 25 in mouse and rat. Since papers using mouse cells reported compact shaped ASC specks, we cloned L25M EGFP-ASC construct and observed similar ASC specks compared to wt EGFP-ASC. Note that the filament formation assay we carried out using EGFP-PYD L25A isolated domain and Co-IP/GST pull-down assay in a previous work showed that L25A did not inhibit PYD-PYD interactions [59]. It appears that L25A mutant full length ASC undergoes a deficiency in the compaction of the ASC speck. The effect of L25A mutation and other mutations that disrupt the ASC speck (e.g. D48A on PYD and R160A on CARD) interfere with the different levels of compaction which further supports that the ASC speck is an organized structure.

Collectively, our results demonstrate that the organized structure of the ASC speck depends on PYD and CARD capable of establishing homotypic interactions as well as presence of 23 amino acids long flexible linker. The compact shape of the ASC speck depends on at least two levels of compaction, first the PYD-PYD and CARD-CARD homotypic interactions which are followed by a second compaction level that can be inhibited by the L25A mutation. Furthermore, homotypic PYD interactions are not limited to type I

mode. Ability of PYD (and probably CARD as well) to exploit several interaction modes might explain how PYD and CARD filaments stack into the compact ASC speck, as proposed here by different levels of compaction.

The aggresome-like properties and organized structure of the ASC speck raises the question whether the ASC speck structurally has any evolutionarily advantage against other oligomeric enzyme complexes. The apoptosome and DISC, which are formed by proteins containing death-fold superfamily domains, are oligomeric structures [30-33]. Another possibility is that the ASC speck might have an alternative function utilizing its aggresome-like properties. The ASC speck has almost all the distinctive properties of the aggresome as comperatively listed in Table 1.2. In aditition to these, we observed non-specific co-aggregation of a set of cytoplasmic proteins on the ASC speck in HEK293T cells (Figure 5.15). Based on this initial observation, we hypothesized that co-aggreagation of cytosolic proteins originating from the pathogen on the ASC speck during the intracellular infection might be instrumental in antigen presentation. Inflammasomes are active in professional antigen presenting cells such as DCs and macrophages and also in other cell types that are frequently in contact with pathogens such as neutrophils and keratinocytes [70]. The ASC protein has already been implicated in antigen presentation via inflammasome dependent and independent mechanisms, most notably as an adaptor protein in the NLRP3 inflammasome for the adjuvant effect of alum. Aggregation of ubiquitinated proteins upon LPS stimulation in dendritic cells, namely DALIS, has been implicated in antigen presentation as well. According to our theory, the ASC speck is a novel member of the induced aggresome-like structures, similar to DALIS. Apart from its role in inflammasome activity, the ASC speck samples the cytosolic protein pool, preferrably defected and ubiquitinated proteins, into an aggresome-like structure which might be important in antigen presentation.

Our initial felicitous observation of non-specific co-aggregation of cytosolic proteins on the ASC speck was detected upon co-transfection of mCherry-ASC fusion protein with EGFP-C3 construct into HEK293T cells. Later, the same experiment was repeated with different EGFP-peptide constructs, and the results suggest that the hydrophobicity of the peptide might contribute to co-aggregation onto the ASC speck (Figure 5.15). We ruled

out the possibility that co-aggregation might be a result of interactions between fluorescent reporters (Figure 5.17). Also, co-aggregation was observed after ASC specks were extracted from the cell and remained after prolonged incubation in solution, indicating the stability of co-aggregates (Figure 5.19). This observation also disproves the possibility that co-localization might be a result of co-existance within the same membrane enclosed organelle rather than co-aggregation.

We observed relatively low expression levels for ASC speck co-aggregating compared to non-aggregating constructs (Figure 5.20, 5.21). This observation raises the possibility that co-aggregating constructs have a relatively short life span, possibly due to misfolding and subsequent proteasomal clearance. Indeed, expression levels of CytOVA-EYFP construct, which is also expressed at lower levels compared to control (EYFP) was increased upon proteasomal inhibition by MG132 treatment (Figure 5.24). Furthermore, co-localization frequency of CytOVA-EYFP on NLRP3-induced ASC specks increases upon MG132 treatment in mCherry-ASC stable HEK293T cells. It is known that MHC-I dependent presentation of the model antigen ovalbumin depends on ubiquitination and subsequent proteasomal processing. We have also confirmed that NLRP3-induced ASC specks are ubiquitinated in EGFP-ASC stable HEK293T cells. Collectively, our data suggests that the ASC speck co-aggregates hydrophobic, probably misfolded and ubiquitinated proteins in a way similar to aggresomes.

Previously, proteasomal inhibition has been shown to promote formation of aggresome and aggresome-like strucures DALIS and JUNQ [77, 79, 81, 82]. Note that in our experimenal system, MG132 treatment did not alter ASC speck formation frequency or protein levels of ASC or NLRP3, but increased ovalbumin levels, suggesting that co-localization increase is due to elevated levels of the co-aggregating protein. Furthermore, the lack of an increase in the ASC speck formation frequency upon MG132 treatment suggests that ASC speck and aggresome formation events are based on different processes, the former depends on the specific homotypic interaction between PYD and CARD and the latter depends on aggregation of misfolded proteins. However, the ASC speck is capable of incorporating apparently misfolded and ubiquitinated proteins and this ability is increased by proteasomal inhibition. Viruses utilize various mechanisms to hijack the host translation

system and maximize viral protein production including shutting-off host protein translation system [97]. Defective ribosomal products (DRiP), which accounts for around 30% of newly synthesized proteins, are thought to be the major source of antigens to be presented by MHC-I [98, 99]. We suggest that these newly synthesized defective viral proteins are likely to be co-aggregated on the ASC speck similar to the ovalbumin construct in our experimental system.

Thereby, we report here that the ASC speck forms stable co-aggregates with cytoplasmic proteins which might be important in antigen presentation. Although the ASC speck is a highly organized structure, co-aggregation of cytoplasmic proteins on the ASC speck is non-specific which suggest that it can accommodate a wide range of proteins. In case of an intracellular infection which can activate an ASC speck forming inflammasome such as NLRP3, NLRC4 and AIM2, we suggest that pathogenic proteins might co-aggregate on the ASC speck as well. Particularly, this scenario is more likely for viral infections triggering NLRP3 and AIM2 inflammasomes but may also be valid for pathogenic proteins escaping from the phagolysosome into the cytosol. Of note, phagolysosomal damage is one of the proposed activation mechanisms of the NLRP3 inflammasome [100, 101]. The presence of the influenze nucleoprotein at DALIS has been shown in DCs before [86]. Since NLRP3 inflammasome can be activated by influenza virus A, it is an interesting question whether influenza nucleoprotein might also be present at the ASC speck upon infection in DCs [18].

We list here three different routes where antigen co-aggregation on the ASC speck might be important in antigen presentation. In the first scenario, the ASC speck might function as a cytosolic storage for antigens thereby prolonging antigen presentation as reported for DALIS [86]. The second scenario involves autophagy, as autophagic clearance of the ASC speck has been reported before [52]. The autopaghy pathway is important for the cross-presentation of cytosolic antigens via MHC-II molecule [67]. Interestingly, it has been reported that activation of the NLRP3 inflammasome is correlated with secretion of inflammasome components and MHC class II containing exosomes. The authors suggested a model in which IL-1β (and other inflammasome components) might be secreted via MHC class II containing exosomes [46, 47, 102]. This pathway was proposed for explain-

ing the non-classical secretion of the IL-1β [45], although co-aggregation of antigen it the ASC speck, followed by autophagy and trafficing to MHC-II compartment might be relevant to cross-presentation as well.

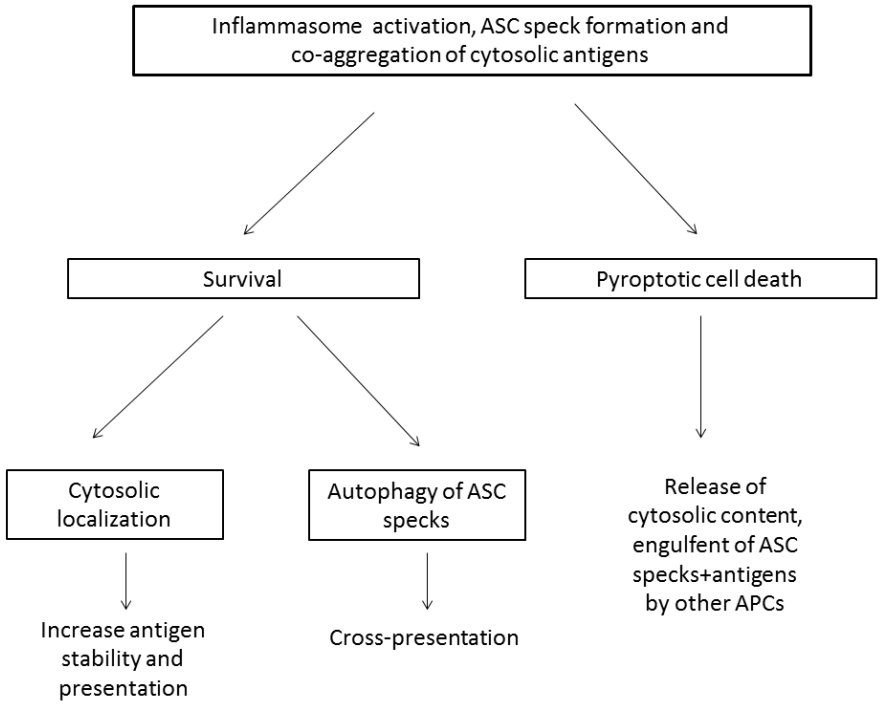

Figure 6.2. Three potential routes for antigen-ASC speck co-aggregates to contribute to antigen presentation.

The first two scenarios involve survival of the cell upon inflammasome activation. The autophagic clearance of the ASC speck has been suggested for the survival of the cell in order to avoid pyroptosis [52, 53]. The third scenario however, involves pyroptosis. Inflammasome activation has been reported to be followed by a specific type of cell death via caspase-1, called pyroptosis [48]. The pyroptotic cell death shares similar features with necrosis such as extracellular release of cytoplasmic content. Indeed, when PMA differentiated stable EGFP-ASC THP-1 cells were stimulated for NLRP3 inflammasome activation with MSU crystals, ASC specks have been observed in the extracellular space (Figure 5.28). We hypothesized that extracellular antigen-ASC speck co-aggregates might be better antigens compared to otherwise soluble, diffuse extracellular pathogenic proteins. There are numerous studies for different nano- or micrometer sized antigen delivery vehicles (particulate adjuvants) which aim to target APCs and increase the stability of the antigen, and thereby duration of antigen presentation [68, 69]. We have shown that purified

ASC specks can be engulfed by THP-1 cells and localized in an acidic organelle upon engulfment (Figure 5.29, 5.20). Furthermore using time-lapse microscopy, we have demostrated dynamic tubular vesicles loaded with degradation products of ASC speck are pinching-off from the phagolysosome (Figure 5.31). These types of vesicles were previously attributed to MHC-II dependent presentation of extracellular antigens [63, 103-105]. We have also demonstrated that phagolysosome contains the large mass of intact ASC speck along with degradation products with a much less fluorescence intensity, suggesting the controlled release of the material in the ASC speck (Figure 5.32). Another interesting point with the extracellular route is that ligands activating AIM2 and NLRC4 inflammasomes, cytosolic DNA and flagellin, also activates TLR9 (unmethylated DNA) and TLR5, respectively [6, 64]. These TLRs are proven adjuvant pathways and their ligands are used as adjuvant molecules in present day vaccines [12]. It has been shown before that cytosolic DNA co-localizes with the ASC speck upon stimulation of the AIM2 inflammasome [35]. Flagellin also physically interacts with NLRC4-NAIP5 hetero-oligomer [14], although for our knowledge co-localization of flagellin has not been reported on the ASC speck. Nevertheless, coupled ligand recognition of cytoplasmic AIM2 and NLRC4 inflammasomes and membrane bound TLR9 and TLR5 might provide additional adjuvanicity to the ASC specks via the extracellular route.

In conclusion, co-aggregation of cytosolic proteins on the ASC speck might be the underlying reason of the ASC speck formation. In that sense, the ASC speck should be classified as an induced aggresome-like structure. The co-aggregation of potential antigenic proteins on the ASC speck has potential implications in antigen presentation and thus provides another link between innate and adaptive immunity.Our results have direct implications on the rational design of novel vaccines. In that sense, we have filed a patent application on 24.04.2012 for using the ASC speck as an antigen delivery vehicle. We have carried out preliminary experiments to show the increased stability of the mCherry on the ASC speck upon intradermal injection in mice (Figure 5.36). Furthermore, ASC specks made of flagellin-ASC fusion protein was shown to induce NF-κB signaling, which might further increase the adjuvanicity of the ASC speck (Figure 5.37). A comprehensive analysis of ASC specks loaded with the model antigen ovalbumin on MHC-I and MHC-II dependent antigen presentation and antibody production is necessary to evaluate the full potential of ASC specks for vaccination applications.

7. APPENDIX A: Plasmid Maps

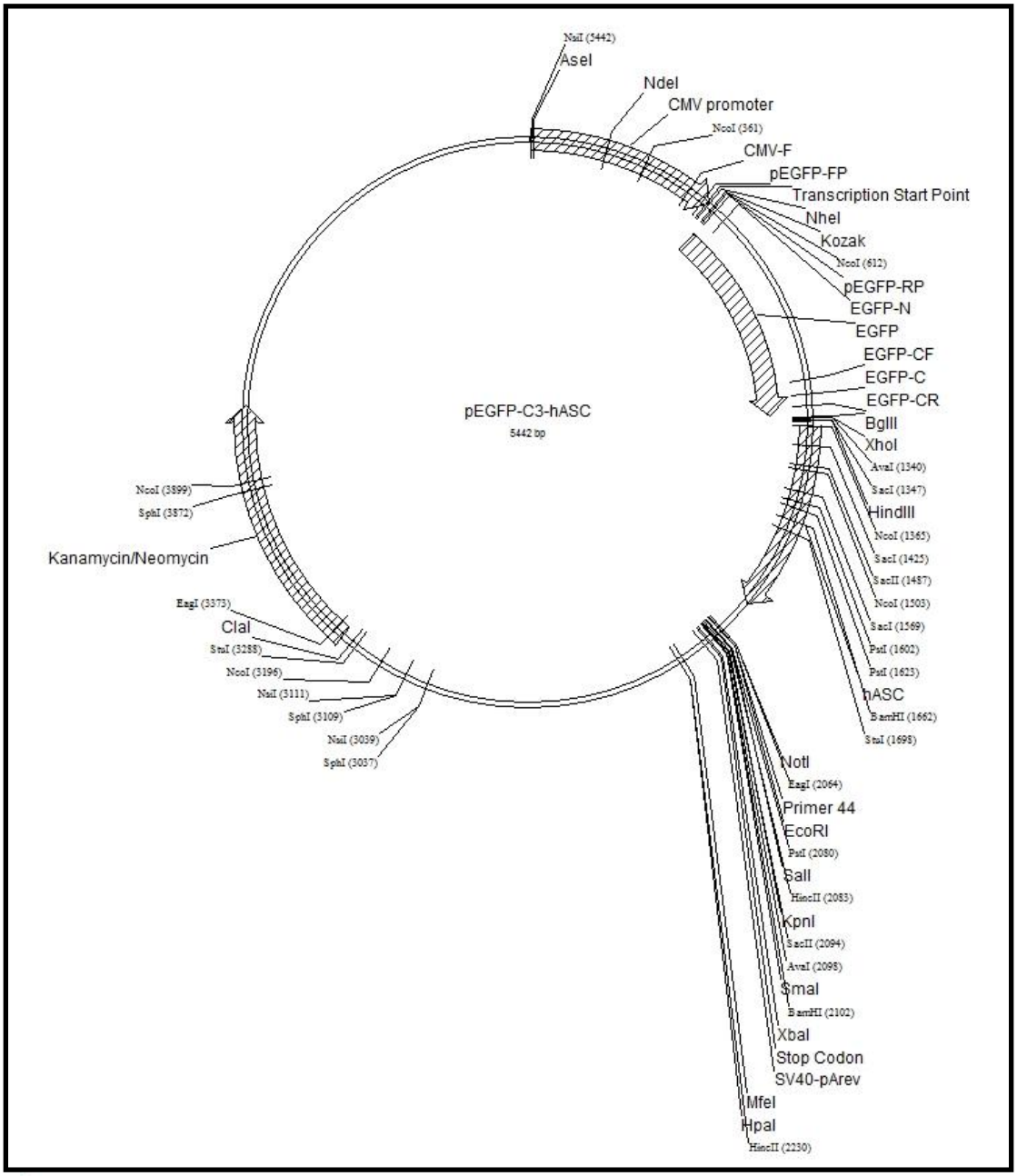

Figure A.1. Plasmid map of pEGFP-C3-hASC. All mutations created on the full length ASC protein were based on this construct.

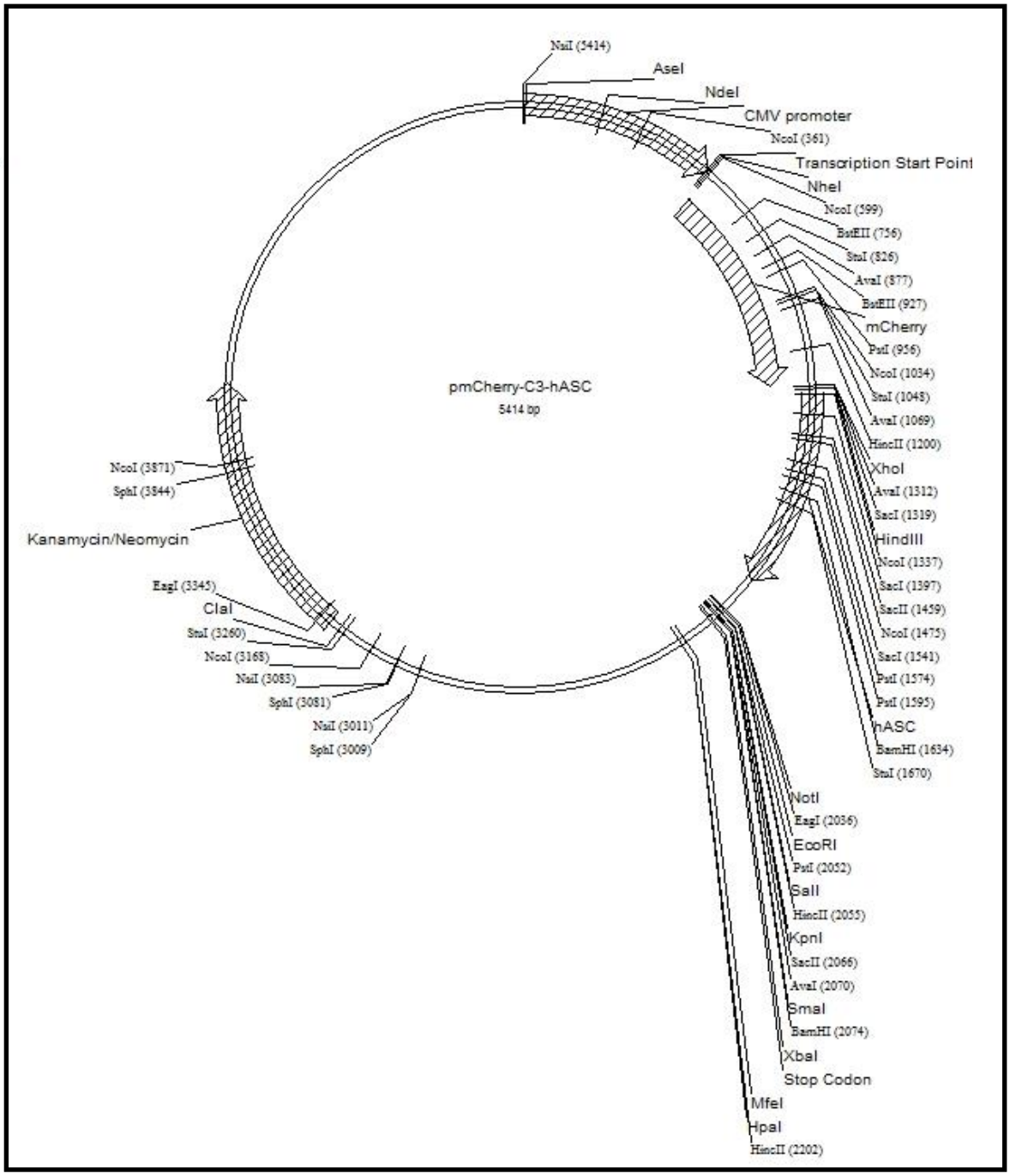

Figure A.2. Plasmid map of pmCherry-C3-hASC.

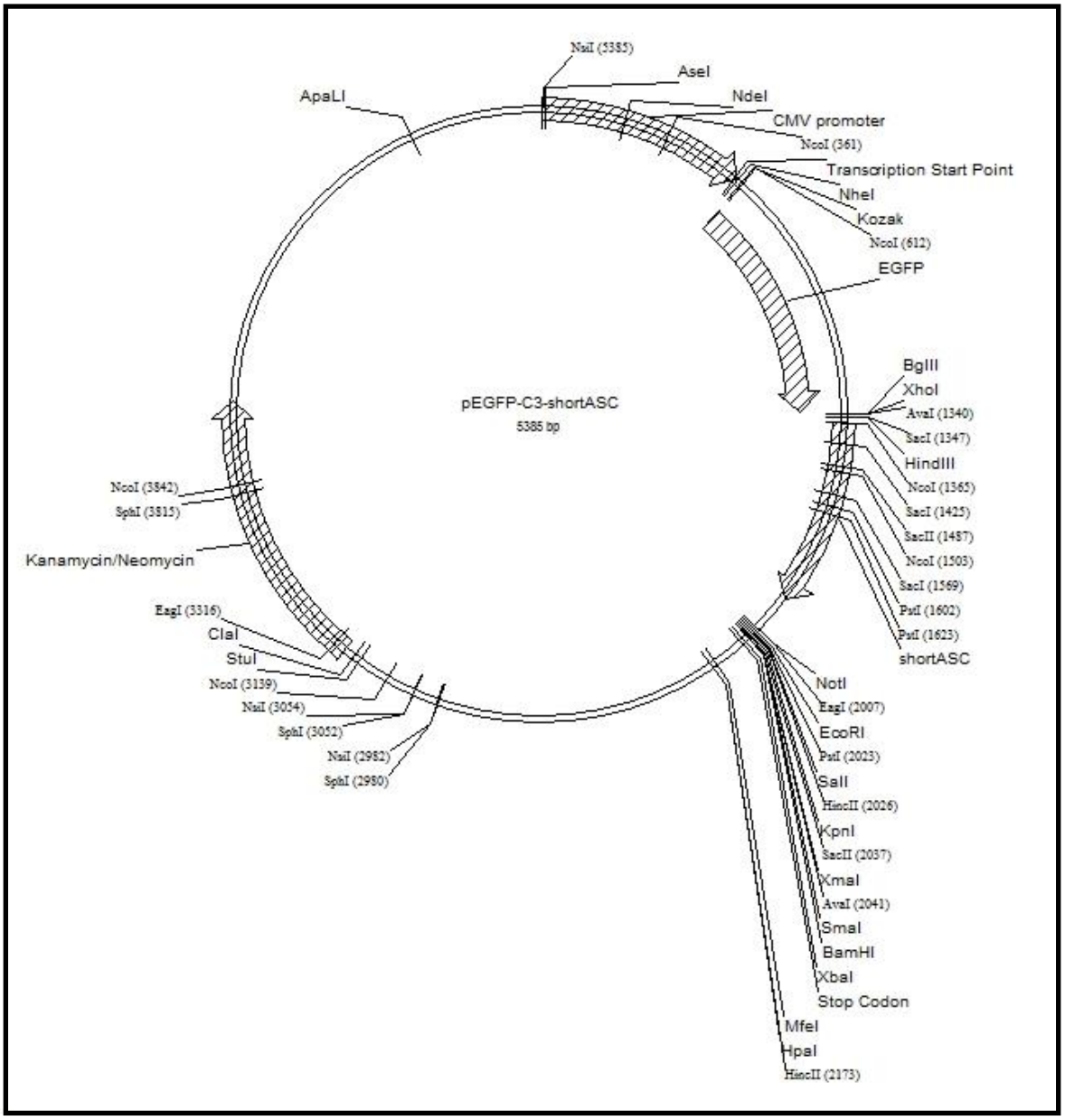

Figure A.3. Plasmid map of pEGFP-C3-shortASC.

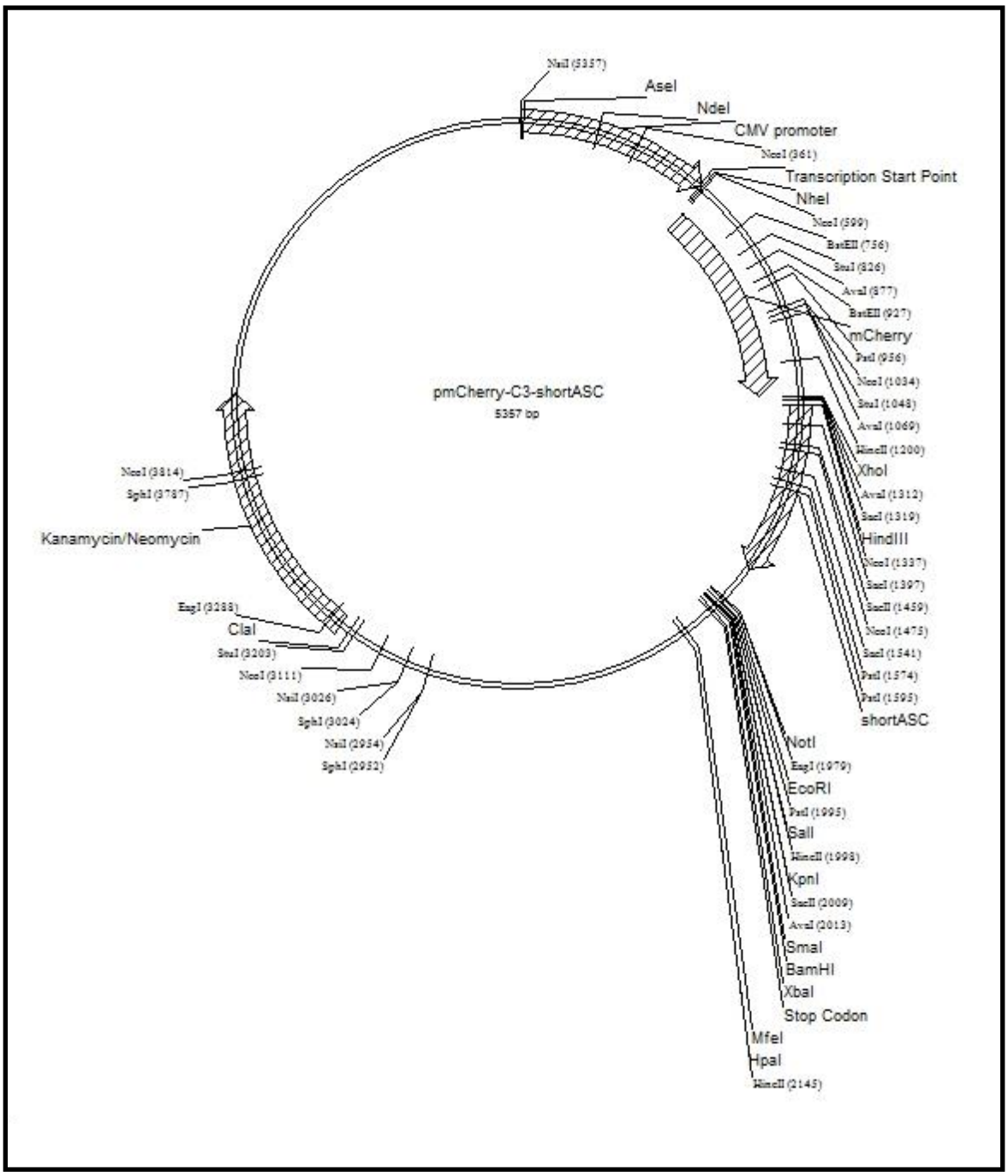

Figure A.4. Plasmid map of pmCherry-C3-shortASC.

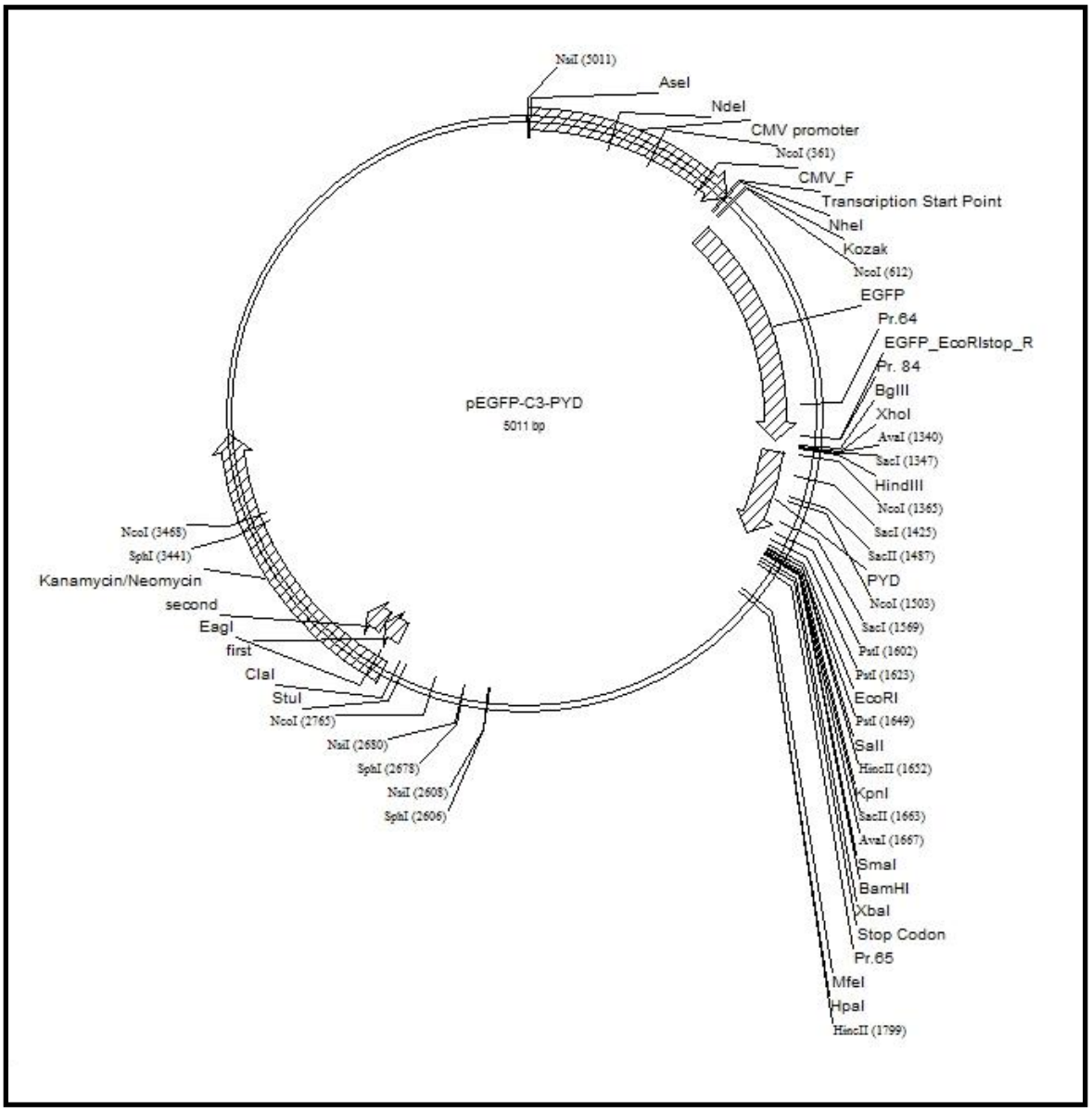

Figure A.5. Plasmid map of pEGFP-C3-PYD

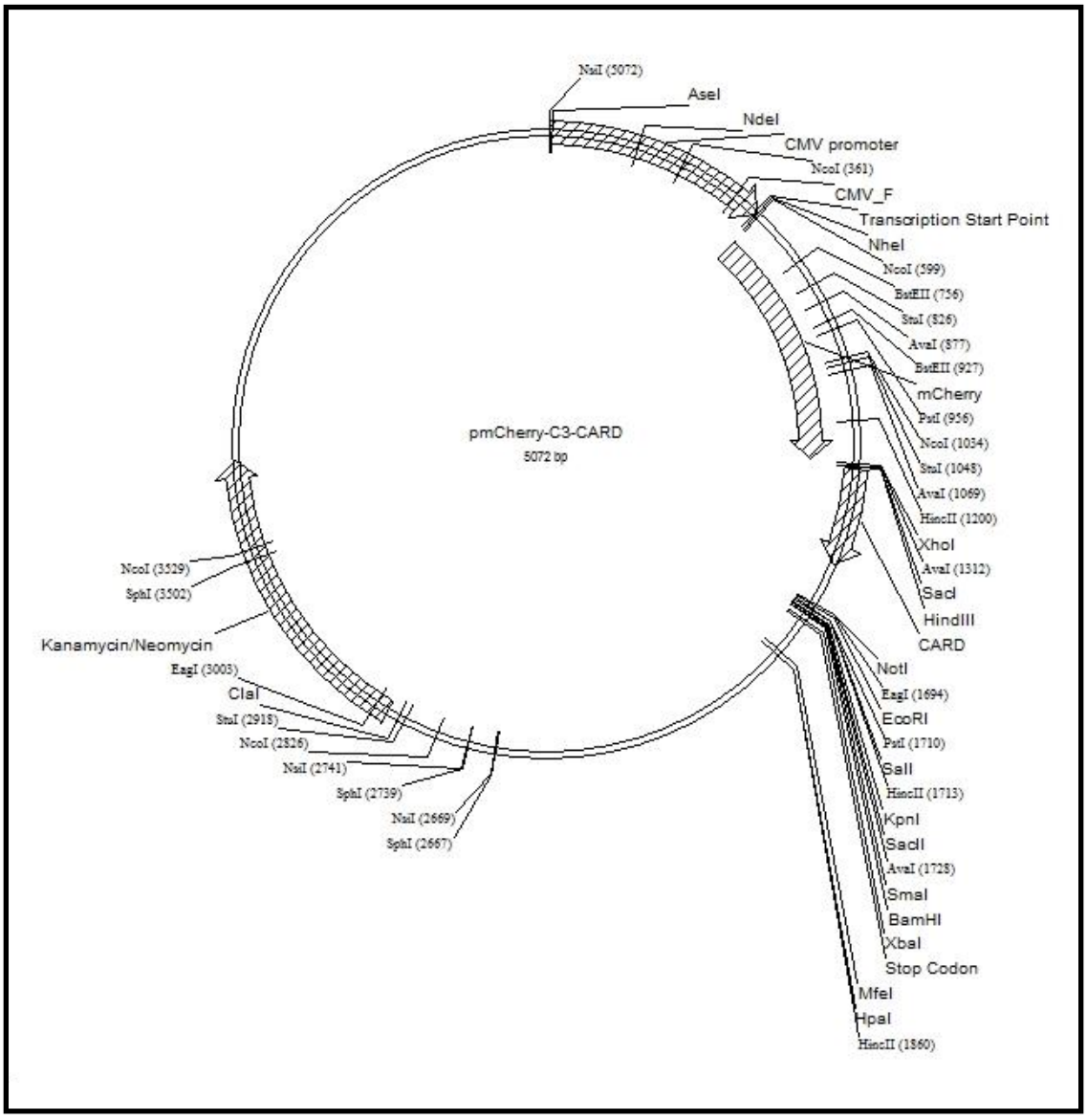

Figure A.6. Plasmid map of pmCherry-C3-CARD.

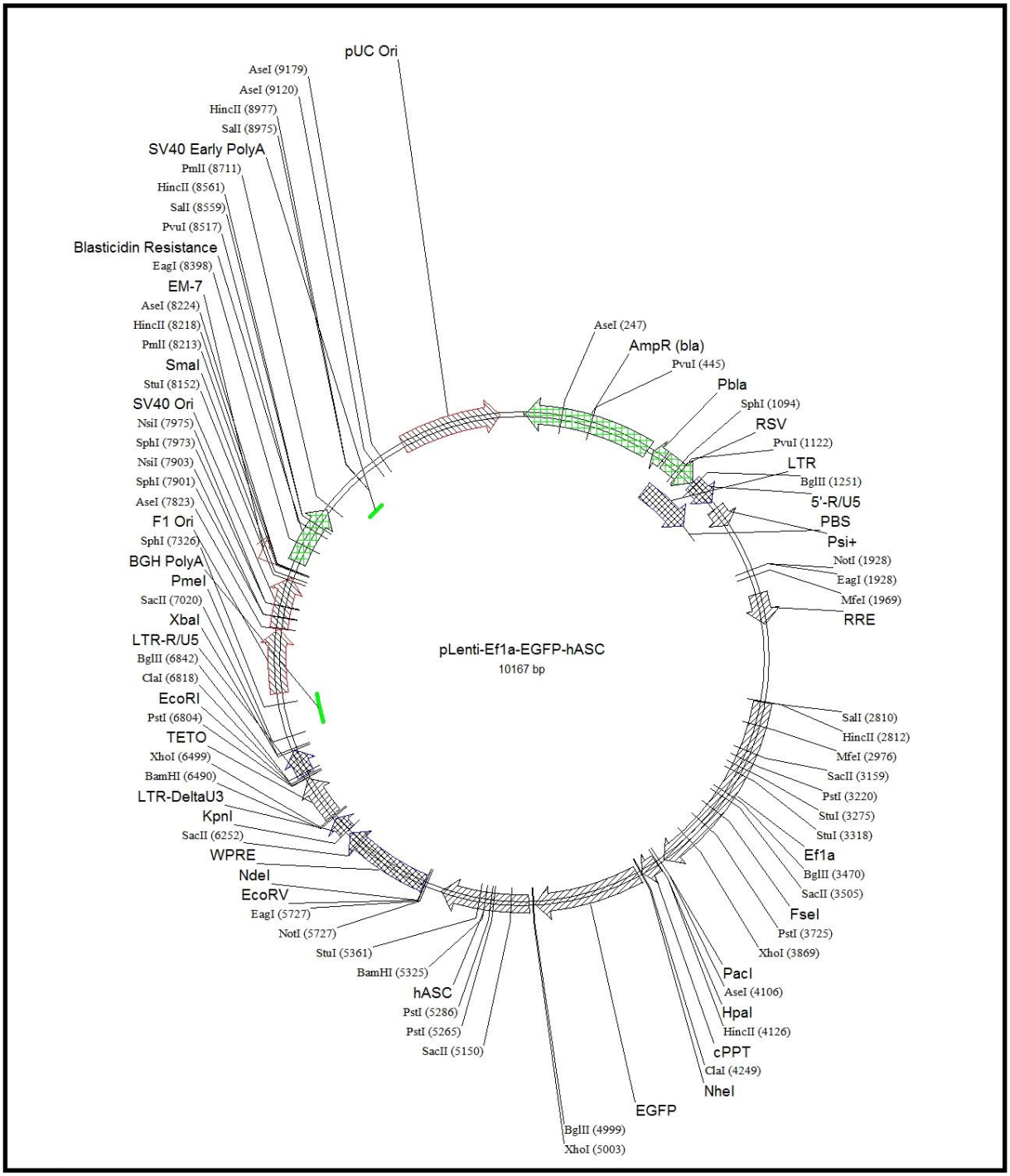

Figure A.7 Plasmid map of pLenti-Ef1a-EGFP-hASC.

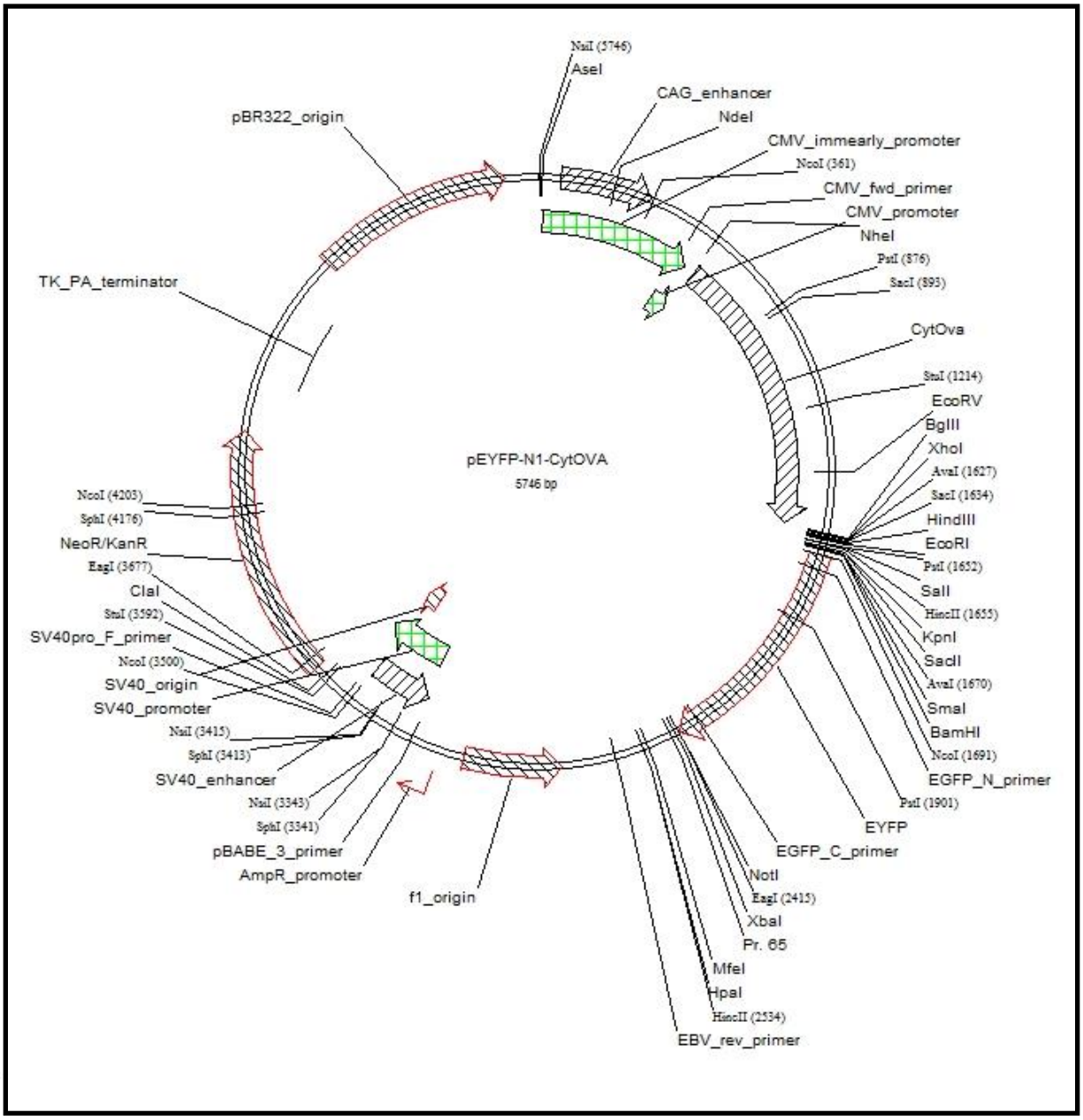

Figure A.8. Plasmid map of peYFP-N1-CytOVA.

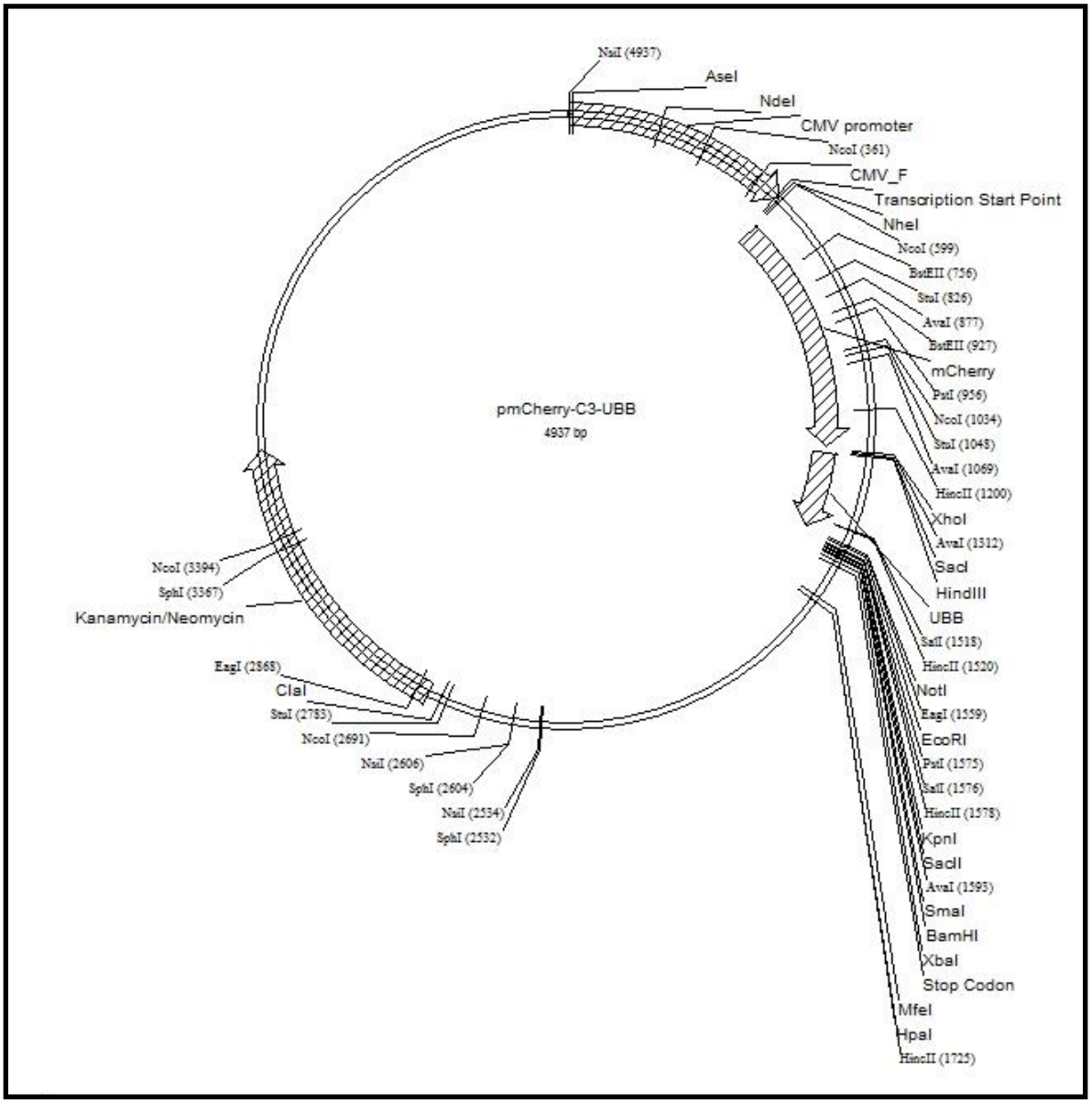

Figure A.9. Plasmid map of pmCherry-C3-UBB.

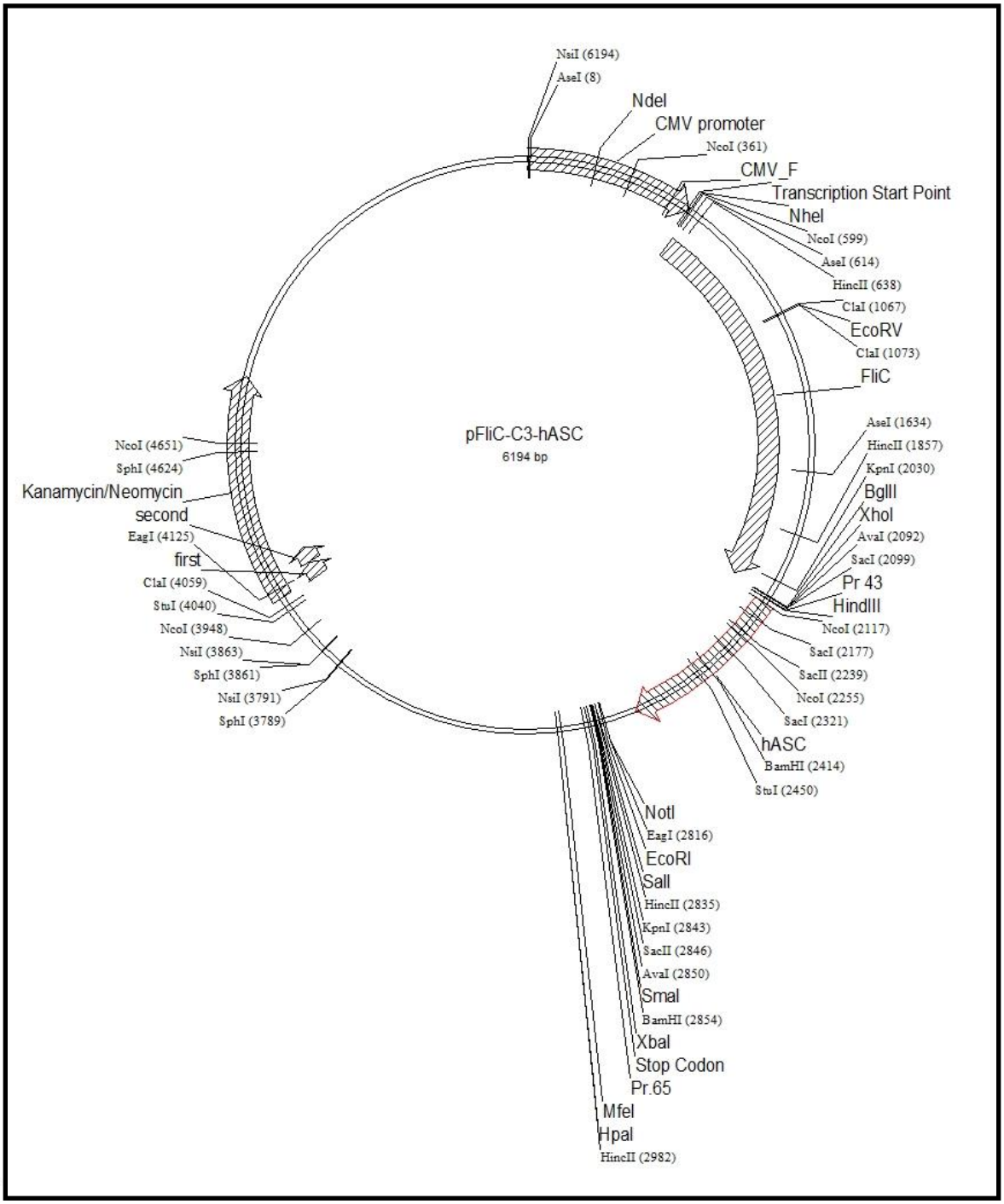

Figure A.10. Plasmid map of pFliC-C3-hASC.

8. APPENDIX B: ASC speck purification from HEK293T cells

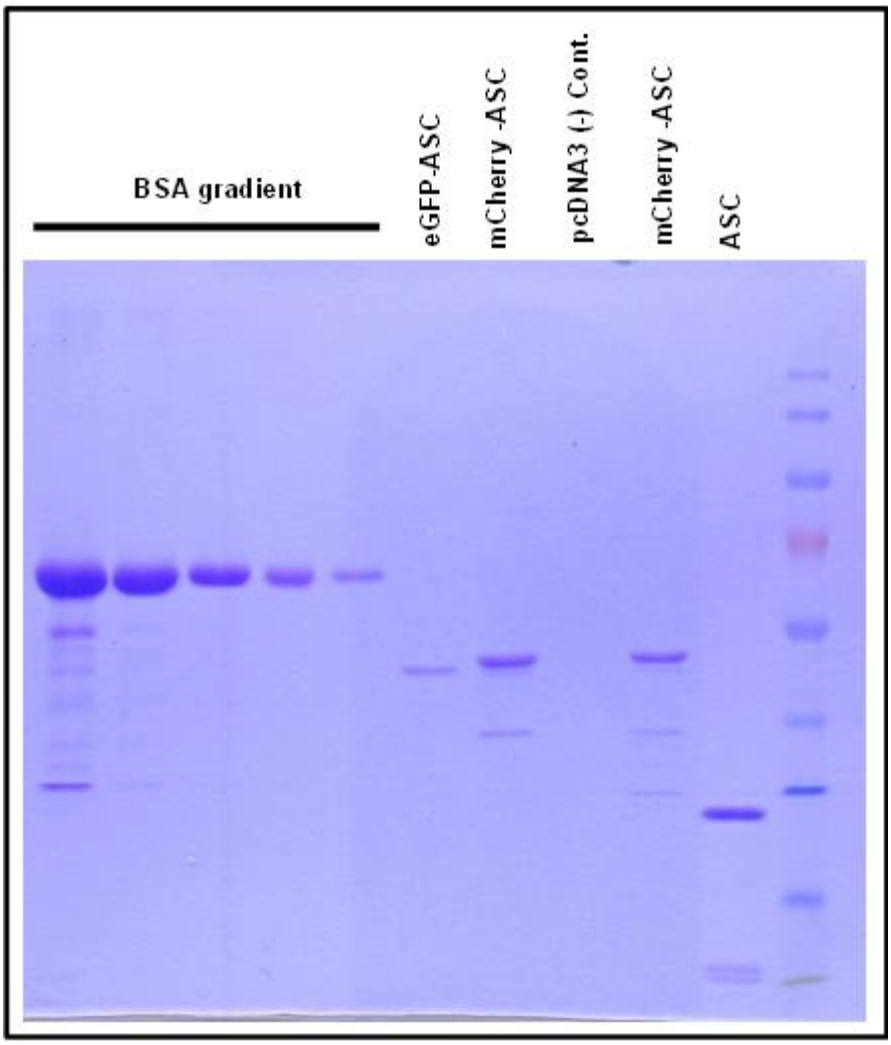

Figure B.1. Typical results of the ASC speck purification from HEK293T cells. EGFP-ASC, mCherry-ASC and untagged ASC specks were purified as in Section 4.6.2. Purified specks were run side by side with BSA standards for concentration determination. Gels were stained with coomassie staining.

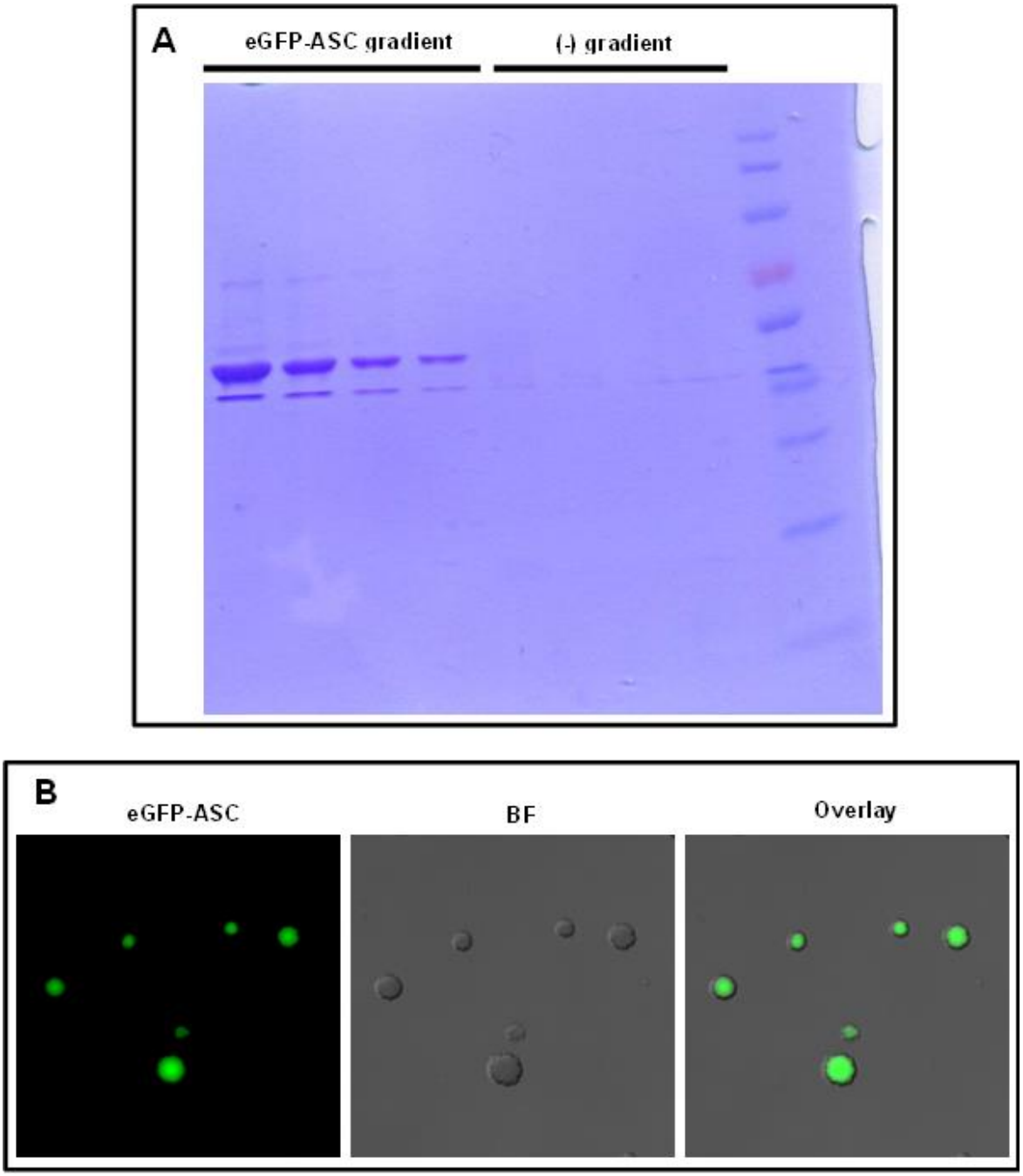

Figure B.2. Purified EGFP-ASC specks from HEK293T cells. (A) Concentration gradient of purified EGFP-ASC specks were run side-by-side with negative control (pcDNA3 transfected HEK293T cells applied to same purification procedure). While mostly one band was detected (apart from the unresolved lower band), high molecular weight smeary bands were also detected. These bands could be either purification impurities or ASC speck co-aggregates. (B) Confocal micrograph of purified EGFP-ASC specks.

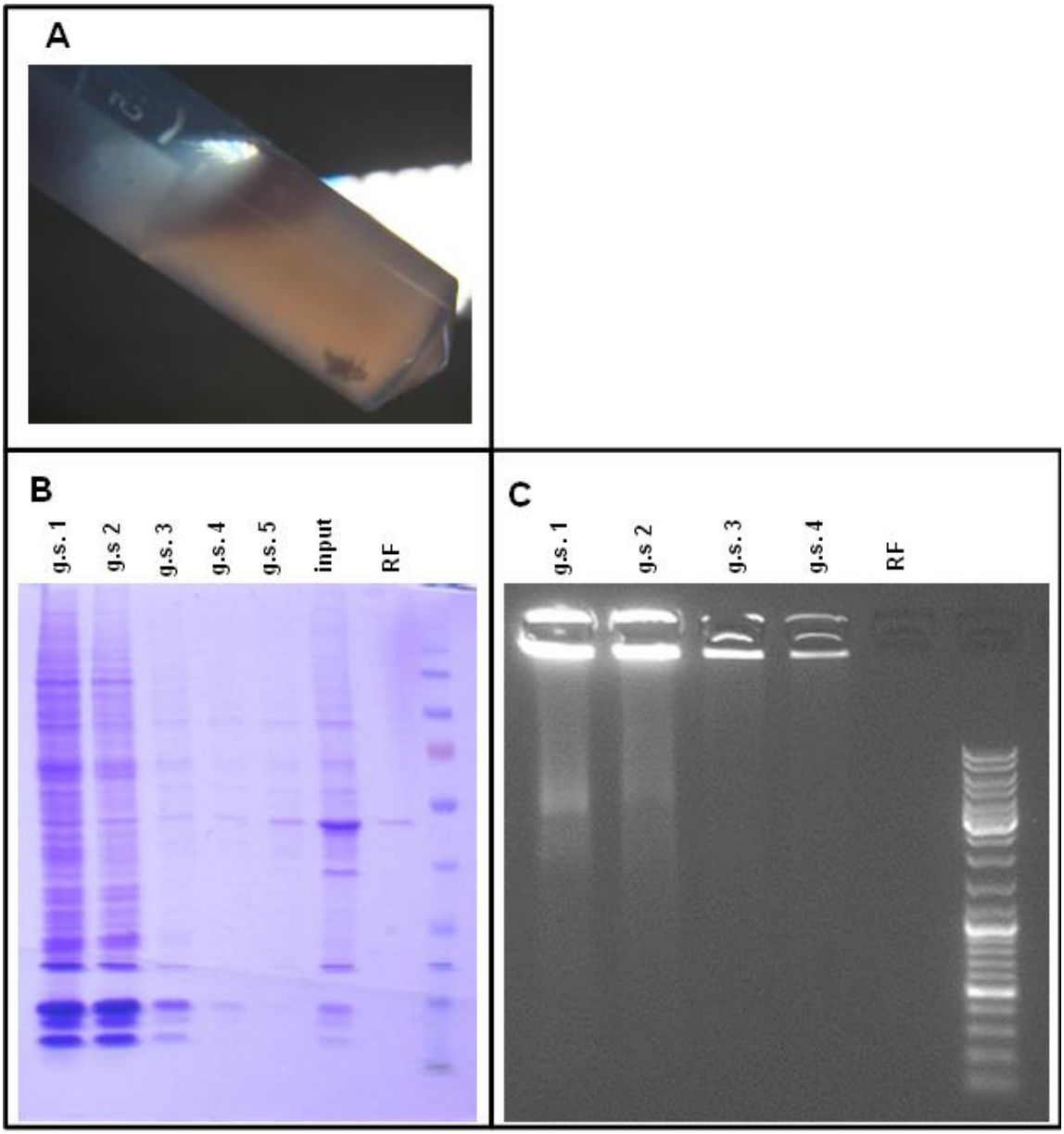

Figure B.3. Gravity sedimenting pellet is rich in nucleic acids and proteins but enriched in ASC specks. (A) Visual appearance of gravity sedimenting pellet. (B) After serial runs of centrifugation and resuspension, gravitiy sedimenting pellets (g.s.) were saved and run with input (syringe filtration input) and RF (reverse flow, end product). Compare non-specific band in gravity sedimentation pellets and RF. (C) Gravity sedimenting pellets were run in agarose gel together with RF. These results indicate that depletion of gravity sedimentation pellet effectively contributes to ASC speck enrichment.

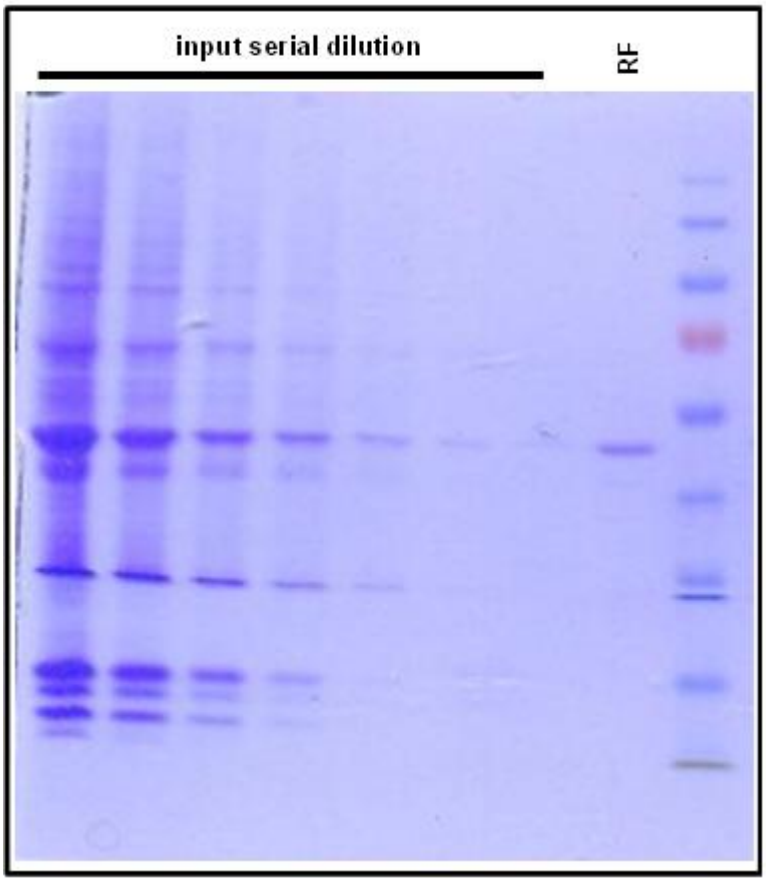

Figure B.4. Effectiveness of the syringe filtration & reverse flow on ASC speck enrichment. The syringe filtration input is run as serial dilution, together with the output (RF, reverse flow). Compare non-specific bands in the lane for with RF.

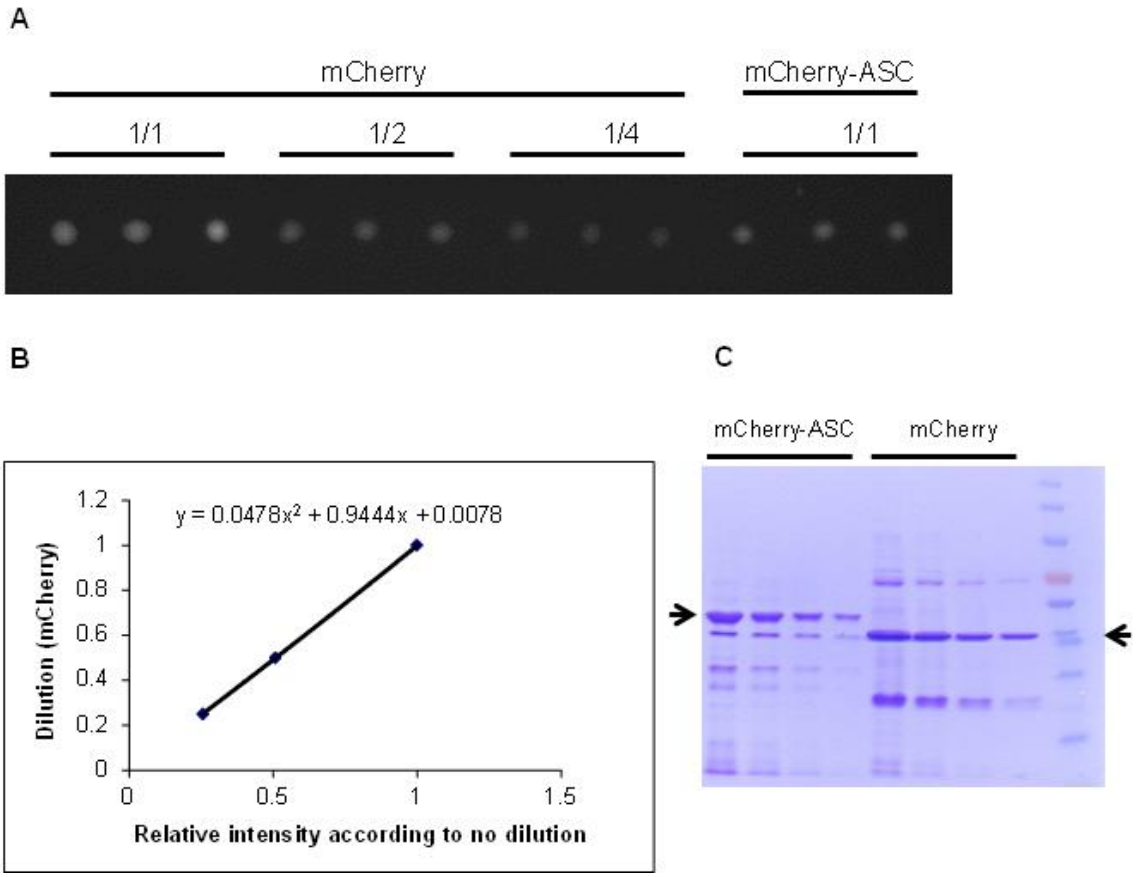

Figure B.5. Relative intensity calculation for mCherry alone and mCherry-ASC specks. (A) Triplicate serial dilutions of mCherry (purified from *E. Coli*) and mCherry-ASC (purified from HEK293T) were excited in a UV box and imaged. (B) A standard curve was plotted for the mCherry dilution and corresponding measured intensities. Measured intensity of mCherry-ASC is inserted in this equation for the unknown x in order to find relative fluorescence. (C) Serial dilutions of mCherry-ASC and mCherry samples visualized by Coomassie staining. Arrows indicate protein of interest.

REFERENCES

1. de Alba, E., "Structure and Interdomain Dynamics of Apoptosis-Associated Speck-Like Protein Containing a Card (Asc)", *The Journal of Biological Chemistry*, Vol. 284, No. 47, pp. 32932-41, 2009.

2. Beutler, B. A., "Tlrs and Innate Immunity", *Blood*, Vol. 113, No. 7, pp. 1399-407, 2009.

3. Theofilopoulos, A. N., R. Gonzalez-Quintial, B. R. Lawson, Y. T. Koh, M. E. Stern, D. H. Kono, B. Beutler, and R. Baccala, "Sensors of the Innate Immune System: Their Link to Rheumatic Diseases", *Nature Reviews Rheumatology*, Vol. 6, No. 3, pp. 146-56, 2010.

4. Jones, J. D. and J. L. Dangl, "The Plant Immune System", *Nature*, Vol. 444, No. 7117, pp. 323-9, 2006.

5. Gross, O., C. J. Thomas, G. Guarda, and J. Tschopp, "The Inflammasome: An Integrated View", *Immunological Reviews*, Vol. 243, No. 1, pp. 136-151, 2011.

6. Schroder, K. and J. Tschopp, "The Inflammasomes", *Cell*, Vol. 140, No. 6, pp. 821-832, 2010.

7. Cederlund, A., G. H. Gudmundsson, and B. Agerberth, "Antimicrobial Peptides Important in Innate Immunity", *FEBS Journal*, Vol. 278, No. 20, pp. 3942-51, 2011.

8. Ganz, T., "The Role of Antimicrobial Peptides in Innate Immunity", *Integrative and Comparative Biology*, Vol. 43, No. 2, pp. 300-4, 2003.

9. Pancer, Z. and M. D. Cooper, "The Evolution of Adaptive Immunity", *Annual Review of Immunology*, Vol. 24, No. pp. 497-518, 2006.

10. Boehm, T., N. McCurley, Y. Sutoh, M. Schorpp, M. Kasahara, and M. D. Cooper, "Vlr-Based Adaptive Immunity", *Annual Review of Immunology*, Vol. 30, No. pp. 203-20, 2012.

11. Takeuchi, O. and S. Akira, "Pattern Recognition Receptors and Inflammation", *Cell*, Vol. 140, No. 6, pp. 805-20, 2010.

12. Duthie, M. S., H. P. Windish, C. B. Fox, and S. G. Reed, "Use of Defined Tlr Ligands as Adjuvants within Human Vaccines", *Immunological Reviews*, Vol. 239, No. 1, pp. 178-196, 2011.

13. Leemans, J. C., S. L. Cassel, and F. S. Sutterwala, "Sensing Damage by the Nlrp3 Inflammasome", *Immunological Reviews*, Vol. 243, No. 1, pp. 152-162, 2011.

14. Halff, E. F., C. A. Diebolder, M. Versteeg, A. Schouten, T. H. Brondijk, and E. G. Huizinga, "Formation and Structure of a Naip5-Nlrc4 Inflammasome Induced by Direct Interactions with Conserved N- and C-Terminal Regions of Flagellin", *The Journal of Biological Chemistry*, Vol. 287, No. 46, pp. 38460-72, 2012.

15. Zhao, Y., J. Yang, J. Shi, Y. N. Gong, Q. Lu, H. Xu, L. Liu, and F. Shao, "The Nlrc4 Inflammasome Receptors for Bacterial Flagellin and Type Iii Secretion Apparatus", *Nature*, Vol. 477, No. 7366, pp. 596-600, 2011.

16. Rathinam, V. A. K., Z. Jiang, S. N. Waggoner, S. Sharma, L. E. Cole, L. Waggoner, S. K. Vanaja, B. G. Monks, S. Ganesan, and E. Latz, "The Aim2 Inflammasome Is Essential for Host Defense against Cytosolic Bacteria and DNA Viruses", *Nature Immunology*, Vol. 11, No. 5, pp. 395-402, 2010.

17. Koizumi, Y., C. Toma, N. Higa, T. Nohara, N. Nakasone, and T. Suzuki, "Inflammasome Activation Via Intracellular Nlrs Triggered by Bacterial Infection", *Cellular Microbiology*, Vol. 14, No. 2, pp. 149-154, 2012.

18. Gram, A. M., J. Frenkel, and M. E. Ressing, "Inflammasomes and Viruses: Cellular Defence Versus Viral Offence", *Journal of General Virology*, Vol. 93, No. Pt 10, pp. 2063-75, 2012.

19. Joly, S. and F. S. Sutterwala, "Fungal Pathogen Recognition by the Nlrp3 Inflammasome", *Virulence*, Vol. 1, No. 4, pp. 276-80, 2010.

20. Cassel, S. L. and F. S. Sutterwala, "Sterile Inflammatory Responses Mediated by the Nlrp3 Inflammasome", *European Journal of Immunology*, Vol. 40, No. 3, pp. 607-11, 2010.

21. Tschopp, J. and K. Schroder, "Nlrp3 Inflammasome Activation: The Convergence of Multiple Signalling Pathways on Ros Production?", *Nature Reviews Immunology*, Vol. 10, No. 3, pp. 210-5, 2010.

22. Latz, E., T. S. Xiao, and A. Stutz, "Activation and Regulation of the Inflammasomes", *Nature Reviews Immunology*, Vol. 13, No. 6, pp. 397-411, 2013.

23. Muzio, M., B. R. Stockwell, H. R. Stennicke, G. S. Salvesen, and V. M. Dixit, "An Induced Proximity Model for Caspase-8 Activation", *The Journal of Biological Chemistry*, Vol. 273, No. 5, pp. 2926-2930, 1998.

24. Salvesen, G. S. and V. M. Dixit, "Caspase Activation: The Induced-Proximity Model", *Proceedings of the National Academy of Sciences of the United States of America*, Vol. 96, No. 20, pp. 10964-7, 1999.

25. Pop, C., J. Timmer, S. Sperandio, and G. S. Salvesen, "The Apoptosome Activates Caspase-9 by Dimerization", *Molecular Cell*, Vol. 22, No. 2, pp. 269-275, 2006.

26. Yang, X., H. Y. Chang, and D. Baltimore, "Autoproteolytic Activation of Pro-Caspases by Oligomerization", *Molecular Cell*, Vol. 1, No. 2, pp. 319, 1998.

27. Chang, D. W., D. Ditsworth, H. Liu, S. M. Srinivasula, E. S. Alnemri, and X. Yang, "Oligomerization Is a General Mechanism for the Activation of Apoptosis Initiator

and Inflammatory Procaspases", *The Journal of Biological Chemistry*, Vol. 278, No. 19, pp. 16466-16469, 2003.

28. MacCorkle, R. A., K. W. Freeman, and D. M. Spencer, "Synthetic Activation of Caspases: Artificial Death Switches", *Proceedings of the National Academy of Sciences of the United States of America*, Vol. 95, No. 7, pp. 3655-3660, 1998.

29. Bao, Q. and Y. Shi, "Apoptosome: A Platform for the Activation of Initiator Caspases", *Cell Death and Differentiation*, Vol. 14, No. 1, pp. 56-65, 2006.

30. Qi, S., Y. Pang, Q. Hu, Q. Liu, H. Li, Y. Zhou, T. He, Q. Liang, Y. Liu, X. Yuan, G. Luo, H. Li, J. Wang, N. Yan, and Y. Shi, "Crystal Structure of the Caenorhabditis Elegans Apoptosome Reveals an Octameric Assembly of Ced-4", *Cell*, Vol. 141, No. 3, pp. 446-57, 2010.

31. Wang, L., J. K. Yang, V. Kabaleeswaran, A. J. Rice, A. C. Cruz, A. Y. Park, Q. Yin, E. Damko, S. B. Jang, S. Raunser, C. V. Robinson, R. M. Siegel, T. Walz, and H. Wu, "The Fas-Fadd Death Domain Complex Structure Reveals the Basis of Disc Assembly and Disease Mutations", *Nature Structural and Molecular Biology*, Vol. 17, No. 11, pp. 1324-9, 2010.

32. Yuan, S., X. Yu, M. Topf, L. Dorstyn, S. Kumar, S. J. Ludtke, and C. W. Akey, "Structure of the Drosophila Apoptosome at 6.9 a Resolution", *Structure*, Vol. 19, No. 1, pp. 128-40, 2011.

33. Yuan, S., X. Yu, M. Topf, S. J. Ludtke, X. Wang, and C. W. Akey, "Structure of an Apoptosome-Procaspase-9 Card Complex", *Structure*, Vol. 18, No. 5, pp. 571-83, 2010.

34. Broz, P., J. von Moltke, J. W. Jones, R. E. Vance, and D. M. Monack, "Differential Requirement for Caspase-1 Autoproteolysis in Pathogen-Induced Cell Death and Cytokine Processing", *Cell Host and Microbe*, Vol. 8, No. 6, pp. 471-83, 2010.

35. Jones, J. W., N. Kayagaki, P. Broz, T. Henry, K. Newton, K. O'Rourke, S. Chan, J. Dong, Y. Qu, M. Roose-Girma, V. M. Dixit, and D. M. Monack, "Absent in Melanoma 2 Is Required for Innate Immune Recognition of Francisella Tularensis", *Proceedings of the National Academy of Sciences of the United States of America*, Vol. 107, No. 21, pp. 9771-9776, 2010.

36. Fernandes-Alnemri, T., J. Wu, J. W. Yu, P. Datta, B. Miller, W. Jankowski, S. Rosenberg, J. Zhang, and E. S. Alnemri, "The Pyroptosome: A Supramolecular Assembly of Asc Dimers Mediating Inflammatory Cell Death Via Caspase-1 Activation", *Cell Death and Differentiation*, Vol. 14, No. 9, pp. 1590-604, 2007.

37. Broz, P., K. Newton, M. Lamkanfi, S. Mariathasan, V. M. Dixit, and D. M. Monack, "Redundant Roles for Inflammasome Receptors Nlrp3 and Nlrc4 in Host Defense against Salmonella", *The Journal of Experimental Medicine*, Vol. 207, No. 8, pp. 1745-55, 2010.

38. Bryan, N. B., A. Dorfleutner, Y. Rojanasakul, and C. Stehlik, "Activation of Inflammasomes Requires Intracellular Redistribution of the Apoptotic Speck-Like Protein Containing a Caspase Recruitment Domain", *The Journal of Immunology*, Vol. 182, No. 5, pp. 3173-82, 2009.

39. Ogura, Y., F. S. Sutterwala, and R. A. Flavell, "The Inflammasome: First Line of the Immune Response to Cell Stress", *Cell*, Vol. 126, No. 4, pp. 659-62, 2006.

40. Li, H., S. B. Willingham, J. P. Ting, and F. Re, "Cutting Edge: Inflammasome Activation by Alum and Alum's Adjuvant Effect Are Mediated by Nlrp3", *The Journal of Immunology*, Vol. 181, No. 1, pp. 17-21, 2008.

41. Dupont, N., S. Jiang, M. Pilli, W. Ornatowski, D. Bhattacharya, and V. Deretic, "Autophagy-Based Unconventional Secretory Pathway for Extracellular Delivery of Il-1beta", *The EMBO Journal*, Vol. 30, No. 23, pp. 4701-11, 2011.

42. Keller, M., A. Rüegg, S. Werner, and H. Beer, "Active Caspase-1 Is a Regulator of Unconventional Protein Secretion", *Cell*, Vol. 132, No. 5, pp. 818-831, 2008.

43. Rubartelli, A., F. Cozzolino, M. Talio, and R. Sitia, "A Novel Secretory Pathway for Interleukin-1 Beta, a Protein Lacking a Signal Sequence", *The EMBO Journal*, Vol. 9, No. 5, pp. 1503-10, 1990.

44. Nickel, W. and C. Rabouille, "Mechanisms of Regulated Unconventional Protein Secretion", *Nature Reviews Molecular Cell Biology*, Vol. 10, No. 2, pp. 148-55, 2009.

45. Eder, C., "Mechanisms of Interleukin-1beta Release", *Immunobiology*, Vol. 214, No. 7, pp. 543-53, 2009.

46. Qu, Y., L. Franchi, G. Nunez, and G. R. Dubyak, "Nonclassical Il-1 Beta Secretion Stimulated by P2x7 Receptors Is Dependent on Inflammasome Activation and Correlated with Exosome Release in Murine Macrophages", *The Journal of Immunology*, Vol. 179, No. 3, pp. 1913-25, 2007.

47. Qu, Y., L. Ramachandra, S. Mohr, L. Franchi, C. V. Harding, G. Nunez, and G. R. Dubyak, "P2x7 Receptor-Stimulated Secretion of Mhc Class Ii-Containing Exosomes Requires the Asc/Nlrp3 Inflammasome but Is Independent of Caspase-1", *The Journal of Immunology*, Vol. 182, No. 8, pp. 5052-5062, 2009.

48. Miao, E. A., J. V. Rajan, and A. Aderem, "Caspase-1-Induced Pyroptotic Cell Death", *Immunological Reviews*, Vol. 243, No. 1, pp. 206-14, 2011.

49. Suzuki, T., L. Franchi, C. Toma, H. Ashida, M. Ogawa, Y. Yoshikawa, H. Mimuro, N. Inohara, C. Sasakawa, and G. Nunez, "Differential Regulation of Caspase-1 Activation, Pyroptosis, and Autophagy Via Ipaf and Asc in Shigella-Infected Macrophages", *PLOS Pathogens*, Vol. 3, No. 8, pp. e111, 2007.

50. Miao, E. A., I. A. Leaf, P. M. Treuting, D. P. Mao, M. Dors, A. Sarkar, S. E. Warren, M. D. Wewers, and A. Aderem, "Caspase-1-Induced Pyroptosis Is an Innate Immune Effector Mechanism against Intracellular Bacteria", *Nature Immunology*, Vol. 11, No. 12, pp. 1136-1142, 2010.

51. Ceballos-Olvera, I., M. Sahoo, M. A. Miller, L. Del Barrio, and F. Re, "Inflammasome-Dependent Pyroptosis and Il-18 Protect against Burkholderia Pseudomallei Lung Infection While Il-1beta Is Deleterious", *PLOS Pathogens*, Vol. 7, No. 12, pp. e1002452, 2011.

52. Shi, C. S., K. Shenderov, N. N. Huang, J. Kabat, M. Abu-Asab, K. A. Fitzgerald, A. Sher, and J. H. Kehrl, "Activation of Autophagy by Inflammatory Signals Limits Il-1beta Production by Targeting Ubiquitinated Inflammasomes for Destruction", *Nature Immunology*, Vol. 13, No. 3, pp. 255-63, 2012.

53. Byrne, B. G., J. F. Dubuisson, A. D. Joshi, J. J. Persson, and M. S. Swanson, "Inflammasome Components Coordinate Autophagy and Pyroptosis as Macrophage Responses to Infection", *MBio*, Vol. 4, No. 1, pp. 2013.

54. Masumoto, J., S. Taniguchi, K. Ayukawa, H. Sarvotham, T. Kishino, N. Niikawa, E. Hidaka, T. Katsuyama, T. Higuchi, and J. Sagara, "Asc, a Novel 22-Kda Protein, Aggregates During Apoptosis of Human Promyelocytic Leukemia Hl-60 Cells", *The Journal of Biological Chemistry*, Vol. 274, No. 48, pp. 33835-8, 1999.

55. Kersse, K., J. Verspurten, T. Vanden Berghe, and P. Vandenabeele, "The Death-Fold Superfamily of Homotypic Interaction Motifs", *Trends in Biochemical Sciences*, Vol. 36, No. 10, pp. 541-52, 2011.

56. Matsushita, K., M. Takeoka, J. Sagara, N. Itano, Y. Kurose, A. Nakamura, and S. Taniguchi, "A Splice Variant of Asc Regulates Il-1beta Release and Aggregates Differently from Intact Asc", *Mediators of Inflammation*, Vol. 2009, No. pp. 287387, 2009.

57. Masumoto, J., W. Zhou, F. F. Chen, F. Su, J. Y. Kuwada, E. Hidaka, T. Katsuyama, J. Sagara, S. Taniguchi, P. Ngo-Hazelett, J. H. Postlethwait, G. Nunez, and N. Inohara, "Caspy, a Zebrafish Caspase, Activated by Asc Oligomerization Is Required for Pharyngeal Arch Development", *The Journal of Biological Chemistry*, Vol. 278, No. 6, pp. 4268-76, 2003.

58. Liepinsh, E., R. Barbals, E. Dahl, A. Sharipo, E. Staub, and G. Otting, "The Death-Domain Fold of the Asc Pyrin Domain, Presenting a Basis for Pyrin/Pyrin Recognition", *Journal of Molecular Biology*, Vol. 332, No. 5, pp. 1155-63, 2003.

59. Vajjhala, P. R., R. E. Mirams, and J. M. Hill, "Multiple Binding Sites on the Pyrin Domain of Asc Protein Allow Self-Association and Interaction with Nlrp3 Protein", *The Journal of Biological Chemistry*, Vol. 287, No. 50, pp. 41732-43, 2012.

60. Moriya, M., S. Taniguchi, P. Wu, E. Liepinsh, G. Otting, and J. Sagara, "Role of Charged and Hydrophobic Residues in the Oligomerization of the Pyrin Domain of Asc", *Biochemistry*, Vol. 44, No. 2, pp. 575-83, 2005.

61. Proell, M., M. Gerlic, P. D. Mace, J. C. Reed, and S. J. Riedl, "The Card Plays a Critical Role in Asc Foci Formation and Inflammasome Signalling", *Biochemical Journal*, Vol. 449, No. 3, pp. 613-21, 2013.

62. Jensen, P. E., "Recent Advances in Antigen Processing and Presentation", *Nature Immunology*, Vol. 8, No. 10, pp. 1041-8, 2007.

63. Neefjes, J., M. L. Jongsma, P. Paul, and O. Bakke, "Towards a Systems Understanding of Mhc Class I and Mhc Class Ii Antigen Presentation", *Nature Reviews Immunology*, Vol. 11, No. 12, pp. 823-36, 2011.

64. Higgins, S. C. and K. H. G. Mills, "Tlr, Nlr Agonists, and Other Immune Modulators as Infectious Disease Vaccine Adjuvants", *Current Infectious Disease Reports*, Vol. 12, No. 1, pp. 4-12, 2010.

65. Watts, C., "The Exogenous Pathway for Antigen Presentation on Major Histocompatibility Complex Class Ii and Cd1 Molecules", *Nature Immunology*, Vol. 5, No. 7, pp. 685-92, 2004.

66. Pieters, J., "Mhc Class Ii Compartments: Specialized Organelles of the Endocytic Pathway in Antigen Presenting Cells", *The Journal of Biological Chemistry*, Vol. 378, No. 8, pp. 751-8, 1997.

67. Crotzer, V. L. and J. S. Blum, "Autophagy and Its Role in Mhc-Mediated Antigen Presentation", *The Journal of Immunology*, Vol. 182, No. 6, pp. 3335-41, 2009.

68. De Temmerman, M. L., J. Rejman, J. Demeester, D. J. Irvine, B. Gander, and S. C. De Smedt, "Particulate Vaccines: On the Quest for Optimal Delivery and Immune Response", *Drug Discovery Today*, Vol. 16, No. 13-14, pp. 569-82, 2011.

69. Xiang, S. D., A. Scholzen, G. Minigo, C. David, V. Apostolopoulos, P. L. Mottram, and M. Plebanski, "Pathogen Recognition and Development of Particulate Vaccines: Does Size Matter?", *Methods*, Vol. 40, No. 1, pp. 1-9, 2006.

70. Yazdi, A. S., S. K. Drexler, and J. Tschopp, "The Role of the Inflammasome in Nonmyeloid Cells", *Journal of Clinical Immunology*, Vol. 30, No. 5, pp. 623-7, 2010.

71. Eisenbarth, S. C., O. R. Colegio, W. O'Connor, F. S. Sutterwala, and R. A. Flavell, "Crucial Role for the Nalp3 Inflammasome in the Immunostimulatory Properties of Aluminium Adjuvants", *Nature*, Vol. 453, No. 7198, pp. 1122-6, 2008.

72. Guo, X. and K. M. Dhodapkar, "Central and Overlapping Role of Cathepsin B and Inflammasome Adaptor Asc in Antigen Presenting Function of Human Dendritic Cells", *Human Immunology*, Vol. 73, No. 9, pp. 871-8, 2012.

73. Ippagunta, S. K., R. K. Malireddi, P. J. Shaw, G. A. Neale, L. V. Walle, D. R. Green, Y. Fukui, M. Lamkanfi, and T. D. Kanneganti, "The Inflammasome Adaptor Asc Regulates the Function of Adaptive Immune Cells by Controlling Dock2-Mediated Rac Activation and Actin Polymerization", *Nature Immunology*, Vol. 12, No. 10, pp. 1010-6, 2011.

74. Ellebedy, A. H., C. Lupfer, H. E. Ghoneim, J. DeBeauchamp, T. D. Kanneganti, and R. J. Webby, "Inflammasome-Independent Role of the Apoptosis-Associated Speck-Like Protein Containing Card (Asc) in the Adjuvant Effect of Mf59", *Proceedings of the National Academy of Sciences of the United States of America*, Vol. 108, No. 7, pp. 2927-32, 2011.

75. Balci-Peynircioglu, B., A. L. Waite, P. Schaner, Z. E. Taskiran, N. Richards, D. Orhan, S. Gucer, S. Ozen, D. Gumucio, and E. Yilmaz, "Expression of Asc in Renal Tissues of Familial Mediterranean Fever Patients with Amyloidosis: Postulating a Role for Asc in Aa Type Amyloid Deposition", *Experimental Biology and Medicine*, Vol. 233, No. 11, pp. 1324-33, 2008.

76. Cheng, J., A. L. Waite, E. R. Tkaczyk, K. Ke, N. Richards, A. J. Hunt, and D. L. Gumucio, "Kinetic Properties of Asc Protein Aggregation in Epithelial Cells", *Journal of Cellular Physiology*, Vol. 222, No. 3, pp. 738-47, 2010.

77. Johnston, J. A., C. L. Ward, and R. R. Kopito, "Aggresomes: A Cellular Response to Misfolded Proteins", *The Journal of Cell Biology*, Vol. 143, No. 7, pp. 1883-98, 1998.

78. Bagola, K. and T. Sommer, "Protein Quality Control: On Ipods and Other Junq", *Current Biology*, Vol. 18, No. 21, pp. R1019-21, 2008.

79. Lelouard, H., E. Gatti, F. Cappello, O. Gresser, V. Camosseto, and P. Pierre, "Transient Aggregation of Ubiquitinated Proteins During Dendritic Cell Maturation", *Nature*, Vol. 417, No. 6885, pp. 177-82, 2002.

80. Opazo, F., A. Krenz, S. Heermann, J. B. Schulz, and B. H. Falkenburger, "Accumulation and Clearance of Alpha-Synuclein Aggregates Demonstrated by Time-Lapse Imaging", *Journal of Neurochemistry*, Vol. 106, No. 2, pp. 529-40, 2008.

81. García-Mata, R., Z. Bebök, E. J. Sorscher, and E. S. Sztul, "Characterization and Dynamics of Aggresome Formation by a Cytosolic Gfp-Chimera", *The Journal of Cell Biology*, Vol. 146, No. 6, pp. 1239-1254, 1999.

82. Kaganovich, D., R. Kopito, and J. Frydman, "Misfolded Proteins Partition between Two Distinct Quality Control Compartments", *Nature*, Vol. 454, No. 7208, pp. 1088-1095, 2008.

83. Kettern, N., C. Rogon, A. Limmer, H. Schild, and J. Hohfeld, "The Hsc/Hsp70 Co-Chaperone Network Controls Antigen Aggregation and Presentation During Maturation of Professional Antigen Presenting Cells", *PLoS One*, Vol. 6, No. 1, pp. e16398, 2011.

84. Lelouard, H., V. Ferrand, D. Marguet, J. Bania, V. Camosseto, A. David, E. Gatti, and P. Pierre, "Dendritic Cell Aggresome-Like Induced Structures Are Dedicated Areas for Ubiquitination and Storage of Newly Synthesized Defective Proteins", *The Journal of Cell Biology*, Vol. 164, No. 5, pp. 667-75, 2004.

85. Szeto, J., N. A. Kaniuk, V. Canadien, R. Nisman, N. Mizushima, T. Yoshimori, D. P. Bazett-Jones, and J. H. Brumell, "Alis Are Stress-Induced Protein Storage Compartments for Substrates of the Proteasome and Autophagy", *Autophagy*, Vol. 2, No. 3, pp. 189-99, 2006.

86. Herter, S., P. Osterloh, N. Hilf, G. Rechtsteiner, J. Hohfeld, H. G. Rammensee, and H. Schild, "Dendritic Cell Aggresome-Like-Induced Structure Formation and Delayed Antigen Presentation Coincide in Influenza Virus-Infected Dendritic Cells", *The Journal of Immunology*, Vol. 175, No. 2, pp. 891-8, 2005.

87. DeFillipo, A. M., J. Dai, and Z. Li, "Heat Shock-Induced Dendritic Cell Maturation Is Coupled by Transient Aggregation of Ubiquitinated Proteins Independently of Heat Shock Factor 1 or Inducible Heat Shock Protein 70", *Molecular Immunology*, Vol. 41, No. 8, pp. 785-92, 2004.

88. Canadien, V., T. Tan, R. Zilber, J. Szeto, A. J. Perrin, and J. H. Brumell, "Cutting Edge: Microbial Products Elicit Formation of Dendritic Cell Aggresome-Like Induced Structures in Macrophages", *The Journal of Immunology*, Vol. 174, No. 5, pp. 2471-5, 2005.

89. Tsuchiya, S., M. Yamabe, Y. Yamaguchi, Y. Kobayashi, T. Konno, and K. Tada, "Establishment and Characterization of a Human Acute Monocytic Leukemia Cell Line (Thp-1)", *International Journal of Cancer*, Vol. 26, No. 2, pp. 171-6, 1980.

90. Auwerx, J., "The Human Leukemia Cell Line, Thp-1: A Multifacetted Model for the Study of Monocyte-Macrophage Differentiation", *Experientia*, Vol. 47, No. 1, pp. 22-31, 1991.

91. Sambrook, J. and D. W. Russell, "Calcium-Phosphate-Mediated Transfection of Eukaryotic Cells with Plasmid Dnas", *Cold Spring Harbor Protocols*, Vol. 2006, No. 1, pp. 2006.

92. Richards, N., P. Schaner, A. Diaz, J. Stuckey, E. Shelden, A. Wadhwa, and D. L. Gumucio, "Interaction between Pyrin and the Apoptotic Speck Protein (Asc) Modulates Asc-Induced Apoptosis", *The Journal of Biological Chemistry*, Vol. 276, No. 42, pp. 39320-9, 2001.

93. Mizel, S. B. and J. T. Bates, "Flagellin as an Adjuvant: Cellular Mechanisms and Potential", *The Journal of Immunology*, Vol. 185, No. 10, pp. 5677-5682, 2010.

94. Masumoto, J., S. Taniguchi, and J. Sagara, "Pyrin N-Terminal Homology Domain- and Caspase Recruitment Domain-Dependent Oligomerization of Asc", *Biochemical and Biophysical Research Communications*, Vol. 280, No. 3, pp. 652-5, 2001.

95. Srinivasula, S. M., J. L. Poyet, M. Razmara, P. Datta, Z. Zhang, and E. S. Alnemri, "The Pyrin-Card Protein Asc Is an Activating Adaptor for Caspase-1", *The Journal of Biological Chemistry*, Vol. 277, No. 24, pp. 21119-21122, 2002.

96. Sutterwala, F. S., Y. Ogura, and R. A. Flavell, "The Inflammasome in Pathogen Recognition and Inflammation", *Journal of Leukocyte Biology*, Vol. 82, No. 2, pp. 259-264, 2007.

97. Walsh, D., M. B. Mathews, and I. Mohr, "Tinkering with Translation: Protein Synthesis in Virus-Infected Cells", *Cold Spring Harbor Perspectives in Biology*, Vol. 5, No. 1, pp. a012351, 2013.

98. Pierre, P., "Dendritic Cells, Drips, and Dalis in the Control of Antigen Processing", *Immunological Reviews*, Vol. 207, No. pp. 184-90, 2005.

99. Dolan, B. P., J. R. Bennink, and J. W. Yewdell, "Translating Drips: Progress in Understanding Viral and Cellular Sources of Mhc Class I Peptide Ligands", *Cellular and Molecular Life Sciences*, Vol. 68, No. 9, pp. 1481-9, 2011.

100. Hornung, V., F. Bauernfeind, A. Halle, E. O. Samstad, H. Kono, K. L. Rock, K. A. Fitzgerald, and E. Latz, "Silica Crystals and Aluminum Salts Activate the Nalp3 Inflammasome through Phagosomal Destabilization", *Nature Immunology*, Vol. 9, No. 8, pp. 847-56, 2008.

101. Duewell, P., H. Kono, K. J. Rayner, C. M. Sirois, G. Vladimer, F. G. Bauernfeind, G. S. Abela, L. Franchi, G. Nunez, M. Schnurr, T. Espevik, E. Lien, K. A. Fitzgerald, K. L. Rock, K. J. Moore, S. D. Wright, V. Hornung, and E. Latz, "Nlrp3 Inflammasomes Are Required for Atherogenesis and Activated by Cholesterol Crystals", *Nature*, Vol. 464, No. 7293, pp. 1357-61, 2010.

102. Ramachandra, L., Y. Qu, Y. Wang, C. J. Lewis, B. A. Cobb, K. Takatsu, W. H. Boom, G. R. Dubyak, and C. V. Harding, "Mycobacterium Tuberculosis Synergizes with Atp to Induce Release of Microvesicles and Exosomes Containing Major Histocompatibility Complex Class Ii Molecules Capable of Antigen Presentation", *Infection and Immunity*, Vol. 78, No. 12, pp. 5116-25, 2010.

103. Kleijmeer, M., G. Ramm, D. Schuurhuis, J. Griffith, M. Rescigno, P. Ricciardi-Castagnoli, A. Y. Rudensky, F. Ossendorp, C. J. Melief, W. Stoorvogel, and H. J. Geuze, "Reorganization of Multivesicular Bodies Regulates Mhc Class Ii Antigen Presentation by Dendritic Cells", *The Journal of Cell Biology*, Vol. 155, No. 1, pp. 53-63, 2001.

104. van Nispen tot Pannerden, H. E., W. J. Geerts, M. J. Kleijmeer, and H. F. Heijnen, "Spatial Organization of the Transforming Mhc Class Ii Compartment", *Biology of the Cell*, Vol. 102, No. 11, pp. 581-91, 2010.

105. Stephen, T. L., M. Fabri, L. Groneck, T. A. Rohn, H. Hafke, N. Robinson, J. Rietdorf, D. Schrama, J. C. Becker, G. Plum, M. Kronke, H. Kropshofer, and W. M. Kalka-

Moll, "Transport of Streptococcus Pneumoniae Capsular Polysaccharide in Mhc Class Ii Tubules", *PLOS Pathogens*, Vol. 3, No. 3, pp. e32, 2007.